

Positivity-Preserving Well-Balanced Central Discontinuous Galerkin Schemes for the Euler Equations under Gravitational Fields

Haili Jiang,^{*} Huazhong Tang,[†] Kailiang Wu[‡]

Abstract

This paper designs and analyzes positivity-preserving well-balanced (WB) central discontinuous Galerkin (CDG) schemes for the Euler equations with gravity. A distinctive feature of these schemes is that they not only are WB for a general known stationary hydrostatic solution, but also can preserve the positivity of the fluid density and pressure. The standard CDG method does not possess this feature, while directly applying some existing WB techniques to the CDG framework may not accommodate the positivity and keep other important properties at the same time. In order to obtain the WB and positivity-preserving properties simultaneously while also maintaining the conservativeness and stability of the schemes, a novel spatial discretization is devised in the CDG framework based on suitable modifications to the numerical dissipation term and the source term approximation. The modifications are based on a crucial projection operator for the stationary hydrostatic solution, which is proposed for the first time in this work. This novel projection has the same order of accuracy as the standard L^2 -projection, can be explicitly calculated, and is easy to implement without solving any optimization problems. More importantly, it ensures that the projected stationary solution has the same cell averages on both the primal and dual meshes, which is a key to achieve the desired properties of our schemes. Based on some convex decomposition techniques, rigorous positivity-preserving analyses for the resulting WB CDG schemes are carried out. Several one- and two-dimensional numerical examples are performed to illustrate the desired properties of these schemes, including the high-order accuracy, the WB property, the robustness for simulations involving the low pressure or density, high resolution for the discontinuous solutions and the small perturbations around the equilibrium state.

Keywords: Euler equations; central discontinuous Galerkin method; well-balanced schemes; positivity-preserving property; gravitational field

^{*}School of Mathematical Sciences, Peking University, Beijing 100871, P.R. China. (jianghaili@pku.edu.cn)

[†]Nanchang Hangkong University, Jiangxi Province, Nanchang 330000, P.R. China; HEDPS, Center for Applied Physics and Technology, and LMAM, School of Mathematical Sciences, Peking University, Beijing 100871, P.R. China. (hztang@math.pku.edu.cn)

[‡]Corresponding author. Department of Mathematics and SUSTech International Center for Mathematics, Southern University of Science and Technology, and National Center for Applied Mathematics Shenzhen (NCAMS), Shenzhen 518055, P.R. China. (wukl@sustech.edu.cn).

1 Introduction

The Euler equations under gravitational fields are widely adopted to model physical phenomena in the atmospheric science and astrophysics, such as numerical weather forecasting [4], climate modeling, and supernova explosions [17]. In the one-dimensional case, this nonlinear system can be written into the form of the hyperbolic balance laws as

$$\mathbf{U}_t + \mathbf{F}(\mathbf{U})_x = \mathbf{S}(\mathbf{U}, \phi_x), \quad (1)$$

with

$$\mathbf{U} = \begin{pmatrix} \rho \\ m \\ E \end{pmatrix}, \quad \mathbf{F}(\mathbf{U}) = \begin{pmatrix} \rho u \\ \rho u^2 + p \\ (E + p)u \end{pmatrix}, \quad \mathbf{S}(\mathbf{U}, \phi_x) = \begin{pmatrix} 0 \\ -\rho \phi_x \\ -m \phi_x \end{pmatrix}.$$

Here ρ denotes the fluid density, u is the velocity, $m = \rho u$ is the momentum, p represents the pressure, $E = \frac{1}{2}\rho u^2 + \rho e$ denotes the total non-gravitational energy, and e is the specific internal energy. The function $\phi(x)$ in the source terms is the static gravitational potential. In order to close the system (1), an equation of state (EOS) is needed and can be written as $p = p(\rho, e)$; for the ideal gas it is given by

$$p = (\gamma - 1)\rho e = (\gamma - 1)\left(E - \frac{m^2}{2\rho}\right), \quad (2)$$

where the constant $\gamma > 1$ denotes the ratio of specific heats. This paper will mainly focus on the ideal EOS (2), and the proposed schemes are readily extensible to a general EOS.

The Euler system (1) under the gravitational potential $\phi(x)$ admits non-trivial stationary hydrostatic solutions, where the velocity is zero and the gravity is exactly balanced by the pressure gradient:

$$\rho = \rho(x), \quad u = 0, \quad p_x = -\rho \phi_x. \quad (3)$$

Two types of equilibria appear frequently in practical applications. They are the isothermal [41] and polytropic [17] hydrostatic equilibrium states. The temperature $T(x) = T_0$ is a constant under the isothermal assumption. For an isothermal ideal gas with $p = \rho RT$, integrating (3) yields

$$\rho = \hat{\rho}_0 \exp\left(-\frac{\phi}{RT_0}\right), \quad u = 0, \quad p = \hat{p}_0 \exp\left(-\frac{\phi}{RT_0}\right),$$

where R is the gas constant, $\hat{\rho}_0$ is the pressure at a reference position x_0 , and $\hat{p}_0 = \hat{\rho}_0 RT_0$. A polytropic hydrostatic equilibrium, which arises from the astrophysical applications, is characterized by $p = K_0 \rho^\nu$, and for this equilibrium, integrating (3) gives

$$\rho = \left(\frac{\nu - 1}{K_0 \nu}(C - \phi)\right)^{\frac{1}{\nu-1}}, \quad u = 0, \quad p = \frac{1}{K_0^{\frac{1}{\nu-1}}}\left(\frac{\nu - 1}{\nu}(C - \phi)\right)^{\frac{\nu}{\nu-1}},$$

with K_0 and C being constants. A special case is $\nu = \gamma$, which corresponds to a constant entropy.

In order to correctly and accurately capture small perturbations around the equilibrium state (3), it is desirable to develop well-balanced (WB) numerical methods that preserve the discrete version

of those steady state solutions exactly up to machine accuracy. In fact, a straightforward numerical discretization may not be WB and can lead to a numerical solution which is inaccurate or oscillates around the hydrostatic equilibrium after a long time simulation. This problem may be improved if the mesh size is extremely refined, which, however, may cause the simulation time-consuming especially in the multidimensional cases. To reduce the computational cost, the exploration of the WB schemes has attracted much attention in the past few decades. Most of those schemes were devised for the nonlinear shallow water equations over varied bottom topology, another typical model of hyperbolic balance laws; see, e.g., [29, 1, 3, 14, 21, 58, 60, 61, 62] for more details. In recent years, various WB schemes for the Euler equations under gravitational fields have been developed within several different frameworks, including but not limited to the non-central finite volume methods [4, 34, 63, 17, 18, 5, 25], the central finite volume methods [43, 16], the finite difference methods [41, 11, 28], and the discontinuous Galerkin (DG) methods [26, 6, 27], etc. A numerical comparison between the high-order DG method and the WB DG method was carried out in [45]. Most of those works assumed that the target equilibrium is explicitly known, which is also adopted in our present work. It is worth mentioning that, recently, there exist some efforts [2, 7, 10, 18, 44] on developing the WB schemes for the Euler system under gravitational field, without requiring a prior knowledge of the stationary hydrostatic solution.

In physics, the fluid density and thermal pressure are positive, implying that the conservative variables \mathbf{U} must stay in the set of admissible states

$$G := \left\{ \mathbf{U} = (\rho, m, E)^\top : \rho > 0, p(\mathbf{U}) = (\gamma - 1) \left(E - \frac{m^2}{2\rho} \right) > 0 \right\}.$$

Given that the initial data in the set G , a scheme is defined to be positivity-preserving if its solutions are always belong to G . Over the past decade, studying the positivity-preserving and more generally bound-preserving high-order numerical methods has attracted much attention and achieved significant progresses for hyperbolic systems. Most of those high-order accurate schemes are designed with two types of limiters: the simple scaling limiter proposed in [68, 69] and the flux-correction limiters proposed in [15, 64]. Based on the simple scaling limiter, the high-order positivity-preserving DG schemes were designed for the Euler equations without source term in [69, 71] and with various source terms including the gravitational source term in [70]. The bound-preserving methods were also extended to, for example, the shallow water equations [61], the special relativistic Euler equations [54, 36, 56, 49], the compressible Navier–Stokes equations [67], and the compressible magnetohydrodynamic systems [48, 50, 51, 55, 53], and the general relativistic Euler equations under strong gravitational fields [47]. Recently, a universal framework, called geometric quasilinearization (GQL), was proposed in [52] for studying general bound-preserving problems involving nonlinear constraints, with applications to a wide variety of physical systems including the Euler equations. For more developments and applications, the readers are referred to the review articles [40, 65] and the references therein.

The present paper is concerned with the central DG (CDG) methods for solving the Euler equations under gravitational fields. The CDG methods are a family of high-order numerical schemes based on the DG methods [8] and the central scheme framework [35, 20, 31], which were originally

introduced for solving the hyperbolic conservation laws [32], and have been applied to the Hamilton-Jacobi equations [24], the ideal magnetohydrodynamic equations [23, 22], and the special relativistic hydrodynamic [72] and magnetohydrodynamic equations [73]. Based on the simple scaling limiter, the high-order bound-preserving CDG schemes were constructed for the scalar conservation laws and the Euler equations [30], the relativistic Euler equations [56], and the shallow water equations [29]. The CDG methods evolve two copies of numerical solutions defined on two sets of meshes (e.g. the primal mesh and its dual mesh), avoiding using any exact or approximate Riemann solvers at the cell interfaces which can be extremely complicated and time-consuming in some cases. Although needing more memory space than standard DG methods, the CDG methods were proven to allow relatively larger time step-sizes [38] and be more accurate in some numerical tests [33].

The aim of this work is to design and rigorously analyze the high-order positivity-preserving WB CDG schemes for the Euler equations under gravitational fields. A second-order positivity-preserving WB finite volume scheme based on a relaxation Riemann solver was developed in [42] for the Euler equations with gravity for arbitrary hydrostatic equilibria. Based on the (non-central) DG framework, the arbitrarily high-order positivity-preserving WB methods were proposed in [57] for the Euler equations with gravitation. It is also worth mentioning that, in the context of the shallow water equations, several positivity-preserving WB schemes have been developed in the literature [19, 59, 61, 29, 66]. However, within the CDG framework, the study of the positivity-preserving WB schemes for the Euler equations with gravitation is still blank.

For the regular (non-central) DG methods [57], a key to achieve the WB and positivity-preserving properties simultaneously is based on a suitable modification of the HLLC numerical flux, which satisfies both the contact property and the positivity. By contrast, the CDG methods have no numerical flux but possess an extra numerical dissipation term (not existing in the regular DG methods). As such, some existing WB and positivity-preserving techniques in the regular DG case [57] do not apply to the CDG case. Therefore, the design and analysis of positivity-preserving WB schemes in the CDG framework have quite different difficulties and require the development of new techniques. Most notably, we need to carefully deal with the numerical dissipation term by proposing a novel critical projection operator, so as to obtain the WB and positivity-preserving properties simultaneously while also maintaining the conservativeness and stability of the CDG schemes. The main efforts in this paper are summarized as follows.

- In order to obtain the WB and positivity-preserving properties simultaneously while also keeping the conservativeness and stability of the schemes, a novel spatial discretization is devised in the CDG framework based on suitable modifications to the numerical dissipation term and the source term approximation.
- The modifications are based on a crucial projection operator for the stationary hydrostatic solution, which is proposed for the first time in this work. This novel projection has the same order of accuracy as the standard L^2 -projection, can be explicitly calculated, and is easy to implement without solving any optimization problems. More importantly, it ensures that the projected stationary solution has the same cell averages on both the primal and dual meshes, which is key to

achieve the desired properties of our schemes.

- Based on some convex decomposition techniques, a weak positivity property of the resulting WB CDG schemes is rigorously proved, which implies that a simple limiter [69, 46] can ensure the positivity-preserving property without losing the high-order accuracy. The WB modifications of the numerical dissipation term and the approximate source term lead to additional difficulties in our positivity-preserving analyses, which are more complicated than the analysis for the standard CDG schemes.

The rest of the paper is organized as follows. Section 2 proposes the novel projection of the stationary hydrostatic solutions. Section 3 constructs the high-order positivity-preserving WB CDG method for the one-dimensional Euler equations under gravitational fields. The proposed CDG schemes are extended to the two-dimensional case in Section 4. Section 5 gives several numerical examples to verify the high-order accuracy, robustness, and effectiveness of our schemes. Concluding remarks are finally presented in Section 6.

2 Novel projection of the stationary hydrostatic solutions

This section presents a novel projection of the stationary hydrostatic solutions, which will play a crucial role in designing our positivity-preserving WB CDG method.

2.1 Notations

Let us introduce some standard notations. The spatial domain Ω is uniformly divided into $\{I_j := (x_{j-\frac{1}{2}}, x_{j+\frac{1}{2}})\}$ with constant stepsize $\Delta x = x_{j+\frac{1}{2}} - x_{j-\frac{1}{2}}$. If denoting $x_j = \frac{1}{2}(x_{j-\frac{1}{2}} + x_{j+\frac{1}{2}})$, then $\{I_{j+\frac{1}{2}} := (x_j, x_{j+1})\}$ forms a dual partition. To approximate the exact solution $\mathbf{U}(x, t)$ in the CDG framework, two discrete function spaces are defined associated with the primal mesh $\{I_j\}_j$ and the dual mesh $\{I_{j+\frac{1}{2}}\}_j$, respectively, as

$$\mathbb{V}_h^{C,k} = \left\{ v \in L^2(\Omega) : v|_{I_j} \in \mathbb{P}^k(I_j) \forall j \right\}, \quad \mathbb{V}_h^{D,k} = \left\{ w \in L^2(\Omega) : w|_{I_{j+\frac{1}{2}}} \in \mathbb{P}^k(I_{j+\frac{1}{2}}) \forall j \right\},$$

where $\mathbb{P}^k(I_j)$ and $\mathbb{P}^k(I_{j+\frac{1}{2}})$ denote the space of the polynomials with degree at most k on the cells I_j and $I_{j+\frac{1}{2}}$, respectively.

2.2 Motivation of the novel projection

Assume that the target equilibrium state is known and denoted by $\{\rho^s(x), u^s(x), p^s(x)\}$. This yields

$$u^s(x) = 0, \quad (p^s(x))_x = -\rho^s(x)\phi_x.$$

Let $\mathbf{U}^s(x) = (\rho^s(x), 0, p^s(x)/(\gamma-1))^\top$. The standard CDG method is generally not WB for the stationary hydrostatic solutions of the Euler system (1), and some modifications are required. As the WB

(non-central) DG and finite volume schemes in [57, 26, 25], our WB CDG methods proposed in the Section 3 are also achieved by suitable modifications based on the projection of the target stationary hydrostatic solution. However, the standard L^2 -projection is not a good choice in the present CDG framework, as it may lose the conservative property and affect the positivity-preserving property of the CDG schemes, which will be clarified in Remarks 3.1 and 3.3. In order to maintain the WB, positivity-preserving and conservative properties at the same time, we need to seek a new projection, which ensures that the projected stationary solutions $\mathbf{U}_h^{s,C} \in [\mathbb{V}_h^{C,k}]^3$ and $\mathbf{U}_h^{s,D} \in [\mathbb{V}_h^{D,k}]^3$, have the same cell averages, namely,

$$\int_{I_j} \mathbf{U}_h^{s,C} dx = \int_{I_j} \mathbf{U}_h^{s,D} dx, \quad \int_{I_{j+\frac{1}{2}}} \mathbf{U}_h^{s,D} dx = \int_{I_{j+\frac{1}{2}}} \mathbf{U}_h^{s,C} dx, \quad \forall j. \quad (4)$$

The projected stationary solutions $\mathbf{U}_h^{s,C}$ and $\mathbf{U}_h^{s,D}$ will be used to modify the numerical dissipation term and discretized source term for the WB property, and the desired condition (4) will be important in guaranteeing the provably positivity-preserving and conservative properties; see more details in Section 3.3.1 and Section 3.4.2.

Remark 2.1. Note that, for the shallow-water equations with (non-flat) bottom topography function $b(x)$, a similar projection of $b(x)$ is also required in designing the positivity-preserving WB CDG methods in [29], where the projection of $b(x)$ is defined by solving a constrained minimization problem

$$\begin{aligned} & \min_{b_h^C \in \mathbb{V}_h^{C,k}, b_h^D \in \mathbb{V}_h^{D,k}} \|b_h^C - b\|_{L^2(\Omega)} + \|b_h^D - b\|_{L^2(\Omega)}, \\ & \text{subject to } \int_{I_j} b_h^C dx = \int_{I_j} b_h^D dx, \quad \int_{I_{j+\frac{1}{2}}} b_h^D dx = \int_{I_{j+\frac{1}{2}}} b_h^C dx. \end{aligned} \quad (5)$$

Although there is no rigorous proof, numerical tests in [29] indicate that the above projected approximations b_h^C and b_h^D have the same high-order accuracy as the standard L^2 -projection, provided that $b(x)$ is a smooth function. The notion of (5) can be extended to our case to construct a projection satisfies (4). However, this projection is not easy to implement due to the involved optimization problem, and its accuracy has not yet been theoretically justified.

We find a new projection, which satisfies (4) and is more efficient than (5). Our new projection can be *explicitly calculated* without solving any (constrained) optimization problems, and thus can be easily implemented. Moreover, we can rigorously prove that our new projection also has the same order of accuracy as the standard L^2 -projection.

2.3 Definition of the novel projection

We first define our new projection operator on the primal mesh. Let $\mathcal{P}_h^C : L^2(\Omega) \longrightarrow \mathbb{V}_h^{C,k}$ denote an operator, which maps any function $f(x) \in L^2(\Omega)$ onto the piecewise polynomial space $\mathbb{V}_h^{C,k}$, and satisfies

$$\int_{I_j^-} \mathcal{P}_h^C(f) dx = \int_{I_j^-} f dx, \quad \int_{I_j^+} \mathcal{P}_h^C(f) dx = \int_{I_j^+} f dx, \quad \forall j, \quad (6)$$

with $I_j^- = (x_{j-\frac{1}{2}}, x_j)$, $I_j^+ = (x_j, x_{j+\frac{1}{2}})$. Note that with only the condition (6), the mapping \mathcal{P}_h^C is not uniquely determined. We uniquely define the mapping \mathcal{P}_h^C by

$$\int_{I_j^-} \mathcal{P}_h^C(f) dx = \int_{I_j^-} f dx, \quad \int_{I_j} \mathcal{P}_h^C(f) v dx = \int_{I_j} f v dx, \quad \forall v \in \mathbb{P}^k(I_j) \setminus \text{span}\{\Phi_1\}, \quad (7)$$

where $\mathbb{P}^k(I_j) \setminus \text{span}\{\Phi_1\} := \text{span}\{\Phi_0, \Phi_2, \Phi_3, \dots, \Phi_k\}$, and $\{\Phi_i\}_{i=0}^k$ denotes an orthogonal basis $\mathbb{P}^k(I_j)$ and is taken as the scaled Legendre polynomials

$$\Phi_0(\xi) = 1, \quad \Phi_1(\xi) = \xi, \quad \Phi_2(\xi) = \xi^2 - \frac{1}{3}, \quad \Phi_3(\xi) = \xi^3 - \frac{3}{5}\xi, \quad \dots, \quad (8)$$

with $\xi = 2(x - x_j)/\Delta x$. Take $v = \Phi_0 = 1$ in (7), one has the equality $\int_{I_j} \mathcal{P}_h^C(f) dx = \int_{I_j} f dx$, which implies that the projection \mathcal{P}_h^C satisfies the desired condition (6). We will show in Lemma 2.1 that the mapping \mathcal{P}_h^C defined by (7) is a projection operator from $L^2(\Omega)$ onto the space $\mathbb{V}_h^{C,k}$.

Similarly, we can define the projection $\mathcal{P}_h^D : L^2(\Omega) \rightarrow \mathbb{V}_h^{D,k}$ on the dual mesh by

$$\int_{I_j^+} \mathcal{P}_h^D(f) dx = \int_{I_j^+} f dx, \quad \int_{I_{j+\frac{1}{2}}} \mathcal{P}_h^D(f) v dx = \int_{I_{j+\frac{1}{2}}} f v dx, \quad \forall v \in \mathbb{P}^k(I_{j+\frac{1}{2}}) \setminus \text{span}\{\Phi_1\},$$

where $\Phi_i(\xi)$, $i = 0, 1, \dots, k$, defined in (8) are with $\xi = 2(x - x_{j+\frac{1}{2}})/\Delta x$. It can be shown that \mathcal{P}_h^D satisfies

$$\int_{I_j^+} \mathcal{P}_h^D(f) dx = \int_{I_j^+} f dx, \quad \int_{I_{j+1}^-} \mathcal{P}_h^D(f) dx = \int_{I_{j+1}^-} f dx, \quad \forall j. \quad (9)$$

Combining (6) with (9) gives

$$\int_{I_j} \mathcal{P}_h^C(f) dx = \int_{I_j} \mathcal{P}_h^D(f) dx, \quad \int_{I_{j+\frac{1}{2}}} \mathcal{P}_h^D(f) dx = \int_{I_{j+\frac{1}{2}}} \mathcal{P}_h^C(f) dx, \quad \forall j. \quad (10)$$

If assuming that $\mathbf{U}_h^{s,C}$ and $\mathbf{U}_h^{s,D}$ denote the new projections of each component of the stationary solutions $\mathbf{U}^s(x)$ onto the space $\mathbb{V}_h^{C,k}$ and $\mathbb{V}_h^{D,k}$, respectively, then it follows from (10) that

$$\int_{I_j} \mathbf{U}_h^{s,C} dx = \int_{I_j} \mathbf{U}^s dx = \int_{I_j} \mathbf{U}_h^{s,D} dx, \quad \int_{I_{j+\frac{1}{2}}} \mathbf{U}_h^{s,D} dx = \int_{I_{j+\frac{1}{2}}} \mathbf{U}^s dx = \int_{I_{j+\frac{1}{2}}} \mathbf{U}_h^{s,C} dx, \quad \forall j. \quad (11)$$

which yields (4). The identity (11) plays an important role in the positivity-preserving analyses in Section 3.4.2.

2.4 Properties of the novel projection

For convenience, we will mainly discuss the properties of the operator \mathcal{P}_h^C on the primal mesh in detail, as those of \mathcal{P}_h^D on the dual mesh are very similar.

Note that, on each cell I_j , the projected solution $\mathcal{P}_h^C(f)$ is a piecewise polynomial and can be explicitly written as

$$f_h^C(x) = \sum_{i=0}^k N_i(f) \Phi_i(x), \quad x \in I_j,$$

with the coefficients $\{N_i(f)\}_{i=0}^k$ given by

$$N_i(f) = \frac{\int_{I_j} f \Phi_i dx}{\int_{I_j} \Phi_i^2 dx}, \quad i \neq 1, \quad N_1(f) = \frac{\int_{I_j} (f - \sum_{i \neq 1} N_i(f) \Phi_i) dx}{\int_{I_j} \Phi_1 dx},$$

where $\int_{I_j} \Phi_1 dx = -\frac{\Delta x}{4} \neq 0$. It is easy to show that the operator \mathcal{P}_h^C satisfies the following properties.

Lemma 2.1. *For any function $g(x) \in \mathbb{V}_h^{C,k}$, one has $\mathcal{P}_h^C(g)(x) = g(x)$, and consequently \mathcal{P}_h^C is a projection operator.*

Proof. For each j , on the cell I_j the function $g(x) \in \mathbb{V}_h^{C,k}$ can be expressed as a linear combination of the orthogonal basis $\{\Phi_i\}_{i=0}^k$, i.e.

$$g(x) = \sum_{i=0}^k \alpha_i \Phi_i(x), \quad x \in I_j.$$

Noting that

$$N_i(g) = \alpha_i, \quad 0 \leq i \leq k,$$

we obtain

$$\mathcal{P}_h^C(g)(x) = \sum_{i=0}^k N_i(g) \Phi_i(x) = \sum_{i=0}^k \alpha_i \Phi_i(x) = g(x), \quad x \in I_j.$$

For any functions $f_1, f_2 \in L^2(\Omega)$ and any real numbers α_1, α_2 , one has

$$N_i(\alpha_1 f_1 + \alpha_2 f_2) = \alpha_1 N_i(f_1) + \alpha_2 N_i(f_2), \quad 0 \leq i \leq k,$$

It follows that

$$\mathcal{P}_h^C(\alpha_1 f_1 + \alpha_2 f_2) = \alpha_1 \mathcal{P}_h^C(f_1) + \alpha_2 \mathcal{P}_h^C(f_2),$$

which implies \mathcal{P}_h^C is a linear operator. Furthermore, for any $f \in L^2(\Omega)$, we have $\mathcal{P}_h^C(f) \in \mathbb{V}_h^{C,k}$ and thus $\mathcal{P}_h^C(\mathcal{P}_h^C(f)) = \mathcal{P}_h^C(f)$. This implies \mathcal{P}_h^C is a projection operator. The proof is completed. ■

Lemma 2.2. *The projection operator \mathcal{P}_h^C is bounded.*

Proof. Let us consider an arbitrary function $f \in L^2(I_j)$. Applying the triangular inequality gives

$$\|\mathcal{P}_h^C(f)\|_{L^2(I_j)} \leq \sum_{i=0}^k |N_i(f)| \|\Phi_i\|_{L^2(I_j)}.$$

If $i \neq 1$, one can derive that

$$|N_i(f)| = \frac{|\int_{I_j} f \Phi_i dx|}{\|\Phi_i\|_{L^2(I_j)}^2} \leq \frac{\|f\|_{L^2(I_j)} \|\Phi_i\|_{L^2(I_j)}}{\|\Phi_i\|_{L^2(I_j)}^2} = \frac{\|f\|_{L^2(I_j)}}{\|\Phi_i\|_{L^2(I_j)}},$$

which leads to

$$|N_i(f)| \|\Phi_i\|_{L^2(I_j)} \leq M_i \|f\|_{L^2(I_j)}, \quad \text{with } M_i = 1. \quad (12)$$

If $i = 1$, we have

$$|N_1(f)| \leq \frac{|\int_{I_j^-} f \, dx| + \sum_{i \neq 1} |N_i(f)| \int_{I_j^-} \Phi_i \, dx}{|\int_{I_j^-} \Phi_1 \, dx|} = \frac{|\int_{I_j^-} f \, dx|}{|\int_{I_j^-} \Phi_1 \, dx|} + \sum_{i \neq 1} \frac{|\int_{I_j^-} \Phi_i \, dx|}{|\int_{I_j^-} \Phi_1 \, dx|} |N_i(f)|.$$

Note that $I_j^- \subseteq I_j$ and $\Phi_0 = 1$, one has

$$\left| \int_{I_j^-} f \, dx \right| = \left| \int_{I_j^-} f \Phi_0 \, dx \right| \leq \|f\|_{L^2(I_j)} \|\Phi_0\|_{L^2(I_j^-)}, \quad \left| \int_{I_j^-} \Phi_i \, dx \right| \leq \|\Phi_i\|_{L^2(I_j)} \|\Phi_0\|_{L^2(I_j^-)}.$$

It follows that

$$\begin{aligned} |N_1(f)| &\leq \frac{\|f\|_{L^2(I_j)} \|\Phi_0\|_{L^2(I_j^-)}}{|\int_{I_j^-} \Phi_1 \, dx|} + \sum_{i \neq 1} \frac{\|\Phi_0\|_{L^2(I_j^-)}}{|\int_{I_j^-} \Phi_1 \, dx|} \|\Phi_i\|_{L^2(I_j)} |N_i(f)| \\ &\leq \frac{\|f\|_{L^2(I_j)} \|\Phi_0\|_{L^2(I_j^-)}}{|\int_{I_j^-} \Phi_1 \, dx|} + \sum_{i \neq 1} \frac{\|\Phi_0\|_{L^2(I_j^-)}}{|\int_{I_j^-} \Phi_1 \, dx|} \|f\|_{L^2(I_j)} \\ &= (k+1) \frac{\|\Phi_0\|_{L^2(I_j^-)}}{|\int_{I_j^-} \Phi_1 \, dx|} \|f\|_{L^2(I_j)}, \end{aligned}$$

where (12) has been used in the second inequality. Therefore, we obtain

$$|N_1(f)| \|\Phi_1\|_{L^2(I_j)} \leq M_1 \|f\|_{L^2(I_j)} \quad (13)$$

with

$$M_1 := (k+1) \times \frac{\|\Phi_1\|_{L^2(I_j)} \|\Phi_0\|_{L^2(I_j^-)}}{|\int_{I_j^-} \Phi_1 \, dx|} = \frac{2\sqrt{6}}{3} (k+1).$$

Combining (12) with (13) yields

$$\|\mathcal{P}_h^C(f)\|_{L^2(I_j)} \leq M \|f\|_{L^2(I_j)}, \quad M = \sum_{i=0}^k M_i = k + \frac{2\sqrt{6}}{3} (k+1).$$

This finishes the proof. ■

Theorem 2.1. For any function $f \in W_2^{k+1}(I_j)$, one has

$$\|f - \mathcal{P}_h^C(f)\|_{L^2(I_j)} \leq C_{k+1} (\Delta x)^{k+1} |f|_{W_2^{k+1}(I_j)}.$$

where $W_2^{k+1}(I_j)$ is the standard Sobolev space, $|\cdot|_{W_2^{k+1}(I_j)}$ is the Sobolev seminorm of order $k+1$, and C_{k+1} is a constant only depending on k .

Proof. For any $g \in \mathbb{P}^k(I_j)$, applying Lemmas 2.1 and 2.2 and then using the triangular inequality give

$$\begin{aligned}
\|f - \mathcal{P}_h^C(f)\|_{L^2(I_j)} &\leq \|f - g\|_{L^2(I_j)} + \|g - \mathcal{P}_h^C(f)\|_{L^2(I_j)} \\
&= \|f - g\|_{L^2(I_j)} + \|\mathcal{P}_h^C(f - g)\|_{L^2(I_j)} \quad (\text{Lemma 2.1}) \\
&\leq \|f - g\|_{L^2(I_j)} + M\|f - g\|_{L^2(I_j)} \quad (\text{Lemma 2.2}) \\
&= (1 + M)\|f - g\|_{L^2(I_j)}. \tag{14}
\end{aligned}$$

Consequently,

$$\begin{aligned}
\|f - \mathcal{P}_h^C(f)\|_{L^2(I_j)} &\leq (1 + M) \inf_{g \in \mathbb{P}^k(I_j)} \|f - g\|_{L^2(I_j)} \\
&\leq (1 + M)\tilde{C}_{k+1}(\Delta x)^{k+1}|f|_{W_2^{k+1}(I_j)} \quad (\text{Bramble – Hilbert}) \\
&= C_{k+1}(\Delta x)^{k+1}|f|_{W_2^{k+1}(I_j)}.
\end{aligned}$$

where we have used the Bramble-Hilbert Lemma [9], and \tilde{C}_{k+1} is a constant only depending on k . \blacksquare

Remark 2.2. Similarly, the operator \mathcal{P}_h^D on the dual mesh is also linear, bounded, and a projection. Furthermore, for any function $f \in W_2^{k+1}(I_{j-\frac{1}{2}})$

$$\|f - \mathcal{P}_h^D(f)\|_{L^2(I_{j-\frac{1}{2}})} \leq C_{k+1}(\Delta x)^{k+1}|f|_{W_2^{k+1}(I_{j-\frac{1}{2}})},$$

where C_{k+1} is a constant only depending on k .

Remark 2.3. By similar arguments, one can prove that the errors $\|f - \mathcal{P}_h^C(f)\|_{L^q(\Omega)}$ and $\|f - \mathcal{P}_h^D(f)\|_{L^q(\Omega)}$ are of order $\mathcal{O}((\Delta x)^{k+1})$ for a general q ($1 \leq q \leq +\infty$) and $f \in W_q^{k+1}(\Omega)$. The details are omitted here.

3 Positivity-preserving WB CDG schemes in one dimension

To solve the system (1), the CDG schemes evolve two copies of numerical solutions, denoted by $\mathbf{U}_h^C(x, t)$ and $\mathbf{U}_h^D(x, t)$, on the primal and dual meshes, respectively.

3.1 Review of the standard CDG method

The semi-discrete formulations of the standard CDG method are given as follows: for any test function $v \in \mathbb{V}_h^{C,k}$ and $w \in \mathbb{V}_h^{D,k}$, look for the numerical solutions $\mathbf{U}_h^C \in [\mathbb{V}_h^{C,k}]^3$ and $\mathbf{U}_h^D \in [\mathbb{V}_h^{D,k}]^3$ satisfying

$$\begin{aligned}
\int_{I_j} \frac{\partial \mathbf{U}_h^C}{\partial t} v dx &= \frac{1}{\tau_{\max}} \int_{I_j} (\mathbf{U}_h^D - \mathbf{U}_h^C) v dx + \int_{I_j} \mathbf{F}(\mathbf{U}_h^D) v_x dx \\
&\quad - \left(\mathbf{F}(\mathbf{U}_h^D(x_{j+\frac{1}{2}})) v(x_{j+\frac{1}{2}}^-) - \mathbf{F}(\mathbf{U}_h^D(x_{j-\frac{1}{2}})) v(x_{j-\frac{1}{2}}^+) \right) + \int_{I_j} \mathbf{S}(\mathbf{U}_h^D, (\phi_h^D)_x) v dx, \tag{15}
\end{aligned}$$

$$\begin{aligned}
\int_{I_{j+\frac{1}{2}}} \frac{\partial \mathbf{U}_h^D}{\partial t} w dx &= \frac{1}{\tau_{max}} \int_{I_{j+\frac{1}{2}}} (\mathbf{U}_h^C - \mathbf{U}_h^D) w dx + \int_{I_{j+\frac{1}{2}}} \mathbf{F}(\mathbf{U}_h^C) w_x dx \\
&\quad - \left(\mathbf{F}(\mathbf{U}_h^C(x_{j+1})) w(x_{j+1}^-) - \mathbf{F}(\mathbf{U}_h^C(x_j)) w(x_j^+) \right) + \int_{I_{j+\frac{1}{2}}} \mathbf{S}(\mathbf{U}_h^C, (\phi_h^C)_x) w dx. \tag{16}
\end{aligned}$$

Here $\tau_{max} = \tau_{max}(t)$ is the maximal time step allowed by the CFL condition at time t , and $f(x^\pm) = \lim_{\varepsilon \rightarrow 0+} f(x \pm \varepsilon)$ denotes the limits at point x taken from the left and right sides, respectively. In general, the standard CDG method is neither positivity-preserving nor WB and does not maintain the stationary hydrostatic solution (3).

3.2 Outline of the positivity-preserving WB CDG schemes

To define the positivity-preserving CDG schemes, we introduce the following two sets

$$\begin{aligned}
\overline{\mathbb{G}}_h^{C,k} &:= \left\{ \mathbf{v} \in [\mathbb{V}_h^{C,k}]^3 : \frac{1}{\Delta x} \int_{I_j} \mathbf{v}(x) dx \in G, \forall j \right\}, \\
\mathbb{G}_h^{C,k} &:= \left\{ \mathbf{v} \in \overline{\mathbb{G}}_h^{C,k} : \mathbf{v}|_{I_j}(x) \in G, \forall x \in \mathbb{S}_j, \forall j \right\},
\end{aligned}$$

where \mathbb{S}_j denotes the set of some critical points in I_j which will be specified in (25). Similarly, we can define the sets $\overline{\mathbb{G}}_h^{D,k}$ and $\mathbb{G}_h^{D,k}$ on the dual mesh as

$$\begin{aligned}
\overline{\mathbb{G}}_h^{D,k} &:= \left\{ \mathbf{w} \in [\mathbb{V}_h^{D,k}]^3 : \frac{1}{\Delta x} \int_{I_{j+\frac{1}{2}}} \mathbf{w}(x) dx \in G, \forall j \right\}, \\
\mathbb{G}_h^{D,k} &:= \left\{ \mathbf{w} \in \overline{\mathbb{G}}_h^{D,k} : \mathbf{w}|_{I_{j+\frac{1}{2}}}(x) \in G, \forall x \in \mathbb{S}_{j+\frac{1}{2}}, \forall j \right\},
\end{aligned}$$

where $\mathbb{S}_{j+\frac{1}{2}}$ denotes the set of some critical points in $I_{j+\frac{1}{2}}$ which will be specified in (26).

We will describe in Section 3.3 a suitable CDG spatial discretization of the Euler system (1), and the resulting semi-discrete CDG schemes can be written in the ODE form as follows

$$\frac{d\mathbf{U}_h^C}{dt} = \mathbf{L}_h^C(\mathbf{U}_h^C, \mathbf{U}_h^D), \quad \frac{d\mathbf{U}_h^D}{dt} = \mathbf{L}_h^D(\mathbf{U}_h^D, \mathbf{U}_h^C), \tag{17}$$

where \mathbf{L}_h^C and \mathbf{L}_h^D are respectively spatial discretization operators on the primal and dual meshes obtained from suitable modifications to the standard CDG discretization.

Definition 3.1. *Suppose the initial data satisfy $\mathbf{U}_h^C(x, 0) = \mathbf{U}_h^{s,C}$, $\mathbf{U}_h^D(x, 0) = \mathbf{U}_h^{s,D}$, a CDG scheme is defined to be WB if the flux and source term approximations balance each other, namely $\mathbf{L}_h^C(\mathbf{U}_h^{s,C}, \mathbf{U}_h^{s,D}) = \mathbf{0}$, $\mathbf{L}_h^D(\mathbf{U}_h^{s,D}, \mathbf{U}_h^{s,C}) = \mathbf{0}$.*

Definition 3.2. *A CDG scheme is defined to be positivity-preserving if its numerical solutions \mathbf{U}_h^C , \mathbf{U}_h^D stay in sets $\mathbb{G}_h^{C,k}$ and $\mathbb{G}_h^{D,k}$, respectively. For clarity, if a CDG scheme preserves the numerical solutions in set $\overline{\mathbb{G}}_h^{C,k}$ and $\overline{\mathbb{G}}_h^{D,k}$, then we say that it satisfies a weak positivity-preserving property.*

We aim at designing the high-order accurate CDG schemes that satisfy the WB and positivity-preserving properties simultaneously. This goal will be achieved by following three steps:

- First, we seek spatial discretization operators $\mathbf{L}_h^C(\mathbf{U}_h^C, \mathbf{U}_h^D)$ and $\mathbf{L}_h^D(\mathbf{U}_h^D, \mathbf{U}_h^C)$ satisfying both the WB property:

$$\mathbf{L}_h^C(\mathbf{U}_h^{s,C}, \mathbf{U}_h^{s,D}) = 0, \quad \mathbf{L}_h^D(\mathbf{U}_h^{s,D}, \mathbf{U}_h^{s,C}) = 0, \quad (18)$$

and the weak positivity-preserving property: if $\mathbf{U}_h^C \in \mathbb{G}_h^{C,k}$, $\mathbf{U}_h^D \in \mathbb{G}_h^{D,k}$, then

$$\mathbf{U}_h^C + \Delta t \mathbf{L}_h^C(\mathbf{U}_h^C, \mathbf{U}_h^D) \in \overline{\mathbb{G}}_h^{C,k}, \quad \mathbf{U}_h^D + \Delta t \mathbf{L}_h^D(\mathbf{U}_h^D, \mathbf{U}_h^C) \in \overline{\mathbb{G}}_h^{D,k}, \quad (19)$$

under some CFL-type condition on time stepsize Δt .

- Second, we further discretize the ODE system (17) in time using a strong-stability-preserving (SSP) explicit Runge-Kutta method [13].
- Finally, a local scaling positivity-preserving limiting procedure, which will be introduced in Section 3.5, is applied to the intermediate solutions of the Runge-Kutta discretization. This procedure corresponds to two operators $\Pi_h^C : \overline{\mathbb{G}}_h^{C,k} \rightarrow \mathbb{G}_h^{C,k}$ and $\Pi_h^D : \overline{\mathbb{G}}_h^{D,k} \rightarrow \mathbb{G}_h^{D,k}$, which satisfy the conservative property

$$\begin{aligned} \frac{1}{\Delta x} \int_{I_j} \Pi_h^C(\mathbf{v}) dx &= \frac{1}{\Delta x} \int_{I_j} \mathbf{v} dx \quad \forall j, \forall \mathbf{v} \in \overline{\mathbb{G}}_h^{C,k}, \\ \frac{1}{\Delta x} \int_{I_{j+\frac{1}{2}}} \Pi_h^D(\mathbf{w}) dx &= \frac{1}{\Delta x} \int_{I_{j+\frac{1}{2}}} \mathbf{w} dx \quad \forall j, \forall \mathbf{w} \in \overline{\mathbb{G}}_h^{D,k}. \end{aligned}$$

For the first order CDG scheme ($k = 0$), both Π_h^C and Π_h^D become the identity operators, so that the positivity-preserving limiting procedure is only operated for the high-order CDG schemes with $k \geq 1$.

Let $\mathbf{U}_h^{C,n}$ and $\mathbf{U}_h^{D,n}$ denote the numerical solution at time $t = t_n$. The resulting fully discrete positivity-preserving WB CDG method, with the third-order accurate SSP Runge-Kutta time discretization as example, is then given as follows.

- Set $\mathbf{U}_h^{C,0} = \Pi_h^C[\mathbf{U}_h^C(x, 0)]$ and $\mathbf{U}_h^{D,0} = \Pi_h^D[\mathbf{U}_h^D(x, 0)]$, where $\mathbf{U}_h^C(x, 0)$ and $\mathbf{U}_h^D(x, 0)$ denote the novel projections of the initial data $\mathbf{U}(x, 0)$ onto the space $[\mathbb{V}_h^{C,k}]^3$ and $[\mathbb{V}_h^{D,k}]^3$, respectively.
- For $n = 0, \dots, N_t - 1$, compute $\mathbf{U}_h^{C,n+1}$ and $\mathbf{U}_h^{D,n+1}$ as follows:

(i) Compute the intermediate solutions $\mathbf{U}_h^{C,(1)}$ and $\mathbf{U}_h^{D,(1)}$ via

$$\begin{aligned} \mathbf{U}_h^{C,(1)} &= \Pi_h^C[\mathbf{U}_h^{C,n} + \Delta t_n \mathbf{L}_h^C(\mathbf{U}_h^{C,n}, \mathbf{U}_h^{D,n})], \\ \mathbf{U}_h^{D,(1)} &= \Pi_h^D[\mathbf{U}_h^{D,n} + \Delta t_n \mathbf{L}_h^D(\mathbf{U}_h^{D,n}, \mathbf{U}_h^{C,n})]. \end{aligned}$$

(ii) Compute the intermediate solutions $\mathbf{U}_h^{C,(2)}$ and $\mathbf{U}_h^{D,(2)}$ via

$$\begin{aligned} \mathbf{U}_h^{C,(2)} &= \Pi_h^C \left[\frac{3}{4} \mathbf{U}_h^{C,n} + \frac{1}{4} \left(\mathbf{U}_h^{C,(1)} + \Delta t_n \mathbf{L}_h^C(\mathbf{U}_h^{C,(1)}, \mathbf{U}_h^{D,(1)}) \right) \right], \\ \mathbf{U}_h^{D,(2)} &= \Pi_h^D \left[\frac{3}{4} \mathbf{U}_h^{D,n} + \frac{1}{4} \left(\mathbf{U}_h^{D,(1)} + \Delta t_n \mathbf{L}_h^D(\mathbf{U}_h^{D,(1)}, \mathbf{U}_h^{C,(1)}) \right) \right]. \end{aligned}$$

(iii) Compute $\mathbf{U}_h^{C,n+1}$ and $\mathbf{U}_h^{D,n+1}$ via

$$\begin{aligned}\mathbf{U}_h^{C,n+1} &= \Pi_h^C \left[\frac{1}{3} \mathbf{U}_h^{C,n} + \frac{2}{3} \left(\mathbf{U}_h^{C,(2)} + \Delta t_n \mathbf{L}_h^C(\mathbf{U}_h^{C,(2)}, \mathbf{U}_h^{D,(2)}) \right) \right], \\ \mathbf{U}_h^{D,n+1} &= \Pi_h^D \left[\frac{1}{3} \mathbf{U}_h^{D,n} + \frac{2}{3} \left(\mathbf{U}_h^{D,(2)} + \Delta t_n \mathbf{L}_h^D(\mathbf{U}_h^{D,(2)}, \mathbf{U}_h^{C,(2)}) \right) \right],\end{aligned}$$

where the SSP Runge-Kutta method has been written into a convex combination of the forward Euler method. In the following subsections, we will describe in detail the operators \mathbf{L}_h^C , \mathbf{L}_h^D and Π_h^C , Π_h^D , and we shall state the WB property (18) of our modified CDG discretization in Theorem 3.1 and the weak positivity-preserving property (19) in Theorem 3.2.

3.3 Spatial discretization operators \mathbf{L}_h^C and \mathbf{L}_h^D

For convenience, we will mainly present the CDG spatial discretization on the primal mesh in detail, as that on the dual mesh is very similar.

3.3.1 WB dissipation term

As well-known, the numerical dissipation term

$$d_j^C(\mathbf{U}_h^C, \mathbf{U}_h^D, v) = \frac{1}{\tau_{\max}} \int_{I_j} (\mathbf{U}_h^D - \mathbf{U}_h^C) v dx, \quad v \in \mathbb{V}_h^{C,k},$$

in the standard CDG method (15) is essential for the numerical stability [33]. However, it would destroy the WB property at the steady state. To address this issue, we propose to modify it into

$$\tilde{d}_j^C(\mathbf{U}_h^C, \mathbf{U}_h^D, v) = \frac{1}{\tau_{\max}} \int_{I_j} (\mathbf{U}_h^D - \mathbf{U}_h^C) v dx + \frac{1}{\tau_{\max}} \int_{I_j} (\mathbf{U}_h^{s,C} - \mathbf{U}_h^{s,D}) v dx, \quad (20)$$

so that

$$\tilde{d}_j^C(\mathbf{U}_h^{s,C}, \mathbf{U}_h^{s,D}, v) = \frac{1}{\tau_{\max}} \int_{I_j} (\mathbf{U}_h^{s,D} - \mathbf{U}_h^{s,C}) v dx + \frac{1}{\tau_{\max}} \int_{I_j} (\mathbf{U}_h^{s,C} - \mathbf{U}_h^{s,D}) v dx = 0.$$

Remark 3.1. Thanks to the key property (11) of our novel projection, it holds

$$\tilde{d}_j^C(\mathbf{U}_h^C, \mathbf{U}_h^D, 1) = d_j^C(\mathbf{U}_h^C, \mathbf{U}_h^D, 1),$$

which implies that the modified numerical dissipation term (20) would not destroy the conservative property of our schemes. It is worth noting that using the standard L^2 -projection for $\mathbf{U}_h^{s,C}$ and $\mathbf{U}_h^{s,D}$ does not lead to this desirable feature.

In addition to the above-mentioned advantages of the modified numerical dissipation term (20), we can also prove that our modification of dissipation term will not affect the high-order accuracy of the CDG schemes as indicated by the following proposition.

Proposition 3.1. Assume $\mathbf{U}^s \in W_2^{k+1}(\Omega)$, $\tau_{\max} = \mathcal{O}(\Delta x)$, then on each cell I_j , it holds that

$$\left| \tilde{d}_j^C(\mathbf{U}_h^C, \mathbf{U}_h^D, v) - d_j^C(\mathbf{U}_h^C, \mathbf{U}_h^D, v) \right| = \frac{1}{\tau_{\max}} \left| \int_{I_j} (\mathbf{U}_h^{s,C} - \mathbf{U}_h^{s,D}) v dx \right| \leq \mathcal{O}((\Delta x)^{k+1}).$$

Proof. Using the triangular inequality gives

$$\frac{1}{\tau_{\max}} \left| \int_{I_j} (\mathbf{U}_h^{s,C} - \mathbf{U}_h^{s,D}) v dx \right| \leq \frac{1}{\tau_{\max}} \int_{I_j} |(\mathbf{U}_h^{s,C} - \mathbf{U}^s) v| dx + \frac{1}{\tau_{\max}} \int_{I_j} |(\mathbf{U}^s - \mathbf{U}_h^{s,D}) v| dx.$$

Under the condition $\|\mathbf{U}^s\|_{W_2^{k+1}(I_j)} \|v\|_{L^2(I_j)} = \mathcal{O}(\Delta x)$, Theorem 2.1 implies

$$\begin{aligned} \frac{1}{\tau_{\max}} \int_{I_j} |(\mathbf{U}_h^{s,C} - \mathbf{U}^s) v| dx &\leq \frac{1}{\tau_{\max}} \|\mathbf{U}_h^{s,C} - \mathbf{U}^s\|_{L^2(I_j)} \|v\|_{L^2(I_j)} \\ &\leq C_{k+1} (\Delta x)^{k+1} \frac{\|\mathbf{U}^s\|_{W_2^{k+1}(I_j)} \|v\|_{L^2(I_j)}}{\tau_{\max}} = \mathcal{O}((\Delta x)^{k+1}). \end{aligned}$$

Similarly, one has

$$\begin{aligned} \frac{1}{\tau_{\max}} \int_{I_j} |(\mathbf{U}^s - \mathbf{U}_h^{s,D}) v| dx &= \frac{1}{\tau_{\max}} \left(\int_{I_j^-} |(\mathbf{U}^s - \mathbf{U}_h^{s,D}) v| dx + \int_{I_j^+} |(\mathbf{U}^s - \mathbf{U}_h^{s,D}) v| dx \right) \\ &\leq \frac{1}{\tau_{\max}} \left(\|\mathbf{U}^s - \mathbf{U}_h^{s,D}\|_{L^2(I_{j-\frac{1}{2}})} \|v\|_{L^2(I_j^-)} + \|\mathbf{U}^s - \mathbf{U}_h^{s,D}\|_{L^2(I_{j+\frac{1}{2}})} \|v\|_{L^2(I_j^+)} \right) = \mathcal{O}((\Delta x)^{k+1}). \end{aligned}$$

Combining these results, we conclude that $\frac{1}{\tau_{\max}} \left| \int_{I_j} (\mathbf{U}_h^{s,C} - \mathbf{U}_h^{s,D}) v dx \right| \leq \mathcal{O}((\Delta x)^{k+1})$. \blacksquare

3.3.2 Numerical flux and source term

Let $\mathbb{Q}_j^{1,x} = \{x_j^{1,\alpha}\}_{\alpha=1}^N$ and $\mathbb{Q}_j^{2,x} = \{x_j^{2,\alpha}\}_{\alpha=1}^N$ denote the N -point Gauss quadrature nodes transformed into the interval $[x_{j-\frac{1}{2}}, x_j]$ and $[x_j, x_{j+\frac{1}{2}}]$, respectively, and $\{\omega_\alpha\}_{\alpha=1}^N$ are the associated weights satisfying $\sum_{\alpha=1}^N \omega_\alpha = 1$, with $N \geq k+1$ for the CDG accuracy requirement.

Because $\mathbf{U}_h^D(x, t)$ can be discontinuous at $x = x_j$, the element integral $\int_{I_j} \mathbf{F}(\mathbf{U}_h^D) v_x dx$ in (15) is usually divided into two parts

$$\int_{I_j} \mathbf{F}(\mathbf{U}_h^D) v_x dx = \int_{I_j^-} \mathbf{F}(\mathbf{U}_h^D) v_x dx + \int_{I_j^+} \mathbf{F}(\mathbf{U}_h^D) v_x dx,$$

which is then approximated by the numerical quadrature rule

$$\int_{I_j} \mathbf{F}(\mathbf{U}_h^D) v_x dx \approx \frac{\Delta x}{2} \sum_{\kappa=1}^2 \sum_{\alpha=1}^N \omega_\alpha \mathbf{F}(\mathbf{U}_h^D(x_j^{\kappa,\alpha})) v_x(x_j^{\kappa,\alpha}).$$

Next, we introduce a non-standard approximation to the source term integral in (15) to achieve the WB property. This idea is similar to [26] but has some key differences owing to carefully accommodate the positivity-preserving property; see Remark 3.2. Reformulate and decompose the integral of the source term in the momentum equation as

$$\int_{I_j} S_2(\mathbf{U}, \phi_x) v dx = - \int_{I_j} \rho \phi_x v dx = \int_{I_j} \frac{\rho}{\rho^s} p_x^s v dx = \int_{I_j} \left(\frac{\rho}{\rho^s} - \frac{\bar{\rho}_j}{\bar{\rho}_j^s} + \frac{\bar{\rho}_j}{\bar{\rho}_j^s} \right) p_x^s v dx,$$

where $\bar{\rho}_j = \frac{1}{\Delta x} \int_{I_j} \rho dx$ denotes the cell average. Our numerical approximation to the source term takes the form of

$$\int_{I_j} S_2(\mathbf{U}_h^D, (\phi_h^D)_x) v dx \approx \int_{I_j} \left(\frac{\rho_h^D}{\rho_h^{s,D}} - \frac{(\overline{\rho_h^D})_j}{(\overline{\rho_h^{s,D}})_j} \right) (p_h^{s,D})_x v dx + \frac{(\overline{\rho_h^D})_j}{(\overline{\rho_h^{s,D}})_j} \int_{I_j} (p_h^{s,D})_x v dx.$$

Applying integration by parts gives

$$\begin{aligned} \int_{I_j} (p_h^{s,D})_x v dx &= - \int_{I_j} p_h^{s,D} v_x dx - \left(p_h^{s,D}(x_j^+) - p_h^{s,D}(x_j^-) \right) v(x_j) \\ &\quad + \left(p_h^{s,D}(x_{j+\frac{1}{2}}) v(x_{j+\frac{1}{2}}^-) - p_h^{s,D}(x_{j-\frac{1}{2}}) v(x_{j-\frac{1}{2}}^+) \right) \\ &\approx - \int_{I_j} p_h^{s,D} v_x dx + \left(p_h^{s,D}(x_{j+\frac{1}{2}}) v(x_{j+\frac{1}{2}}^-) - p_h^{s,D}(x_{j-\frac{1}{2}}) v(x_{j-\frac{1}{2}}^+) \right), \end{aligned}$$

where the following term has been omitted

$$p_h^{s,D}(x_j^+) - p_h^{s,D}(x_j^-) = (p_h^{s,D}(x_j^+) - p^s(x_j)) + (p^s(x_j) - p_h^{s,D}(x_j^-)) = \mathcal{O}(\Delta x^{k+1}).$$

This leads to

$$\begin{aligned} \int_{I_j} S_2(\mathbf{U}_h^D, (\phi_h^D)_x) v dx &\approx \int_{I_j} \left(\frac{\rho_h^D}{\rho_h^{s,D}} - \frac{(\overline{\rho_h^D})_j}{(\rho_h^{s,D})_j} \right) (p_h^{s,D})_x v dx - \frac{(\overline{\rho_h^D})_j}{(\rho_h^{s,D})_j} \int_{I_j} p_h^{s,D} v_x dx \\ &\quad + \frac{(\overline{\rho_h^D})_j}{(\rho_h^{s,D})_j} \left(p_h^{s,D}(x_{j+\frac{1}{2}}) v(x_{j+\frac{1}{2}}^-) - p_h^{s,D}(x_{j-\frac{1}{2}}) v(x_{j-\frac{1}{2}}^+) \right). \end{aligned}$$

Therefore, the source term $\int_{I_j} S_2(\mathbf{U}_h^D, (\phi_h^D)_x) v dx$ in the momentum equation can further be approximated by

$$\begin{aligned} \langle S_{h,2}^D, v \rangle_j &= \frac{(\overline{\rho_h^D})_j}{(\rho_h^{s,D})_j} \left(p_h^{s,D}(x_{j+\frac{1}{2}}) v(x_{j+\frac{1}{2}}^-) - p_h^{s,D}(x_{j-\frac{1}{2}}) v(x_{j-\frac{1}{2}}^+) \right) \\ &+ \frac{\Delta x}{2} \sum_{\kappa=1}^2 \sum_{\alpha=1}^N \omega_\alpha \left[\left(\frac{\rho_h^D(x_j^{\kappa,\alpha})}{\rho_h^{s,D}(x_j^{\kappa,\alpha})} - \frac{(\overline{\rho_h^D})_j}{(\rho_h^{s,D})_j} \right) (p_h^{s,D})_x(x_j^{\kappa,\alpha}) v(x_j^{\kappa,\alpha}) - \frac{(\overline{\rho_h^D})_j}{(\rho_h^{s,D})_j} p_h^{s,D}(x_j^{\kappa,\alpha}) v_x(x_j^{\kappa,\alpha}) \right]. \end{aligned} \quad (21)$$

Similarly, we approximate the source term $\int_{I_j} S_3(\mathbf{U}_h^D, (\phi_h^D)_x) v dx$ in the energy equation by

$$\begin{aligned} \langle S_{h,3}^D, v \rangle_j &= \frac{(\overline{m_h^D})_j}{(\rho_h^{s,D})_j} \left(p_h^{s,D}(x_{j+\frac{1}{2}}) v(x_{j+\frac{1}{2}}^-) - p_h^{s,D}(x_{j-\frac{1}{2}}) v(x_{j-\frac{1}{2}}^+) \right) \\ &+ \frac{\Delta x}{2} \sum_{\kappa=1}^2 \sum_{\alpha=1}^N \omega_\alpha \left[\left(\frac{m_h^D(x_j^{\kappa,\alpha})}{\rho_h^{s,D}(x_j^{\kappa,\alpha})} - \frac{(\overline{m_h^D})_j}{(\rho_h^{s,D})_j} \right) (p_h^{s,D})_x(x_j^{\kappa,\alpha}) v(x_j^{\kappa,\alpha}) - \frac{(\overline{m_h^D})_j}{(\rho_h^{s,D})_j} p_h^{s,D}(x_j^{\kappa,\alpha}) v_x(x_j^{\kappa,\alpha}) \right]. \end{aligned}$$

3.3.3 Semi-discrete WB CDG schemes

Combining the modified dissipation term in Section 3.3.1 with the discrete source term in Section 3.3.2, we obtain the final semi-discrete WB CDG method on the primal mesh

$$\begin{aligned} \int_{I_j} \frac{\partial \mathbf{U}_h^C}{\partial t} v dx &= \frac{1}{\tau_{max}} \int_{I_j} (\mathbf{U}_h^D - \mathbf{U}_h^C) v dx + \frac{1}{\tau_{max}} \int_{I_j} (\mathbf{U}_h^{s,C} - \mathbf{U}_h^{s,D}) v dx \\ &\quad - \left(\mathbf{F}(\mathbf{U}_h^D(x_{j+\frac{1}{2}})) v(x_{j+\frac{1}{2}}^-) - \mathbf{F}(\mathbf{U}_h^D(x_{j-\frac{1}{2}})) v(x_{j-\frac{1}{2}}^+) \right) \\ &\quad + \frac{\Delta x}{2} \sum_{\kappa=1}^2 \sum_{\alpha=1}^N \omega_\alpha \mathbf{F}(\mathbf{U}_h^D(x_j^{\kappa,\alpha})) v_x(x_j^{\kappa,\alpha}) + \langle \mathbf{S}_h^D, v \rangle_j \quad \forall v \in \mathbb{V}_h^{C,k}, \end{aligned} \quad (22)$$

where $\langle \mathbf{S}_h^D, v \rangle_j = (0, \langle \mathbf{S}_{h,2}^D, v \rangle_j, \langle \mathbf{S}_{h,3}^D, v \rangle_j)^\top$.

The WB CDG spatial discretization on the dual mesh is very similar. Denote $\mathbf{Q} = (0, \rho, m)^\top$, one has $\mathbf{S}(\mathbf{U}, \phi_x) = -\phi_x \mathbf{Q}$, and the modified source term approximation $\langle \mathbf{S}_h^C, w \rangle_{j+\frac{1}{2}}$ is given by

$$\begin{aligned} \langle \mathbf{S}_h^C, w \rangle_{j+\frac{1}{2}} &= \frac{(\overline{\mathbf{Q}_h^C})_{j+\frac{1}{2}}}{(\rho_h^{s,C})_{j+\frac{1}{2}}} \left(p_h^{s,C}(x_{j+1}) w(x_{j+1}^-) - p_h^{s,C}(x_j) w(x_j^+) \right) \\ &+ \frac{\Delta x}{2} \sum_{\kappa=1}^2 \sum_{\alpha=1}^N \omega_\alpha \left[\left(\frac{\mathbf{Q}_h^C(x_{j+\frac{1}{2}}^{\kappa,\alpha})}{(\rho_h^{s,C}(x_{j+\frac{1}{2}}^{\kappa,\alpha}))} - \frac{(\overline{\mathbf{Q}_h^C})_{j+\frac{1}{2}}}{(\rho_h^{s,C})_{j+\frac{1}{2}}} \right) ((p_h^{s,C})_x w)(x_{j+\frac{1}{2}}^{\kappa,\alpha}) - \frac{(\overline{\mathbf{Q}_h^C})_{j+\frac{1}{2}}}{(\rho_h^{s,C})_{j+\frac{1}{2}}} (p_h^{s,C} w_x)(x_{j+\frac{1}{2}}^{\kappa,\alpha}) \right], \end{aligned}$$

where $w \in \mathbb{V}_h^{D,k}$, $\{x_{j+\frac{1}{2}}^{1,\alpha}\}_{\alpha=1}^N = \mathbb{Q}_j^{2,x}$ and $\{x_{j+\frac{1}{2}}^{2,\alpha}\}_{\alpha=1}^N = \mathbb{Q}_{j+1}^{1,x}$ denote the Gauss quadrature nodes transformed into the interval $[x_j, x_{j+\frac{1}{2}}]$ and $[x_{j+\frac{1}{2}}, x_{j+1}]$, respectively. Then the WB CDG method on the dual mesh reads

$$\begin{aligned} \int_{I_{j+\frac{1}{2}}} \frac{\partial \mathbf{U}_h^D}{\partial t} w dx &= \frac{1}{\tau_{max}} \int_{I_{j+\frac{1}{2}}} (\mathbf{U}_h^C - \mathbf{U}_h^D) w dx + \frac{1}{\tau_{max}} \int_{I_{j+\frac{1}{2}}} (\mathbf{U}_h^{s,D} - \mathbf{U}_h^{s,C}) w dx \\ &\quad - \left(\mathbf{F}(\mathbf{U}_h^C(x_{j+1})) w(x_{j+1}^-) - \mathbf{F}(\mathbf{U}_h^C(x_j)) w(x_j^+) \right) \\ &\quad + \frac{\Delta x}{2} \sum_{\kappa=1}^2 \sum_{\alpha=1}^N \omega_\alpha \mathbf{F}(\mathbf{U}_h^C(x_{j+\frac{1}{2}}^{\kappa,\alpha})) w_x(x_{j+\frac{1}{2}}^{\kappa,\alpha}) + \langle \mathbf{S}_h^C, w \rangle_{j+\frac{1}{2}} \quad \forall w \in \mathbb{V}_h^{D,k}. \end{aligned} \quad (23)$$

As the standard CDG schemes (15) and (16), the semi-discrete WB CDG schemes (22) and (23) can be rewritten in the ODE form as

$$\frac{d\mathbf{U}_h^C}{dt} = \mathbf{L}_h^C(\mathbf{U}_h^C, \mathbf{U}_h^D), \quad \frac{d\mathbf{U}_h^D}{dt} = \mathbf{L}_h^D(\mathbf{U}_h^D, \mathbf{U}_h^C),$$

after choosing suitable bases of $\mathbb{V}_h^{C,k}, \mathbb{V}_h^{D,k}$ and representing $\mathbf{U}_h^C, \mathbf{U}_h^D$ as linear combinations of the basis functions.

Remark 3.2. *It is worth noting that the above WB discretization has carefully accommodated the positivity-preserving property. For example, if we are only concerned with the WB property (see, for*

example, [26]), the choice of $\frac{\overline{(\rho_h^D)_j}}{(\rho_h^{s,D})_j}$ in (21) is not unique and can be replaced with any other suitable term that can reduce to one at the steady state (3), e.g. $\frac{\rho_h^D(x_\beta)}{\rho_h^{s,D}(x_\beta)}$ with an arbitrary $x_\beta \in I_j$. However, our analyses show that choosing $\frac{\overline{(\rho_h^D)_j}}{(\rho_h^{s,D})_j}$ in the source term approximation of the momentum equation is advantageous for achieving the positivity-preserving property under a milder and more concise CFL condition. Similar consideration is also applied to the integral of the source term in the energy equation. For example, one can simply approximate

$$- \int_{I_j} (\rho u)_h^D (\phi_h^D)_x v dx$$

by using any standard quadrature rule and does not affect the WB property. However, our analyses indicate that it is crucial to employ a “unified” discretization for the source terms in the momentum and energy equations to simultaneously accommodate the positivity-preserving property.

3.4 Proofs of WB and positivity-preserving properties

3.4.1 WB property

Theorem 3.1. *For the one-dimensional Euler equations (1) under the gravitational field, the modified semi-discrete CDG schemes, given by (22) and (23), are WB for a general stationary hydrostatic solution (3).*

Proof. Suppose that the initial solution is \mathbf{U}^s . By the construction of $\mathbf{U}_h^{s,C}, \mathbf{U}_h^{s,D}$, one has

$$\mathbf{U}_h^C(x, 0) = \mathbf{U}_h^{s,C}, \quad \mathbf{U}_h^D(x, 0) = \mathbf{U}_h^{s,D},$$

and

$$\rho_h^D(x, 0) = \rho_h^{s,D}, \quad u_h^D(x, 0) = 0, \quad p_h^D(x, 0) = p_h^{s,D}.$$

The modified dissipation term becomes

$$\tilde{d}_j^C(\mathbf{U}_h^C, \mathbf{U}_h^D, v) = \frac{1}{\tau_{max}} \int_{I_j} (\mathbf{U}_h^D - \mathbf{U}_h^C) v dx + \frac{1}{\tau_{max}} \int_{I_j} (\mathbf{U}_h^{s,C} - \mathbf{U}_h^{s,D}) v dx = 0.$$

It is observed that the WB property holds for the density and energy equations, as both the flux and source term approximations in those equations become zero. For the momentum equation, because $\frac{\overline{(\rho_h^D)_j}}{(\rho_h^{s,D})_j} = 1$, the modified source term becomes

$$\langle S_{h,2}^D, v \rangle_j = \left(p_h^{s,D}(x_{j+\frac{1}{2}}) v(x_{j+\frac{1}{2}}^-) - p_h^{s,D}(x_{j-\frac{1}{2}}) v(x_{j-\frac{1}{2}}^+) \right) - \frac{\Delta x}{2} \sum_{\kappa=1}^2 \sum_{\alpha=1}^N \omega_\alpha p_h^{s,D}(x_j^{\kappa,\alpha}) v_x(x_j^{\kappa,\alpha}).$$

Since $u = 0$, the flux term $F_2 = \rho u^2 + p$ reduces to p , and its numerical approximation is given by

$$\begin{aligned} & \frac{\Delta x}{2} \sum_{\kappa=1}^2 \sum_{\alpha=1}^N \omega_\alpha F_2(\mathbf{U}_h^D(x_j^{\kappa,\alpha})) v_x(x_j^{\kappa,\alpha}) - \left(F_2(\mathbf{U}_h^D(x_{j+\frac{1}{2}})) v(x_{j+\frac{1}{2}}^-) - F_2(\mathbf{U}_h^D(x_{j-\frac{1}{2}})) v(x_{j-\frac{1}{2}}^+) \right) \\ &= \frac{\Delta x}{2} \sum_{\kappa=1}^2 \sum_{\alpha=1}^N \omega_\alpha p_h^{s,D}(x_j^{\kappa,\alpha}) v_x(x_j^{\kappa,\alpha}) - \left(p_h^{s,D}(x_{j+\frac{1}{2}}) v(x_{j+\frac{1}{2}}^-) - p_h^{s,D}(x_{j-\frac{1}{2}}) v(x_{j-\frac{1}{2}}^+) \right) = -\langle S_{h,2}^D, v \rangle_j. \end{aligned}$$

Therefore, the flux and source term approximations balance each other, implying

$$\int_{I_j} \frac{\partial \mathbf{U}_h^C}{\partial t} v dx = 0, \quad \forall v \in \mathbb{V}_h^{C,k}.$$

Similarly, on the dual mesh, one can establish

$$\int_{I_{j+\frac{1}{2}}} \frac{\partial \mathbf{U}_h^D}{\partial t} w dx = 0, \quad \forall w \in \mathbb{V}_h^{D,k}.$$

Hence our CDG schemes, given by (22) and (23), are WB for a general stationary hydrostatic solution (3). ■

3.4.2 Positivity-preserving property

This subsection will discuss the positivity-preserving property of the WB CDG schemes (22) and (23). The WB modifications of the numerical dissipation and source terms lead to additional difficulties in the positivity-preserving analyses, which are more complicated than that for the standard CDG method. We introduce several basic properties of the admissible state set G , which will be useful in our positivity-preserving analyses.

Lemma 3.1 (Convexity). *The set G is a convex set.*

Proof. This property can be verified by definition and Jensen's inequality; see [69, Page 8919]. ■

Lemma 3.2. *For any $\mathbf{U} \in G$ and $b \in \mathbb{R}$, the state $\mathbf{U} + \lambda \mathbf{S}(\mathbf{U}, b) \in G$ under the condition*

$$|\lambda| < \frac{1}{|b|} \sqrt{\frac{2p}{(\gamma-1)\rho}}.$$

Proof. The proof can be found in [57, Page A476] for the details. ■

Lemma 3.3. *For any $\mathbf{U} \in G$ and $\lambda \in \mathbb{R}$, the state $\mathbf{U} - \lambda \mathbf{F}(\mathbf{U}) \in G$ under the condition*

$$|\lambda| a_x(\mathbf{U}) \leq 1, \quad \text{with } a_x(\mathbf{U}) := |u| + \sqrt{\frac{\gamma p}{\rho}}.$$

Proof. A proof can be found in [69, Page 8921]. See also [52] for another simple proof based on the GQL approach. ■

Next, we consider the semi-discrete scheme satisfied by the cell averages of the WB CDG solution. Denote

$$\bar{\mathbf{U}}_j^C(t) = \frac{1}{\Delta x} \int_{I_j} \mathbf{U}_h^C(x, t) dx, \quad \bar{\mathbf{U}}_{j+\frac{1}{2}}^D(t) = \frac{1}{\Delta x} \int_{I_{j+\frac{1}{2}}} \mathbf{U}_h^D(x, t) dx.$$

Taking the test function $v = 1$ in (22) and $w = 1$ in (23) and using the identities in (11) gives

$$\begin{aligned} \frac{d\bar{\mathbf{U}}_j^C}{dt} &= \mathbf{L}_j^C(\mathbf{U}_h^C, \mathbf{U}_h^D) := \frac{(\bar{\mathbf{U}}_j^D - \bar{\mathbf{U}}_j^C)}{\tau_{\max}} - \frac{(\mathbf{F}(\mathbf{U}_{j+\frac{1}{2}}^D) - \mathbf{F}(\mathbf{U}_{j-\frac{1}{2}}^D))}{\Delta x} + \frac{\langle \mathbf{S}_h^D, 1 \rangle_j}{\Delta x}, \\ \frac{d\bar{\mathbf{U}}_{j+\frac{1}{2}}^D}{dt} &= \mathbf{L}_{j+\frac{1}{2}}^D(\mathbf{U}_h^D, \mathbf{U}_h^C) := \frac{(\bar{\mathbf{U}}_{j+\frac{1}{2}}^C - \bar{\mathbf{U}}_{j+\frac{1}{2}}^D)}{\tau_{\max}} - \frac{(\mathbf{F}(\mathbf{U}_{j+1}^C) - \mathbf{F}(\mathbf{U}_j^C))}{\Delta x} + \frac{\langle \mathbf{S}_h^C, 1 \rangle_{j+\frac{1}{2}}}{\Delta x}, \end{aligned} \quad (24)$$

where $\mathbf{U}_{j+\frac{1}{2}}^D = \mathbf{U}_h^D(x_{j+\frac{1}{2}})$, $\mathbf{U}_{j+1}^C = \mathbf{U}_h^C(x_{j+1})$.

Remark 3.3. Recall that the two key identities in (11) are derived from the novel projection operators \mathcal{P}_h^C and \mathcal{P}_h^D and do not hold for the standard L^2 -projection. Benefited from this remarkable feature, our modification of the numerical dissipation term does not destroy the positivity-preserving property.

Let $\mathbb{L}_j^{1,x} = \{\hat{x}_j^{1,\beta}\}_{\beta=1}^L$ and $\mathbb{L}_j^{2,x} = \{\hat{x}_j^{2,\beta}\}_{\beta=1}^L$ denote the Gauss-Lobatto quadrature nodes transformed into the interval $[x_{j-\frac{1}{2}}, x_j]$ and $[x_j, x_{j+\frac{1}{2}}]$, respectively, and $\{\hat{\omega}_\beta\}_{\beta=1}^L$ are the associated weights satisfying $\sum_{\beta=1}^L \hat{\omega}_\beta = 1$. We take $L = \lceil \frac{k+3}{2} \rceil$, which gives $2L - 3 \geq k$, so that the L -point Gauss-Lobatto quadrature rule is exact for polynomials of degree up to k . For each primal cell I_j , we define the point set

$$\mathbb{S}_j = \mathbb{Q}_j^{1,x} \cup \mathbb{Q}_j^{2,x} \cup \mathbb{L}_j^{1,x} \cup \mathbb{L}_j^{2,x}, \quad \mathbb{Q}_j = \mathbb{Q}_j^{1,x} \cup \mathbb{Q}_j^{2,x}, \quad (25)$$

and the parameter $\tilde{\alpha}_j^D$ as

$$\tilde{\alpha}_j^D = \tilde{\alpha}_{1,j}^D + \tilde{\alpha}_{2,j}^D, \quad \tilde{\alpha}_{1,j}^D = \max_{x \in \{x_{j-\frac{1}{2}}, x_{j+\frac{1}{2}}\}} a_x(\mathbf{U}_h^D),$$

$$\tilde{\alpha}_{2,j}^D = \frac{\hat{\omega}_1 \Delta x}{2} \max_{x \in \mathbb{Q}_j} \left\{ |(\hat{\phi}_h^D)_x| \sqrt{\frac{(\gamma-1)\rho_h^D}{2p_h^D}} \right\}, \quad (\hat{\phi}_h^D)_x = \frac{p_h^{s,D}(x_j^-) - p_h^{s,D}(x_j^+)}{(\rho_h^{s,D})_j \Delta x} - \frac{(p_h^{s,D})_x}{\rho_h^{s,D}}.$$

Similarly, in each dual cell $I_{j+\frac{1}{2}}$, we define the point set

$$\mathbb{S}_{j+\frac{1}{2}} = \mathbb{Q}_j^{2,x} \cup \mathbb{Q}_{j+1}^{1,x} \cup \mathbb{L}_j^{2,x} \cup \mathbb{L}_{j+1}^{1,x}, \quad \mathbb{Q}_{j+\frac{1}{2}} = \mathbb{Q}_j^{2,x} \cup \mathbb{Q}_{j+1}^{1,x} \quad (26)$$

and the parameter $\tilde{\alpha}_{j+\frac{1}{2}}^C$ as

$$\tilde{\alpha}_{j+\frac{1}{2}}^C = \tilde{\alpha}_{1,j+\frac{1}{2}}^C + \tilde{\alpha}_{2,j+\frac{1}{2}}^C, \quad \tilde{\alpha}_{1,j+\frac{1}{2}}^C = \max_{x \in \{x_j, x_{j+1}\}} a_x(\mathbf{U}_h^C),$$

$$\tilde{\alpha}_{2,j+\frac{1}{2}}^C = \frac{\hat{\omega}_1 \Delta x}{2} \max_{x \in \mathbb{Q}_{j+\frac{1}{2}}} \left\{ |(\hat{\phi}_h^C)_x| \sqrt{\frac{(\gamma-1)\rho_h^C}{2p_h^C}} \right\}, \quad (\hat{\phi}_h^C)_x = \frac{p_h^{s,C}(x_{j+\frac{1}{2}}^-) - p_h^{s,C}(x_{j+\frac{1}{2}}^+)}{(\rho_h^{s,C})_{j+\frac{1}{2}} \Delta x} - \frac{(p_h^{s,C})_x}{\rho_h^{s,C}}.$$

Then we have the following CFL-type condition for the high-order CDG schemes (22) and (23) to be positivity-preserving.

Theorem 3.2. Assume that the numerical solutions $\mathbf{U}_h^C(x,t), \mathbf{U}_h^D(x,t)$ and the projected stationary hydrostatic solutions $\mathbf{U}_h^{s,C}(x), \mathbf{U}_h^{s,D}(x)$ satisfy

$$\begin{cases} \mathbf{U}_h^C(x,t) \in G, & \mathbf{U}_h^{s,C}(x) \in G & \forall x \in \mathbb{S}_j, \forall j, \\ \mathbf{U}_h^D(x,t) \in G, & \mathbf{U}_h^{s,D}(x) \in G & \forall x \in \mathbb{S}_{j+\frac{1}{2}}, \forall j. \end{cases} \quad (27)$$

If $\bar{\mathbf{U}}_j^C, \bar{\mathbf{U}}_{j+\frac{1}{2}}^D \in G$, then the weak positivity-preserving property

$$\bar{\mathbf{U}}_j^C + \Delta t \mathbf{L}_j^C(\mathbf{U}_h^C, \mathbf{U}_h^D) \in G, \quad \bar{\mathbf{U}}_{j+\frac{1}{2}}^D + \Delta t \mathbf{L}_{j+\frac{1}{2}}^D(\mathbf{U}_h^D, \mathbf{U}_h^C) \in G, \quad \forall j,$$

holds under the CFL-type condition

$$\frac{\Delta t}{\Delta x} \tilde{\alpha}_x < \frac{\theta \hat{\omega}_1}{2}, \quad \tilde{\alpha}_x = \max_j \max\{\tilde{\alpha}_j^D, \tilde{\alpha}_{j+\frac{1}{2}}^C\}, \quad \theta = \frac{\Delta t}{\tau_{\max}} \in (0, 1].$$

Proof. Using (24) gives

$$\begin{aligned}\bar{\mathbf{U}}_j^C + \Delta t \mathbf{L}_j^C(\mathbf{U}_h^C, \mathbf{U}_h^D) &= (1 - \theta) \bar{\mathbf{U}}_j^C + \left[\eta \theta \bar{\mathbf{U}}_j^D + \lambda_x \langle \mathbf{S}_h^D, 1 \rangle_j \right] \\ &\quad + \left[(1 - \eta) \theta \bar{\mathbf{U}}_j^D - \lambda_x \left(\mathbf{F}(\mathbf{U}_{j+\frac{1}{2}}^D) - \mathbf{F}(\mathbf{U}_{j-\frac{1}{2}}^D) \right) \right] \\ &= (1 - \theta) \bar{\mathbf{U}}_j^C + \eta \theta \mathbf{L}_{h,S} + (1 - \eta) \theta \mathbf{L}_{h,F},\end{aligned}$$

where $\lambda_x = \frac{\Delta t}{\Delta x}$, $\theta = \frac{\Delta t}{\tau_{\max}}$, $\eta \in (0, 1)$ is a constant, and $\mathbf{L}_{h,F}, \mathbf{L}_{h,S}$ are given by

$$\mathbf{L}_{h,F} = \bar{\mathbf{U}}_j^D - \frac{\lambda_x}{(1 - \eta) \theta} \left(\mathbf{F}(\mathbf{U}_{j+\frac{1}{2}}^D) - \mathbf{F}(\mathbf{U}_{j-\frac{1}{2}}^D) \right), \quad \mathbf{L}_{h,S} = \bar{\mathbf{U}}_j^D + \frac{\lambda_x}{\eta \theta} \langle \mathbf{S}_h^D, 1 \rangle_j.$$

Due to the exactness of the Gauss-Lobatto quadrature rule, one has

$$\bar{\mathbf{U}}_j^D = \sum_{\kappa=1}^2 \sum_{\beta=1}^L \frac{\hat{\omega}_\beta}{2} \mathbf{U}_h^D(\hat{x}_j^{\kappa,\beta}).$$

Let us first consider $\mathbf{L}_{h,F}$ and reformulate it as follows

$$\begin{aligned}\mathbf{L}_{h,F} &= \sum_{\kappa=1}^2 \sum_{\beta=1}^L \frac{\hat{\omega}_\beta}{2} \mathbf{U}_h^D(\hat{x}_j^{\kappa,\beta}) - \frac{\lambda_x}{(1 - \eta) \theta} \left(\mathbf{F}(\mathbf{U}_{j+\frac{1}{2}}^D) - \mathbf{F}(\mathbf{U}_{j-\frac{1}{2}}^D) \right) \\ &= \sum_{\beta=2}^L \frac{\hat{\omega}_\beta}{2} \mathbf{U}_h^D(\hat{x}_j^{1,\beta}) + \frac{\hat{\omega}_1}{2} \left(\mathbf{U}_{j-\frac{1}{2}}^D + \frac{2\lambda_x}{(1 - \eta) \theta \hat{\omega}_1} \mathbf{F}(\mathbf{U}_{j-\frac{1}{2}}^D) \right) \\ &\quad + \sum_{\beta=1}^{L-1} \frac{\hat{\omega}_\beta}{2} \mathbf{U}_h^D(\hat{x}_j^{2,\beta}) + \frac{\hat{\omega}_L}{2} \left(\mathbf{U}_{j+\frac{1}{2}}^D - \frac{2\lambda_x}{(1 - \eta) \theta \hat{\omega}_L} \mathbf{F}(\mathbf{U}_{j+\frac{1}{2}}^D) \right) \\ &= \sum_{\beta=2}^L \frac{\hat{\omega}_\beta}{2} \mathbf{U}_h^D(\hat{x}_j^{1,\beta}) + \frac{\hat{\omega}_1}{2} \mathbb{E}_{j-\frac{1}{2}}^+ + \sum_{\beta=1}^{L-1} \frac{\hat{\omega}_\beta}{2} \mathbf{U}_h^D(\hat{x}_j^{2,\beta}) + \frac{\hat{\omega}_L}{2} \mathbb{E}_{j+\frac{1}{2}}^-, \end{aligned}$$

where

$$\mathbb{E}_{j-\frac{1}{2}}^+ = \mathbf{U}_{j-\frac{1}{2}}^D + \frac{2\lambda_x}{(1 - \eta) \theta \hat{\omega}_1} \mathbf{F}(\mathbf{U}_{j-\frac{1}{2}}^D), \quad \mathbb{E}_{j+\frac{1}{2}}^- = \mathbf{U}_{j+\frac{1}{2}}^D - \frac{2\lambda_x}{(1 - \eta) \theta \hat{\omega}_L} \mathbf{F}(\mathbf{U}_{j+\frac{1}{2}}^D).$$

Thanks to the Lax-Friedrichs splitting property, we have $\mathbb{E}_{j-\frac{1}{2}}^+ \in G$ and $\mathbb{E}_{j+\frac{1}{2}}^- \in G$, as long as

$$\lambda_x \max_{x \in \{x_{j-\frac{1}{2}}, x_{j+\frac{1}{2}}\}} a_x(\mathbf{U}_h^D) = \lambda_x \tilde{\alpha}_{1,j}^D < \frac{(1 - \eta) \theta \hat{\omega}_1}{2}.$$

Using the convexity of set G , we obtain $\mathbf{L}_{h,F} \in G$. Next, we discuss the term $\mathbf{L}_{h,S}$, and reformulate the source term $\langle \mathbf{S}_h^D, 1 \rangle_j$ as follows

$$\begin{aligned}\langle \mathbf{S}_h^D, 1 \rangle_j &= \frac{(\rho_h^D)_j}{(\rho_h^{s,D})_j} \left(\left(p_h^{s,D}(x_{j+\frac{1}{2}}) - p_h^{s,D}(x_{j-\frac{1}{2}}) \right) - \frac{\Delta x}{2} \sum_{\kappa=1}^2 \sum_{\alpha=1}^N \omega_\alpha (p_h^{s,D})_x(x_j^{\kappa,\alpha}) \right) \\ &\quad + \frac{\Delta x}{2} \sum_{\kappa=1}^2 \sum_{\alpha=1}^N \omega_\alpha \frac{\rho_h^D(x_j^{\kappa,\alpha})}{\rho_h^{s,D}(x_j^{\kappa,\alpha})} (p_h^{s,D})_x(x_j^{\kappa,\alpha}).\end{aligned}$$

Notice that

$$\frac{\Delta x}{2} \sum_{\kappa=1}^2 \sum_{\alpha=1}^N \omega_{\alpha} (p_h^{s,D})_x(x_j^{\kappa,\alpha}) = \int_{I_j} (p_h^{s,D})_x dx,$$

which leads to

$$\begin{aligned} \langle S_{h,2}^D, 1 \rangle_j &= \frac{\overline{(\rho_h^D)}_j}{(\rho_h^{s,D})_j} \left(p_h^{s,D}(x_j^+) - p_h^{s,D}(x_j^-) \right) + \frac{\Delta x}{2} \sum_{\kappa=1}^2 \sum_{\alpha=1}^N \omega_{\alpha} \frac{\rho_h^D(x_j^{\kappa,\alpha})}{\rho_h^{s,D}(x_j^{\kappa,\alpha})} (p_h^{s,D})_x(x_j^{\kappa,\alpha}) \\ &= -\frac{\Delta x}{2} \sum_{\kappa=1}^2 \sum_{\alpha=1}^N \omega_{\alpha} \rho_h^D(x_j^{\kappa,\alpha}) (\hat{\phi}_h^D)_x(x_j^{\kappa,\alpha}), \end{aligned}$$

with

$$-(\hat{\phi}_h^D)_x(x_j^{\kappa,\alpha}) := \frac{p_h^{s,D}(x_j^+) - p_h^{s,D}(x_j^-)}{(\rho_h^{s,D})_j \Delta x} + \frac{(p_h^{s,D})_x(x_j^{\kappa,\alpha})}{\rho_h^{s,D}(x_j^{\kappa,\alpha})}.$$

Similarly, one can derive

$$\begin{aligned} \langle S_{h,3}^D, 1 \rangle_j &= \frac{\overline{(m_h^D)}_j}{(\rho_h^{s,D})_j} \left(p_h^{s,D}(x_j^+) - p_h^{s,D}(x_j^-) \right) + \frac{\Delta x}{2} \sum_{\kappa=1}^2 \sum_{\alpha=1}^N \omega_{\alpha} \frac{m_h^D(x_j^{\kappa,\alpha})}{\rho_h^{s,D}(x_j^{\kappa,\alpha})} (p_h^{s,D})_x(x_j^{\kappa,\alpha}) \\ &= -\frac{\Delta x}{2} \sum_{\kappa=1}^2 \sum_{\alpha=1}^N \omega_{\alpha} m_h^D(x_j^{\kappa,\alpha}) (\hat{\phi}_h^D)_x(x_j^{\kappa,\alpha}). \end{aligned}$$

Thus $\mathbf{L}_{h,S}$ is reformulated as

$$\begin{aligned} \mathbf{L}_{h,S} &= \bar{\mathbf{U}}_j^D + \frac{\lambda_x}{\eta \theta} \langle S_{h,1}^D, 1 \rangle_j = \bar{\mathbf{U}}_j^D + \frac{\Delta t}{\eta \theta} \sum_{\kappa=1}^2 \sum_{\alpha=1}^N \omega_{\alpha} \hat{\mathbf{S}}_h^D(x_j^{\kappa,\alpha}) \\ &= \sum_{\kappa=1}^2 \sum_{\alpha=1}^N \frac{\omega_{\alpha}}{2} \left(\mathbf{U}_h^D(x_j^{\kappa,\alpha}) + \frac{\Delta t}{\eta \theta} \hat{\mathbf{S}}_h^D(x_j^{\kappa,\alpha}) \right). \end{aligned}$$

where

$$\hat{\mathbf{S}}_h^D := (0, -\rho_h^D (\hat{\phi}_h^D)_x, -m_h^D (\hat{\phi}_h^D)_x)^{\top}.$$

Thanks to Lemma 3.2, we have $\mathbf{L}_{h,S} \in G$ under the condition

$$\Delta t < \eta \theta \min_{x \in \mathbb{Q}_j} \left\{ \frac{1}{|(\hat{\phi}_h^D)_x|} \sqrt{\frac{2\rho_h^D}{(\gamma-1)\rho_h^D}} \right\}.$$

or equivalently

$$\lambda_x \tilde{\alpha}_{2,j}^D < \frac{\eta \theta \hat{\omega}_1}{2}.$$

Combining those results, we conclude that if

$$\lambda_x \in \left\{ \lambda \in \mathbb{R}^+ : \lambda \tilde{\alpha}_{1,j}^D < \frac{(1-\eta)\theta \hat{\omega}_1}{2}, \lambda \tilde{\alpha}_{2,j}^D < \frac{\eta \theta \hat{\omega}_1}{2} \right\}, \quad (28)$$

then $\bar{\mathbf{U}}_j^C + \Delta t \mathbf{L}_j^C(\mathbf{U}_h^C, \mathbf{U}_h^D) \in G$. Since the parameters η can be chosen arbitrarily in this proof, we specify $\eta = \tilde{\alpha}_{2,j}^D / \tilde{\alpha}_j^D = \tilde{\alpha}_{2,j}^D / (\tilde{\alpha}_{1,j}^D + \tilde{\alpha}_{2,j}^D)$ such that the condition (28) becomes

$$\lambda_x(\tilde{\alpha}_{1,j}^D + \tilde{\alpha}_{2,j}^D) = \lambda_x \tilde{\alpha}_j^D < \frac{\theta \hat{\omega}_1}{2}.$$

Similar arguments show that $\bar{\mathbf{U}}_{j+\frac{1}{2}}^D + \Delta t \mathbf{L}_{j+\frac{1}{2}}^D(\mathbf{U}_h^D, \mathbf{U}_h^C) \in G$. The proof is completed. \blacksquare

3.5 Positivity-preserving limiting operators Π_h^C and Π_h^D

A simple positivity-preserving limiter can be applied to enforce the condition (27). Because the limiting procedures for $\mathbf{U}_h^C(x)$ and $\mathbf{U}_h^D(x)$ are similar and implemented separately, we only present that for $\mathbf{U}_h^C(x)$. For any $\mathbf{U}_h^C \in \bar{\mathbb{G}}_h^{C,k}$ with $\mathbf{U}_h^C|_{I_j} := \mathbf{U}_j^C(x)$, we follow [46, 69] and define the positivity-preserving limiting operator $\Pi_h^C : \bar{\mathbb{G}}_h^{C,k} \rightarrow \mathbb{G}_h^{C,k}$ as follows

$$(\Pi_h^C \mathbf{U}_h^C)|_{I_j} = \theta_j^{(2)} (\hat{\mathbf{U}}_j^C(x) - \bar{\mathbf{U}}_j^C) + \bar{\mathbf{U}}_j^C, \quad \theta_j^{(2)} = \min \left\{ 1, \frac{p(\bar{\mathbf{U}}_j^C) - \varepsilon_2}{p(\bar{\mathbf{U}}_j^C) - \min_{x \in \mathbb{S}_j} p(\hat{\mathbf{U}}_j^C(x))} \right\},$$

where $\hat{\mathbf{U}}_j^C(x) = (\hat{\rho}_j^C(x), m_j^C(x), E_j^C(x))^\top$, and $\hat{\rho}_j^C(x)$ is a modification of the density $\rho_j^C(x)$ given by

$$\hat{\rho}_j^C(x) = \theta_j^{(1)} (\rho_j^C(x) - \bar{\rho}_j^C) + \bar{\rho}_j^C, \quad \theta_j^{(1)} = \min \left\{ 1, \frac{\bar{\rho}_j^C - \varepsilon_1}{\bar{\rho}_j^C - \min_{x \in \mathbb{S}_j} \rho_j^C(x)} \right\}.$$

Here ε_1 and ε_2 are two small positive numbers for avoiding the effect of round-off error, and in the computation, one can take $\varepsilon_1 = \min\{10^{-13}, \bar{\rho}_j^C\}$, $\varepsilon_2 = \min\{10^{-13}, p(\bar{\mathbf{U}}_j^C)\}$. Note that such a local scaling limiter keeps the local conservation and does not destroy the high-order accuracy; see [68, 67] for more details. The positivity-preserving limiting operator $\Pi_h^D : \bar{\mathbb{G}}_h^{D,k} \rightarrow \mathbb{G}_h^{D,k}$ defined on the dual mesh is similar.

Suppose the initial numerical solutions are defined as $\mathbf{U}_h^{C,0} = \Pi_h^C[\mathbf{U}_h^C(x, 0)]$, $\mathbf{U}_h^{D,0} = \Pi_h^D[\mathbf{U}_h^D(x, 0)]$. For the WB CDG schemes (22) and (23) coupled with an third order SSP Runge-Kutta method, if the positivity-preserving limiter is used at each Runge-Kutta stage, then our fully discrete CDG schemes are positivity-preserving, namely, $\mathbf{U}_h^{C,n} \in \mathbb{G}_h^{C,k}$ and $\mathbf{U}_h^{D,n} \in \mathbb{G}_h^{D,k}$.

Remark 3.4 (WB Implementation of Non-oscillatory Limiters). *When the exact solution contains strong discontinuities, the above positivity-preserving limiter may not control the nonphysical numerical oscillations in the CDG solutions, and a standard non-oscillatory limiter, such as the TVD/TVB or WENO limiter, is still needed in the “troubled” cells. We will adopt the WENO limiter [37] in the numerical examples involving discontinuities (Examples 4, 9, and 11 in Section 5). However, the traditional use of non-oscillatory limiters may destroy the WB property of our schemes. This issue can be easily addressed by slightly modifying the procedure of identifying the “troubled” cells, based on the perturbations of the solutions and cell averages*

$$\tilde{\mathbf{U}}_h^C(x) = \mathbf{U}_h^C(x) - \mathbf{U}_h^{s,C}(x), \quad \tilde{\bar{\mathbf{U}}}_j^C = \bar{\mathbf{U}}_j^C - \bar{\mathbf{U}}_j^{s,C}.$$

More specifically, for each j we first use the TVB corrected minmod function (see, e.g., [37])

$$\tilde{m}(a_1, a_2, \dots, a_n) = \begin{cases} a_1, & \text{if } |a_1| \leq M(\Delta x)^2, \\ m(a_1, a_2, \dots, a_n), & \text{otherwise,} \end{cases} \quad (29)$$

to check if the cell I_j is “troubled” based on the cell-averaged values $\bar{\mathbf{U}}_j^C$, $\bar{\mathbf{U}}_{j\pm 1}^C$, and the endpoint values $\tilde{\mathbf{U}}_h^C(x_{j-\frac{1}{2}}^+)$, $\tilde{\mathbf{U}}_h^C(x_{j+\frac{1}{2}}^-)$ on the cell I_j . Only if cell I_j is identified as “troubled” cell, we then apply the WENO limiter on $\mathbf{U}_h^C(x)$ as usual before the positivity-preserving limiter. The same implementation is also used separately on the dual mesh. Note that if the steady state is reached, then $\tilde{\mathbf{U}}_h^C(x)$ becomes zero so that no cell will be flagged as “troubled”, and thus the WB property is preserved. Numerical results in Example 11 will further confirm that our implementation of the WENO limiter does not affect the WB property.

4 Extension to the two-dimensional case

This section will extend the positivity-preserving WB CDG schemes to the two-dimensional Euler equations under the gravitational field $\phi(x, y)$

$$\mathbf{U}_t + \nabla \cdot \mathbf{F}(\mathbf{U}) = \mathbf{S}(\mathbf{U}, \nabla \phi), \quad (30)$$

where $\mathbf{U} = (\rho, \rho u_1, \rho u_2, E)^\top$ denotes the conservative variables, $\mathbf{F}(\mathbf{U}) = (\mathbf{F}_1(\mathbf{U}), \mathbf{F}_2(\mathbf{U}))$ with

$$\mathbf{F}_1(\mathbf{U}) = (\rho u_1, \rho u_1^2 + p, \rho u_1 u_2, (E + p)u_1)^\top,$$

$$\mathbf{F}_2(\mathbf{U}) = (\rho u_2, \rho u_1 u_2, \rho u_2^2 + p, (E + p)u_2)^\top,$$

denote the fluxes, and $\mathbf{S}(\mathbf{U}, \nabla \phi) = (0, -\rho \phi_x, -\rho \phi_y, -\mathbf{m} \cdot \nabla \phi)^\top$ is the source term with $\mathbf{m} = (\rho u_1, \rho u_2)$ being the momentum vector.

Let $\mathcal{T}_h^C = \{I_{i,j}, \forall i, j\}$ and $\mathcal{T}_h^D = \{I_{i+\frac{1}{2}, j+\frac{1}{2}}, \forall i, j\}$ respectively denote two overlapping uniform meshes for the rectangular computational domain $\Omega = [x_{\min}, x_{\max}] \times [y_{\min}, y_{\max}]$ with $I_{i,j} = (x_{i-\frac{1}{2}}, x_{i+\frac{1}{2}}) \times (y_{j-\frac{1}{2}}, y_{j+\frac{1}{2}})$ and $I_{i+\frac{1}{2}, j+\frac{1}{2}} = (x_i, x_{i+1}) \times (y_j, y_{j+1})$. The spatial stepsizes are $\Delta x = x_{i+\frac{1}{2}} - x_{i-\frac{1}{2}}$ in the x -direction and $\Delta y = y_{j+\frac{1}{2}} - y_{j-\frac{1}{2}}$ in the y -direction. We define two discrete function spaces associated with the overlapping meshes $\{I_{i,j}\}$ and $\{I_{i+\frac{1}{2}, j+\frac{1}{2}}\}$

$$\mathbb{V}_h^{C,k} = \left\{ v : v|_{I_{i,j}} \in \mathbb{P}^k(I_{i,j}), \forall i, j \right\}, \quad \mathbb{V}_h^{D,k} = \left\{ v : v|_{I_{i+\frac{1}{2}, j+\frac{1}{2}}} \in \mathbb{P}^k(I_{i+\frac{1}{2}, j+\frac{1}{2}}), \forall i, j \right\},$$

where $\mathbb{P}^k(I_{i,j})$ and $\mathbb{P}^k(I_{i+\frac{1}{2}, j+\frac{1}{2}})$ denote the space of two-dimensional polynomials in the cells $I_{i,j}$ and $I_{i+\frac{1}{2}, j+\frac{1}{2}}$ with degree of at most k , respectively. To solve the system (30), the standard CDG method

in the semi-discrete form looks for two numerical solutions $\mathbf{U}_h^C \in [\mathbb{V}_h^{C,k}]^4$ and $\mathbf{U}_h^D \in [\mathbb{V}_h^{D,k}]^4$ such that

$$\begin{aligned} \int_{I_{i,j}} \frac{\partial \mathbf{U}_h^C}{\partial t} v dx dy &= \frac{1}{\tau_{max}} \int_{I_{i,j}} (\mathbf{U}_h^D - \mathbf{U}_h^C) v dx dy + \int_{I_{i,j}} \mathbf{F}(\mathbf{U}_h^D) \cdot \nabla v dx dy \\ &\quad - \int_{y_{j-\frac{1}{2}}}^{y_{j+\frac{1}{2}}} \left(\mathbf{F}_1(\mathbf{U}_h^D(x_{i+\frac{1}{2}}, y)) v(x_{i+\frac{1}{2}}^-, y) - \mathbf{F}_1(\mathbf{U}_h^D(x_{i-\frac{1}{2}}, y)) v(x_{i-\frac{1}{2}}^+, y) \right) dy \\ &\quad - \int_{x_{i-\frac{1}{2}}}^{x_{i+\frac{1}{2}}} \left(\mathbf{F}_2(\mathbf{U}_h^D(x, y_{j+\frac{1}{2}})) v(x, y_{j+\frac{1}{2}}^-) - \mathbf{F}_2(\mathbf{U}_h^D(x, y_{j-\frac{1}{2}})) v(x, y_{j-\frac{1}{2}}^+) \right) dx \\ &\quad + \int_{I_{i,j}} \mathbf{S}(\mathbf{U}_h^D, \nabla \phi_h^D) v dx dy \quad \forall v \in \mathbb{V}_h^{C,k}, \end{aligned} \quad (31)$$

$$\begin{aligned} \int_{I_{i+\frac{1}{2}, j+\frac{1}{2}}} \frac{\partial \mathbf{U}_h^D}{\partial t} w dx dy &= \frac{1}{\tau_{max}} \int_{I_{i+\frac{1}{2}, j+\frac{1}{2}}} (\mathbf{U}_h^C - \mathbf{U}_h^D) w dx dy + \int_{I_{i+\frac{1}{2}, j+\frac{1}{2}}} \mathbf{F}(\mathbf{U}_h^C) \cdot \nabla w dx dy \\ &\quad - \int_{y_j}^{y_{j+1}} \left(\mathbf{F}_1(\mathbf{U}_h^C(x_{i+1}, y)) w(x_{i+1}^-, y) - \mathbf{F}_1(\mathbf{U}_h^C(x_i, y)) w(x_i^+, y) \right) dy \\ &\quad - \int_{x_i}^{x_{i+1}} \left(\mathbf{F}_2(\mathbf{U}_h^C(x, y_{j+1})) w(x, y_{j+1}^-) - \mathbf{F}_2(\mathbf{U}_h^C(x, y_j)) w(x, y_j^+) \right) dx \\ &\quad + \int_{I_{i+\frac{1}{2}, j+\frac{1}{2}}} \mathbf{S}(\mathbf{U}_h^C, \nabla \phi_h^C) w dx dy \quad \forall w \in \mathbb{V}_h^{D,k}, \end{aligned} \quad (32)$$

where $\tau_{max} = \tau_{max}(t)$ is the maximal time step allowed by the CFL restriction at time t . As the one-dimensional case, the two-dimensional standard CDG method (31)–(32) is generally not WB for the stationary hydrostatic solutions.

4.1 Novel projection of the stationary hydrostatic solutions

Assume that the target equilibrium state of the system (30) is known and denoted by

$$\{\rho^s(x, y), u_1^s(x, y), u_2^s(x, y), p^s(x, y)\},$$

which satisfies

$$u_1^s(x, y) = 0, \quad u_2^s(x, y) = 0, \quad \nabla p^s = -\rho^s \nabla \phi. \quad (33)$$

Let $\mathbf{U}^s(x, y) = (\rho^s(x, y), 0, 0, p^s(x, y)/(\gamma - 1))^\top$, and define

$$\begin{aligned} I_{i,j}^0 &= (x_{i-\frac{1}{2}}, x_i) \times (y_{j-\frac{1}{2}}, y_j), & I_{i,j}^1 &= (x_i, x_{i+\frac{1}{2}}) \times (y_{j-\frac{1}{2}}, y_j), \\ I_{i,j}^2 &= (x_{i-\frac{1}{2}}, x_i) \times (y_j, y_{j+\frac{1}{2}}), & I_{i,j}^3 &= (x_i, x_{i+\frac{1}{2}}) \times (y_j, y_{j+\frac{1}{2}}). \end{aligned}$$

Following the ideas in the one-dimensional case, we first introduce the novel projection of the stationary solution $\mathbf{U}^s(x, y)$ on the primal mesh. Define the operator $\mathcal{P}_h^C : L^2(\Omega) \rightarrow \mathbb{V}_h^{C,k}$, such that for any function $f \in L^2(\Omega)$,

$$\begin{aligned} \int_{I_{i,j}^m} \mathcal{P}_h^C(f) dx dy &= \int_{I_{i,j}^m} f dx dy, \quad m \in \{0, 1, 2\}, \\ \int_{I_{i,j}} \mathcal{P}_h^C(f) v dx dy &= \int_{I_{i,j}} f v dx dy, \quad \forall v \in \text{span}\{\Phi_0, \Phi_4, \dots, \Phi_K\}, \end{aligned} \quad (34)$$

where $K = k(k+3)/2$, and $\{\Phi_l\}_{l=0}^K$ is an orthogonal basis of $\mathbb{P}^k(I_{i,j})$ and taken as the scaled Legendre polynomials

$$\begin{aligned}\Phi_0(\xi, \eta) &= 1, \quad \Phi_1(\xi, \eta) = \xi, \quad \Phi_2(\xi, \eta) = \eta, \quad \Phi_3(\xi, \eta) = \xi\eta, \\ \Phi_4(\xi, \eta) &= \xi^2 - \frac{1}{3}, \quad \Phi_5(\xi, \eta) = \eta^2 - \frac{1}{3}, \quad \dots,\end{aligned}$$

with $\xi = 2(x - x_i)/\Delta x$ and $\eta = 2(y - y_j)/\Delta y$. It follows from (34) that the operator \mathcal{P}_h^C satisfies

$$\int_{I_{i,j}^m} \mathcal{P}_h^C(f) dx dy = \int_{I_{i,j}^m} f dx dy, \quad \forall m \in \{0, 1, 2, 3\}, \quad \forall i, j, \quad (35)$$

for any function $f \in L^2(\Omega)$. As the one-dimensional case, the operator \mathcal{P}_h^C defined by (34) can be explicitly expressed. In fact, the piecewise polynomial $\mathcal{P}_h^C(f)$ on each cell $I_{i,j}$ takes the form of

$$\mathcal{P}_h^C(f) = \sum_{l=0}^K N_l(f) \Phi_l,$$

with the polynomial coefficients $\{N_l(f)\}_{l=0}^K$ given by

$$\begin{aligned}N_l(f) &= \frac{\int_{I_{i,j}} f \Phi_l dx dy}{\int_{I_{i,j}} \Phi_l^2 dx dy}, \quad l \neq 1, 2, 3, \\ N_1(f) &= \frac{-4(b_0 + b_2)}{\Delta x \Delta y}, \quad N_2(f) = \frac{-4(b_0 + b_1)}{\Delta x \Delta y}, \quad N_3(f) = \frac{-8(b_1 + b_2)}{\Delta x \Delta y},\end{aligned}$$

where the parameter $b_m = \int_{I_{i,j}^m} (f - \sum_{l \in \{1,2,3\}} N_l(f) \Phi_l) dx dy$, $m \in \{0, 1, 2\}$.

Similarly, we can define the projection $\mathcal{P}_h^D : L^2(\Omega) \rightarrow \mathbb{V}_h^{D,k}$ on the dual mesh such that

$$\int_{I_{i+\frac{1}{2}, j+\frac{1}{2}}^m} \mathcal{P}_h^D(f) dx dy = \int_{I_{i+\frac{1}{2}, j+\frac{1}{2}}^m} f dx dy, \quad \forall m \in \{0, 1, 2, 3\}, \quad \forall i, j, \quad (36)$$

where $I_{i+\frac{1}{2}, j+\frac{1}{2}}^m$ is a shift of $I_{i,j}^m$ with $\frac{\Delta x}{2}$ in the x -direction and $\frac{\Delta y}{2}$ in the y -direction. Combining (35) with (36) leads to the following crucial identities

$$\int_{I_{i,j}} \mathcal{P}_h^C(f) dx dy = \int_{I_{i,j}} \mathcal{P}_h^D(f) dx dy, \quad \int_{I_{i+\frac{1}{2}, j+\frac{1}{2}}} \mathcal{P}_h^D(f) dx dy = \int_{I_{i+\frac{1}{2}, j+\frac{1}{2}}} \mathcal{P}_h^C(f) dx dy. \quad (37)$$

If let $\mathbf{U}_h^{s,C}$ and $\mathbf{U}_h^{s,D}$ denote the above novel projections of the steady state solutions $\mathbf{U}^s(x, y)$ onto the space $[\mathbb{V}_h^{C,k}]^4$ and $[\mathbb{V}_h^{D,k}]^4$, respectively, then the identities in (37) imply

$$\int_{I_{i,j}} \mathbf{U}_h^{s,C} dx dy = \int_{I_{i,j}} \mathbf{U}_h^{s,D} dx dy, \quad \int_{I_{i+\frac{1}{2}, j+\frac{1}{2}}} \mathbf{U}_h^{s,D} dx dy = \int_{I_{i+\frac{1}{2}, j+\frac{1}{2}}} \mathbf{U}_h^{s,C} dx dy, \quad \forall i, j. \quad (38)$$

4.2 WB CDG schemes

The design of our two-dimensional WB CDG method on the rectangular mesh is similar to the procedure described in the one-dimensional case.

The numerical dissipation term in the semi-discrete CDG method (31) is modified as

$$\tilde{d}_{ij}^C(\mathbf{U}_h^C, \mathbf{U}_h^D, v) = \frac{1}{\tau_{max}} \int_{I_{i,j}} (\mathbf{U}_h^D - \mathbf{U}_h^C) v dx dy + \frac{1}{\tau_{max}} \int_{I_{i,j}} (\mathbf{U}_h^{s,C} - \mathbf{U}_h^{s,D}) v dx dy,$$

where \tilde{d}_{ij}^C satisfies the WB property $\tilde{d}_{ij}^C(\mathbf{U}_h^{s,C}, \mathbf{U}_h^{s,D}, v) = \mathbf{0}$. Such modification does not affect the spatial accuracy.

In order to discretize the flux and source term integrals, we need to introduce the two-dimensional numerical quadrature. The notations for the quadrature points in the x -direction is the same as the one-dimensional case. For the y -direction, let $\mathbb{Q}_j^{1,y} = \{y_j^{1,\mu}\}_{\mu=1}^N$ and $\mathbb{Q}_j^{2,y} = \{y_j^{2,\mu}\}_{\mu=1}^N$ denote the N -point Gauss quadrature nodes transformed into the interval $[y_{j-\frac{1}{2}}, y_j]$ and $[y_j, y_{j+\frac{1}{2}}]$, respectively, and $\{\omega_\mu\}_{\mu=1}^N$ are the associated weights satisfying $\sum_{\mu=1}^N \omega_\mu = 1$, with $N \geq k+1$ for the CDG accuracy requirement. Then the flux integrals can be approximated by the numerical quadrature

$$\int_{I_{i,j}} \mathbf{F}(\mathbf{U}_h^D) \nabla v dx dy \approx \frac{\Delta x \Delta y}{4} \sum_{\kappa, \alpha} \sum_{\sigma, \mu} \omega_\alpha \omega_\mu \mathbf{F}(\mathbf{U}_h^D(x_i^{\kappa, \alpha}, y_j^{\sigma, \mu})) \nabla v(x_i^{\kappa, \alpha}, y_j^{\sigma, \mu}),$$

$$\int_{\partial I_{i,j}} (\mathbf{F}(\mathbf{U}_h^D) \cdot \mathbf{n}) v ds \approx \Delta y \delta_{ij}^x (\mathbf{F}_1(\mathbf{U}_h^D) v) + \Delta x \delta_{ij}^y (\mathbf{F}_2(\mathbf{U}_h^D) v),$$

where $\sigma, \kappa \in \{1, 2\}$ and $\mu, \alpha \in \{1, \dots, N\}$, \mathbf{n} is the outward unit normal vector of the cell $I_{i,j}$, and the operators $\delta_{ij}^x, \delta_{ij}^y$ are defined by

$$\begin{aligned} \delta_{ij}^x(f) &:= \sum_{\kappa, \alpha} \frac{\omega_\alpha}{2} \left(f(x_{i+\frac{1}{2}}, y_j^{\kappa, \alpha}) - f(x_{i-\frac{1}{2}}, y_j^{\kappa, \alpha}) \right), \\ \delta_{ij}^y(f) &:= \sum_{\kappa, \alpha} \frac{\omega_\alpha}{2} \left(f(x_i^{\kappa, \alpha}, y_{j+\frac{1}{2}}) - f(x_i^{\kappa, \alpha}, y_{j-\frac{1}{2}}) \right). \end{aligned}$$

The last step for designing our WB CDG spatial discretization is to suitably discretize the source term integral. The source term integrals in the momentum equations are reformulated into

$$\begin{aligned} \int_{I_{i,j}} (S_2, S_3)^\top v dx dy &= - \int_{I_{i,j}} \rho \nabla \phi v dx dy = \int_{I_{i,j}} \frac{\rho}{\rho^s} \nabla p^s v dx dy \\ &= \int_{I_{i,j}} \left(\frac{\rho}{\rho^s} - \frac{\bar{\rho}_{ij}}{\bar{\rho}_{ij}^s} + \frac{\bar{\rho}_{ij}}{\bar{\rho}_{ij}^s} \right) \nabla p^s v dx dy, \end{aligned}$$

where $\bar{\rho}_{ij} = \frac{1}{\Delta x \Delta y} \int_{I_{i,j}} \rho dx dy$ is the cell average. Following the one-dimensional design, we observe

that

$$\begin{aligned}
\int_{I_{i,j}} (S_2, S_3)^\top v dx dy &\approx \int_{I_{i,j}} \left(\frac{\rho_h^D}{\rho_h^{s,D}} - \frac{\overline{(\rho_h^D)_{ij}}}{\overline{(\rho_h^{s,D})_{ij}}} \right) \nabla p_h^{s,D} v dx dy + \frac{\overline{(\rho_h^D)_{ij}}}{\overline{(\rho_h^{s,D})_{ij}}} \int_{I_{i,j}} \nabla p_h^{s,D} v dx dy \\
&\approx \int_{I_{i,j}} \left(\frac{\rho_h^D}{\rho_h^{s,D}} - \frac{\overline{(\rho_h^D)_{ij}}}{\overline{(\rho_h^{s,D})_{ij}}} \right) \nabla p_h^{s,D} v dx dy - \frac{\overline{(\rho_h^D)_{ij}}}{\overline{(\rho_h^{s,D})_{ij}}} \int_{I_{i,j}} p_h^{s,D} \nabla v dx dy \\
&\quad + \frac{\overline{(\rho_h^D)_{ij}}}{\overline{(\rho_h^{s,D})_{ij}}} \int_{\partial I_{i,j}} p_h^{s,D} v n ds.
\end{aligned}$$

Therefore, the source term integrals $\int_{I_{i,j}} (S_2, S_3)^\top v dx dy$ can be approximated by

$$\begin{aligned}
\langle (S_{2,h}^D, S_{3,h}^D)^\top, v \rangle_{ij} &:= \frac{\Delta x \Delta y}{4} \sum_{\kappa, \alpha} \sum_{\sigma, \mu} \omega_\alpha \omega_\mu \left(\frac{\rho_h^D(x_i^{\kappa, \alpha}, y_j^{\sigma, \mu})}{\rho_h^{s,D}(x_i^{\kappa, \alpha}, y_j^{\sigma, \mu})} - \frac{\overline{(\rho_h^D)_{ij}}}{\overline{(\rho_h^{s,D})_{ij}}} \right) (\nabla p_h^{s,D} v)(x_i^{\kappa, \alpha}, y_j^{\sigma, \mu}) \\
&\quad - \frac{\overline{(\rho_h^D)_{ij}}}{\overline{(\rho_h^{s,D})_{ij}}} \frac{\Delta x \Delta y}{4} \sum_{\kappa, \alpha} \sum_{\sigma, \mu} \omega_\alpha \omega_\mu (p_h^{s,D} \nabla v)(x_i^{\kappa, \alpha}, y_j^{\sigma, \mu}) + \frac{\overline{(\rho_h^D)_{ij}}}{\overline{(\rho_h^{s,D})_{ij}}} \left(\Delta y \delta_{ij}^x (p_h^{s,D} v), \Delta x \delta_{ij}^y (p_h^{s,D} v) \right)^\top.
\end{aligned}$$

Similarly, the source term integral $\int_{I_{i,j}} S_4 v dx dy$ in the energy equation can be approximated by

$$\begin{aligned}
\langle S_{4,h}^D, v \rangle_{ij} &:= \frac{\Delta x \Delta y}{4} \sum_{\kappa, \alpha} \sum_{\sigma, \mu} \omega_\alpha \omega_\mu \left(\frac{\mathbf{m}_h^D(x_i^{\kappa, \alpha}, y_j^{\sigma, \mu})}{\rho_h^{s,D}(x_i^{\kappa, \alpha}, y_j^{\sigma, \mu})} - \frac{\overline{(\mathbf{m}_h^D)_{ij}}}{\overline{(\rho_h^{s,D})_{ij}}} \right) (\nabla p_h^{s,D} v)(x_i^{\kappa, \alpha}, y_j^{\sigma, \mu}) \\
&\quad - \frac{\overline{(\mathbf{m}_h^D)_{ij}}}{\overline{(\rho_h^{s,D})_{ij}}} \frac{\Delta x \Delta y}{4} \sum_{\kappa, \alpha} \sum_{\sigma, \mu} \omega_\alpha \omega_\mu (p_h^{s,D} \nabla v)(x_i^{\kappa, \alpha}, y_j^{\sigma, \mu}) + \frac{\overline{(\mathbf{m}_h^D)_{ij}}}{\overline{(\rho_h^{s,D})_{ij}}} \left(\Delta y \delta_{ij}^x (p_h^{s,D} v), \Delta x \delta_{ij}^y (p_h^{s,D} v) \right)^\top.
\end{aligned}$$

Combining those leads to the following WB CDG discretization for the two-dimensional Euler equations with gravity on the primal mesh

$$\begin{aligned}
\int_{I_{i,j}} \frac{\partial \mathbf{U}_h^C}{\partial t} v dx dy &= \frac{1}{\tau_{max}} \int_{I_{i,j}} (\mathbf{U}_h^D - \mathbf{U}_h^C) v dx dy + \frac{1}{\tau_{max}} \int_{I_{i,j}} (\mathbf{U}_h^{s,C} - \mathbf{U}_h^{s,D}) v dx dy + \langle \mathbf{S}_h^D, v \rangle_{ij} \\
&\quad + \frac{\Delta x \Delta y}{4} \sum_{\kappa, \alpha} \sum_{\sigma, \mu} \omega_\alpha \omega_\mu \mathbf{F}(\mathbf{U}_h^D(x_i^{\kappa, \alpha}, y_j^{\sigma, \mu})) \nabla v(x_i^{\kappa, \alpha}, y_j^{\sigma, \mu}) - \Delta y \delta_{ij}^x (\mathbf{F}_1(\mathbf{U}_h^D) v) - \Delta x \delta_{ij}^y (\mathbf{F}_2(\mathbf{U}_h^D) v), \quad (39)
\end{aligned}$$

where $\langle \mathbf{S}_h^D, v \rangle_{ij} = (0, \langle S_{h,2}^D, v \rangle_{ij}, \langle S_{h,3}^D, v \rangle_{ij}, \langle S_{h,4}^D, v \rangle_{ij})^\top$. The WB CDG spatial discretization on the dual mesh is very similar. Denote $\mathbf{Q} = (\mathbf{Q}_1, \mathbf{Q}_2)$, with $\mathbf{Q}_1 = (0, \rho, 0, \rho u_1)^\top$, $\mathbf{Q}_2 = (0, 0, \rho, \rho u_2)^\top$, one has $\mathbf{S}(\mathbf{U}) = -\mathbf{Q} \cdot \nabla \phi$, and the source term integrals on the dual mesh are approximated by

$$\begin{aligned}
\langle \mathbf{S}_h^C, w \rangle_{i+\frac{1}{2}, j+\frac{1}{2}} &= \frac{\Delta x \Delta y}{4} \sum_{\kappa, \alpha} \sum_{\sigma, \mu} \omega_\alpha \omega_\mu \left(\frac{\mathbf{Q}_h^C(x_{i+\frac{1}{2}}^{\kappa, \alpha}, y_{j+\frac{1}{2}}^{\sigma, \mu})}{\rho_h^{s,C}(x_{i+\frac{1}{2}}^{\kappa, \alpha}, y_{j+\frac{1}{2}}^{\sigma, \mu})} - \frac{\overline{(\mathbf{Q}_h^C)_{i+\frac{1}{2}, j+\frac{1}{2}}}}{\overline{(\rho_h^{s,C})_{i+\frac{1}{2}, j+\frac{1}{2}}}} \right) (\nabla p_h^{s,C} w)(x_{i+\frac{1}{2}}^{\kappa, \alpha}, y_{j+\frac{1}{2}}^{\sigma, \mu}) \\
&\quad - \frac{\overline{(\mathbf{Q}_h^C)_{i+\frac{1}{2}, j+\frac{1}{2}}}}{\overline{(\rho_h^{s,C})_{i+\frac{1}{2}, j+\frac{1}{2}}}} \frac{\Delta x \Delta y}{4} \sum_{\kappa, \alpha} \sum_{\sigma, \mu} \omega_\alpha \omega_\mu (p_h^{s,C} \nabla w)(x_{i+\frac{1}{2}}^{\kappa, \alpha}, y_{j+\frac{1}{2}}^{\sigma, \mu})
\end{aligned}$$

$$+ \frac{\overline{(\mathbf{Q}_h^C)_{i+\frac{1}{2},j+\frac{1}{2}}}}{(\rho_h^{s,C})_{i+\frac{1}{2},j+\frac{1}{2}}} \left(\Delta y \delta_{i+\frac{1}{2},j+\frac{1}{2}}^x (p_h^{s,C} w), \Delta x \delta_{i+\frac{1}{2},j+\frac{1}{2}}^y (p_h^{s,C} w) \right)^\top,$$

where $\{y_{j+\frac{1}{2}}^{1,\mu}\}_{\mu=1}^N = \mathbb{Q}_j^{2,y}$, $\{y_{j+\frac{1}{2}}^{2,\mu}\}_{\mu=1}^N = \mathbb{Q}_{j+1}^{1,y}$, and operators $\delta_{i+\frac{1}{2},j+\frac{1}{2}}^x, \delta_{i+\frac{1}{2},j+\frac{1}{2}}^y$ are defined by

$$\begin{aligned} \delta_{i+\frac{1}{2},j+\frac{1}{2}}^x(f) &:= \sum_{\kappa,\alpha} \frac{\omega_\alpha}{2} \left(f(x_{i+1}, y_{j+\frac{1}{2}}^{\kappa,\alpha}) - f(x_i, y_{j+\frac{1}{2}}^{\kappa,\alpha}) \right), \\ \delta_{i+\frac{1}{2},j+\frac{1}{2}}^y(f) &:= \sum_{\kappa,\alpha} \frac{\omega_\alpha}{2} \left(f(x_{i+\frac{1}{2}}, y_{j+1}^{\kappa,\alpha}) - f(x_{i+\frac{1}{2}}, y_j^{\kappa,\alpha}) \right). \end{aligned}$$

Then the WB CDG discretization on the dual mesh is given by

$$\begin{aligned} \int_{I_{i+\frac{1}{2},j+\frac{1}{2}}} \frac{\partial \mathbf{U}_h^D}{\partial t} w dx dy &= \frac{1}{\tau_{max}} \int_{I_{i+\frac{1}{2},j+\frac{1}{2}}} (\mathbf{U}_h^C - \mathbf{U}_h^D) w dx dy + \frac{1}{\tau_{max}} \int_{I_{i+\frac{1}{2},j+\frac{1}{2}}} (\mathbf{U}_h^{s,D} - \mathbf{U}_h^{s,C}) w dx dy \\ &+ \frac{\Delta x \Delta y}{4} \sum_{\kappa,\alpha} \sum_{\sigma,\mu} \omega_\alpha \omega_\mu \mathbf{F}(\mathbf{U}_h^C(x_{i+\frac{1}{2}}^{\kappa,\alpha}, y_{j+\frac{1}{2}}^{\sigma,\mu})) \nabla w(x_{i+\frac{1}{2}}^{\kappa,\alpha}, y_{j+\frac{1}{2}}^{\sigma,\mu}) \\ &- \Delta y \delta_{i+\frac{1}{2},j+\frac{1}{2}}^x (\mathbf{F}_1(\mathbf{U}_h^C) w) - \Delta x \delta_{i+\frac{1}{2},j+\frac{1}{2}}^y (\mathbf{F}_2(\mathbf{U}_h^C) w) + \langle \mathbf{S}_h^C, w \rangle_{i+\frac{1}{2},j+\frac{1}{2}}. \end{aligned} \quad (40)$$

Theorem 4.1. *For the two-dimensional Euler equations (30) with gravity, our semi-discrete CDG schemes (39)–(40) are WB for the stationary hydrostatic solution (33).*

Proof. The proof is similar to that of Theorem 3.1 and thus is omitted here. ■

Remark 4.1 (WB Implementation of Boundary Conditions). *A suitable implementation of boundary conditions is also essential for preserving the WB property. Take the solid wall boundary as example, which may appear in the bottom of atmosphere as in weather modeling (see, e.g., the rising thermal bubble problem in Section 5.2.6). Suppose the spatial domain $\Omega = [x_{\min}, x_{\max}] \times [y_{\min}, y_{\max}]$ is divided into $N_x \times N_y$ uniform cells, with*

$$x_{\min} = x_{\frac{1}{2}} < x_{\frac{3}{2}} < \dots < x_{N_x+\frac{1}{2}} = x_{\max}, \quad y_{\min} = y_{\frac{1}{2}} < y_{\frac{3}{2}} < \dots < y_{N_y+\frac{1}{2}} = y_{\max}.$$

We implement the reflective boundary conditions on the solid wall as follows:

- *For the right boundary, we set*

$$\begin{aligned} \rho_{N_x+1,j}^C(x,y) &= \rho_{N_x,j}^C(2x_{\max} - x, y), \quad \rho_{N_x+\frac{1}{2},j+\frac{1}{2}}^D(x,y) = \rho_{N_x+\frac{1}{2},j+\frac{1}{2}}^D(2x_{\max} - x, y), \\ m_{1,N_x+1,j}^C(x,y) &= -m_{1,N_x,j}^C(2x_{\max} - x, y), \quad m_{1,N_x+\frac{1}{2},j+\frac{1}{2}}^D(x,y) = -m_{1,N_x+\frac{1}{2},j+\frac{1}{2}}^D(2x_{\max} - x, y). \end{aligned}$$

The boundary conditions for $m_{2,h}^C(x,y), E_h^C(x,y)$ and $m_{2,h}^D(x,y), E_h^D(x,y)$ are same as the density. The left boundary condition is similar to the right.

- *Analogously, for the top boundary, we set*

$$\begin{aligned} \rho_{i,N_y+1}^C(x,y) &= \rho_{i,N_y}^C(x, 2y_{\max} - y), \quad \rho_{i+\frac{1}{2},N_y+\frac{1}{2}}^D(x,y) = \rho_{i+\frac{1}{2},N_y+\frac{1}{2}}^D(x, 2y_{\max} - y), \\ m_{2,i,N_y+1}^C(x,y) &= -m_{2,i,N_y}^C(x, 2y_{\max} - y), \quad m_{2,i+\frac{1}{2},N_y+\frac{1}{2}}^D(x,y) = -m_{2,i+\frac{1}{2},N_y+\frac{1}{2}}^D(x, 2y_{\max} - y). \end{aligned}$$

The boundary conditions for $m_{1,h}^C(x,y), E_h^C(x,y)$ and $m_{1,h}^D(x,y), E_h^D(x,y)$ are same as the density. The bottom boundary condition is similar to the top.

It is worth noting that, in order to preserve the WB property, we should also apply the same reflective boundary conditions to the projected hydrostatic solutions $\rho_h^{s,C}, p_h^{s,C}$ and $\rho_h^{s,D}, p_h^{s,D}$ for consistency. The implementations for other boundary conditions are similar and omitted here.

4.3 Positivity-preserving WB CDG schemes

4.3.1 Properties of admissible states

The set of admissible states of the two-dimensional Euler equations (30) is defined by

$$G = \left\{ \mathbf{U} = (\rho, \mathbf{m}, E)^\top : \rho > 0, p(\mathbf{U}) = (\gamma - 1) \left(E - \frac{|\mathbf{m}|^2}{2\rho} \right) > 0 \right\},$$

which is a convex set [69].

Lemma 4.1. For any $\mathbf{U} \in G$ and $\mathbf{b} \in \mathbb{R}^2$, one has $\mathbf{U} + \lambda \mathbf{S}(\mathbf{U}, \mathbf{b}) \in G$ under the condition

$$|\lambda| < \frac{1}{|\mathbf{b}|} \sqrt{\frac{2p}{(\gamma - 1)\rho}}.$$

Proof. The proof can be found in, for example, [57, Page A476]. ■

Lemma 4.2. For any $\mathbf{U} \in G$ and $\lambda \in \mathbb{R}$, the states $\mathbf{U} - \lambda \mathbf{F}_1(\mathbf{U}) \in G$ and $\mathbf{U} - \lambda \mathbf{F}_2(\mathbf{U}) \in G$ under the conditions $|\lambda| a_x(\mathbf{U}) \leq 1$ and $|\lambda| a_y(\mathbf{U}) \leq 1$, respectively. Here $a_x(\mathbf{U}) := |u_1| + \sqrt{\gamma p / \rho}$ and $a_y(\mathbf{U}) := |u_2| + \sqrt{\gamma p / \rho}$.

Proof. The proof is similar to that of Lemma 3.3 and can be found in, for example, [69, 52]. ■

4.3.2 Positivity-preserving analysis

Let us derive the semi-discrete scheme satisfied by the cell averages of the WB CDG method (39)–(40). Denote

$$\bar{\mathbf{U}}_{ij}^C(t) = \frac{1}{\Delta x \Delta y} \int_{I_{i,j}} \mathbf{U}_h^C(x, y, t) dx dy, \quad \bar{\mathbf{U}}_{i+\frac{1}{2}, j+\frac{1}{2}}^D(t) = \frac{1}{\Delta x \Delta y} \int_{I_{i+\frac{1}{2}, j+\frac{1}{2}}} \mathbf{U}_h^D(x, y, t) dx dy.$$

Taking the test function $v = 1$ in (39) and $w = 1$ in (40) and using the crucial identities in (38) gives

$$\frac{d\bar{\mathbf{U}}_{ij}^C}{dt} = \frac{(\bar{\mathbf{U}}_{ij}^D - \bar{\mathbf{U}}_{ij}^C)}{\tau_{max}} - \frac{\delta_{ij}^x(\mathbf{F}_1(\mathbf{U}_h^D))}{\Delta x} - \frac{\delta_{ij}^y(\mathbf{F}_2(\mathbf{U}_h^D))}{\Delta y} + \frac{\langle \mathbf{S}_h^D, 1 \rangle_{ij}}{\Delta x \Delta y}, \quad (41)$$

$$\begin{aligned} \frac{d\bar{\mathbf{U}}_{i+\frac{1}{2}, j+\frac{1}{2}}^D}{dt} &= \frac{(\bar{\mathbf{U}}_{i+\frac{1}{2}, j+\frac{1}{2}}^C - \bar{\mathbf{U}}_{i+\frac{1}{2}, j+\frac{1}{2}}^D)}{\tau_{max}} - \frac{\delta_{i+\frac{1}{2}, j+\frac{1}{2}}^x(\mathbf{F}_1(\mathbf{U}_h^C))}{\Delta x} \\ &\quad - \frac{\delta_{i+\frac{1}{2}, j+\frac{1}{2}}^y(\mathbf{F}_2(\mathbf{U}_h^C))}{\Delta y} + \frac{\langle \mathbf{S}_h^C, 1 \rangle_{i+\frac{1}{2}, j+\frac{1}{2}}}{\Delta x \Delta y}. \end{aligned} \quad (42)$$

Denote the right-hand sides of (41) and (42) by $\mathbf{L}_{ij}^C(\mathbf{U}_h^C, \mathbf{U}_h^D)$ and $\mathbf{L}_{i+\frac{1}{2},j+\frac{1}{2}}^D(\mathbf{U}_h^D, \mathbf{U}_h^C)$, respectively. In other words, we have

$$\frac{d\bar{\mathbf{U}}_{ij}^C}{dt} = \mathbf{L}_{ij}^C(\mathbf{U}_h^C, \mathbf{U}_h^D), \quad \frac{d\bar{\mathbf{U}}_{i+\frac{1}{2},j+\frac{1}{2}}^D}{dt} = \mathbf{L}_{i+\frac{1}{2},j+\frac{1}{2}}^D(\mathbf{U}_h^D, \mathbf{U}_h^C). \quad (43)$$

On each primal cell $I_{i,j}$, we define the point set

$$\mathbb{S}_{ij} = \mathbb{S}_{ij}^{1,1} \cup \mathbb{S}_{ij}^{1,2} \cup \mathbb{S}_{ij}^{2,1} \cup \mathbb{S}_{ij}^{2,2}, \quad \mathbb{Q}_{ij} = \mathbb{Q}_{ij}^{1,1} \cup \mathbb{Q}_{ij}^{1,2} \cup \mathbb{Q}_{ij}^{2,1} \cup \mathbb{Q}_{ij}^{2,2},$$

$$\mathbb{S}_{ij}^{\kappa,\tau} = (\mathbb{Q}_i^{\kappa,x} \otimes \mathbb{L}_j^{\tau,y}) \cup (\mathbb{L}_i^{\kappa,x} \otimes \mathbb{Q}_j^{\tau,y}) \cup (\mathbb{Q}_i^{\kappa,x} \otimes \mathbb{Q}_j^{\tau,y}), \quad \mathbb{Q}_{ij}^{\kappa,\tau} = \mathbb{Q}_i^{\kappa,x} \otimes \mathbb{Q}_j^{\tau,y}, \quad \kappa, \tau \in \{1, 2\},$$

and the parameters $\tilde{\alpha}_{x,ij}^D$ and $\tilde{\alpha}_{y,ij}^D$ by

$$\tilde{\alpha}_{x,ij}^D = \tilde{\alpha}_{x,1}^D + \tilde{\alpha}_{x,2}^D, \quad \tilde{\alpha}_{x,1}^D = \max_{(x,y) \in \mathbb{S}_{ij}} a_x(U_h^D), \quad \tilde{\alpha}_{x,2}^D = \frac{\hat{\omega}_1 \Delta x}{4} \tilde{\alpha}_s^D,$$

$$\tilde{\alpha}_{y,ij}^D = \tilde{\alpha}_{y,1}^D + \tilde{\alpha}_{y,2}^D, \quad \tilde{\alpha}_{y,1}^D = \max_{(x,y) \in \mathbb{S}_{ij}} a_y(U_h^D), \quad \tilde{\alpha}_{y,2}^D = \frac{\hat{\omega}_1 \Delta y}{4} \tilde{\alpha}_s^D,$$

where

$$\tilde{\alpha}_s^D = \max_{(x,y) \in \mathbb{Q}_{ij}} \left\{ |\nabla \hat{\phi}_h^D| \sqrt{\frac{(\gamma-1)\rho_h^D}{2p_h^D}} \right\}, \quad \nabla \hat{\phi}_h^D = -\frac{\nabla p_h^{s,D}}{\rho_h^{s,D}} - \frac{\left(\llbracket p_h^{s,D} \rrbracket_{ij}^x, \llbracket p_h^{s,D} \rrbracket_{ij}^y \right)^\top}{(\rho_h^{s,D})_{ij} \Delta x \Delta y},$$

$$\llbracket p_h^{s,D} \rrbracket_{ij}^x := \int_{y_{j-\frac{1}{2}}}^{y_{j+\frac{1}{2}}} \left(p_h^{s,D}(x_i^+, y) - p_h^{s,D}(x_i^-, y) \right) dy, \quad \llbracket p_h^{s,D} \rrbracket_{ij}^y := \int_{x_{i-\frac{1}{2}}}^{x_{i+\frac{1}{2}}} \left(p_h^{s,D}(x, y_j^+) - p_h^{s,D}(x, y_j^-) \right) dx.$$

Similarly, on each dual cell $I_{i+\frac{1}{2},j+\frac{1}{2}}$, we define the point set $\mathbb{S}_{i+\frac{1}{2},j+\frac{1}{2}}$ and $\mathbb{Q}_{i+\frac{1}{2},j+\frac{1}{2}}$, which are respectively the shifts of the point sets $\mathbb{S}_{i,j}$ and $\mathbb{Q}_{i,j}$ with $\frac{\Delta x}{2}$ in the x -direction and $\frac{\Delta y}{2}$ in the y -direction, and the parameters $\tilde{\alpha}_{x,i+\frac{1}{2},j+\frac{1}{2}}^C$ and $\tilde{\alpha}_{y,i+\frac{1}{2},j+\frac{1}{2}}^C$ by

$$\tilde{\alpha}_{x,i+\frac{1}{2},j+\frac{1}{2}}^C = \tilde{\alpha}_{x,1}^C + \tilde{\alpha}_{x,2}^C, \quad \tilde{\alpha}_{x,1}^C = \max_{(x,y) \in \mathbb{S}_{i+\frac{1}{2},j+\frac{1}{2}}} a_x(\mathbf{U}_h^C), \quad \tilde{\alpha}_{x,2}^C = \frac{\hat{\omega}_1 \Delta x}{4} \tilde{\alpha}_s^C,$$

$$\tilde{\alpha}_{y,i+\frac{1}{2},j+\frac{1}{2}}^C = \tilde{\alpha}_{y,1}^C + \tilde{\alpha}_{y,2}^C, \quad \tilde{\alpha}_{y,1}^C = \max_{(x,y) \in \mathbb{S}_{i+\frac{1}{2},j+\frac{1}{2}}} a_y(\mathbf{U}_h^C), \quad \tilde{\alpha}_{y,2}^C = \frac{\hat{\omega}_1 \Delta y}{4} \tilde{\alpha}_s^C,$$

where

$$\tilde{\alpha}_s^C = \max_{(x,y) \in \mathbb{Q}_{i+\frac{1}{2},j+\frac{1}{2}}} \left\{ |\nabla \hat{\phi}_h^C| \sqrt{\frac{(\gamma-1)\rho_h^C}{2p_h^C}} \right\}, \quad \nabla \hat{\phi}_h^C = -\frac{\nabla p_h^{s,C}}{\rho_h^{s,C}} - \frac{\left(\llbracket p_h^{s,C} \rrbracket_{i+\frac{1}{2},j+\frac{1}{2}}^x, \llbracket p_h^{s,C} \rrbracket_{i+\frac{1}{2},j+\frac{1}{2}}^y \right)^\top}{(\rho_h^{s,C})_{i+\frac{1}{2},j+\frac{1}{2}} \Delta x \Delta y},$$

with

$$\llbracket p_h^{s,C} \rrbracket_{i+\frac{1}{2},j+\frac{1}{2}}^x := \int_{y_j}^{y_{j+1}} \left(p_h^{s,C}(x_{i+\frac{1}{2}}^+, y) - p_h^{s,C}(x_{i+\frac{1}{2}}^-, y) \right) dy,$$

$$\llbracket p_h^{s,C} \rrbracket_{i+\frac{1}{2},j+\frac{1}{2}}^y := \int_{x_i}^{x_{i+1}} \left(p_h^{s,C}(x, y_{j+\frac{1}{2}}^+) - p_h^{s,C}(x, y_{j+\frac{1}{2}}^-) \right) dx.$$

Theorem 4.2. Assume that the numerical solutions $\mathbf{U}_h^C(x, y), \mathbf{U}_h^D(x, y)$ satisfy

$$\mathbf{U}_h^C(x, y) \in G \quad \forall (x, y) \in \mathbb{S}_{ij}, \quad \mathbf{U}_h^D(x, y) \in G \quad \forall (x, y) \in \mathbb{S}_{i+\frac{1}{2}, j+\frac{1}{2}}, \quad \forall i, j, \quad (44)$$

and the projected stationary hydrostatic solutions $\mathbf{U}_h^{s,C}(x, y), \mathbf{U}_h^{s,D}(x, y)$ satisfy

$$\mathbf{U}_h^{s,C}(x, y) \in G \quad \forall (x, y) \in \mathbb{S}_{ij}, \quad \mathbf{U}_h^{s,D}(x, y) \in G \quad \forall (x, y) \in \mathbb{S}_{i+\frac{1}{2}, j+\frac{1}{2}}, \quad \forall i, j.$$

If $\bar{\mathbf{U}}_{ij}^C, \bar{\mathbf{U}}_{i+\frac{1}{2}, j+\frac{1}{2}}^D \in G$, then the positivity-preserving property

$$\bar{\mathbf{U}}_{ij}^C + \Delta t \mathbf{L}_{ij}^C(\mathbf{U}_h^C, \mathbf{U}_h^D) \in G, \quad \bar{\mathbf{U}}_{i+\frac{1}{2}, j+\frac{1}{2}}^D + \Delta t \mathbf{L}_{i+\frac{1}{2}, j+\frac{1}{2}}^D(\mathbf{U}_h^D, \mathbf{U}_h^C) \in G, \quad \forall i, j,$$

holds under the CFL-type condition

$$\frac{\Delta t}{\Delta x} \tilde{\alpha}_x + \frac{\Delta t}{\Delta y} \tilde{\alpha}_y < \frac{\theta \hat{\omega}_1}{2}, \quad \theta = \frac{\Delta t}{\tau_{max}} \in (0, 1],$$

with

$$\tilde{\alpha}_x = \max_{i,j} \max \{ \tilde{\alpha}_{x,ij}^D, \tilde{\alpha}_{x,i+\frac{1}{2},j+\frac{1}{2}}^C \}, \quad \tilde{\alpha}_y = \max_{i,j} \max \{ \tilde{\alpha}_{y,ij}^D, \tilde{\alpha}_{y,i+\frac{1}{2},j+\frac{1}{2}}^C \}.$$

Proof. Using (43) gives

$$\begin{aligned} \bar{\mathbf{U}}_{ij}^C + \Delta t \mathbf{L}_{ij}^C(\mathbf{U}_h^C, \mathbf{U}_h^D) &= (1 - \theta) \bar{\mathbf{U}}_{ij}^C + \theta \bar{\mathbf{U}}_{ij}^D + \frac{\Delta t}{\Delta x \Delta y} \langle \mathbf{S}_h^D, \mathbf{1} \rangle_{ij} \\ &\quad - \lambda_x \delta_{ij}^x(\mathbf{F}_1(\mathbf{U}_h^D)) - \lambda_y \delta_{ij}^y(\mathbf{F}_2(\mathbf{U}_h^D)) \\ &= (1 - \theta) \bar{\mathbf{U}}_{ij}^C + \left(\eta \theta \bar{\mathbf{U}}_{ij}^D + \frac{\Delta t}{\Delta x \Delta y} \langle \mathbf{S}_h^D, \mathbf{1} \rangle_{ij} \right) \\ &\quad + \left((1 - \eta) \theta \bar{\mathbf{U}}_{ij}^D - \lambda_x \delta_{ij}^x(\mathbf{F}_1(\mathbf{U}_h^D)) - \lambda_y \delta_{ij}^y(\mathbf{F}_2(\mathbf{U}_h^D)) \right) \\ &= (1 - \theta) \bar{\mathbf{U}}_{ij}^C + \eta \theta \mathbf{L}_{h,S} + (1 - \eta) \theta \mathbf{L}_{h,F}, \end{aligned}$$

where $\lambda_x = \frac{\Delta t}{\Delta x}, \lambda_y = \frac{\Delta t}{\Delta y}, \theta = \frac{\Delta t}{\tau_{max}}, \eta \in (0, 1)$ is a constant, and $\mathbf{L}_{h,F}$ and $\mathbf{L}_{h,S}$ are defined by

$$\begin{aligned} \mathbf{L}_{h,F} &= \bar{\mathbf{U}}_{ij}^D - \frac{\lambda_x}{(1 - \eta) \theta} \delta_{ij}^x(\mathbf{F}_1(\mathbf{U}_h^D)) - \frac{\lambda_y}{(1 - \eta) \theta} \delta_{ij}^y(\mathbf{F}_2(\mathbf{U}_h^D)), \\ \mathbf{L}_{h,S} &= \bar{\mathbf{U}}_{ij}^D + \frac{\Delta t}{\eta \theta \Delta x \Delta y} \langle \mathbf{S}_h^D, \mathbf{1} \rangle_{ij}. \end{aligned}$$

Using the convexity of set G and the exactness of the quadrature rule can derive that

$$\begin{aligned} \bar{\mathbf{U}}_{ij}^D &= \frac{1}{\Delta x \Delta y} \int_{I_{ij}} \mathbf{U}_h^D(x, y) dx dy = \frac{1}{\Delta x} \int_{x_{i-\frac{1}{2}}}^{x_{i+\frac{1}{2}}} \left(\frac{1}{2} \sum_{\kappa=1}^2 \sum_{\alpha=1}^N \omega_\alpha \mathbf{U}_h^D(x, y_j^{\kappa, \alpha}) \right) dx \\ &= \frac{1}{2} \sum_{\kappa=1}^2 \sum_{\alpha=1}^N \omega_\alpha \left(\frac{1}{\Delta x} \int_{x_{i-\frac{1}{2}}}^{x_{i+\frac{1}{2}}} \mathbf{U}_h^D(x, y_j^{\kappa, \alpha}) dx \right) = \frac{1}{2} \sum_{\kappa=1}^2 \sum_{\alpha=1}^N \omega_\alpha \left(\frac{1}{2} \sum_{\tau=1}^2 \sum_{\beta=1}^L \hat{\omega}_\beta \mathbf{U}_h^D(\hat{x}_i^{\tau, \beta}, y_j^{\kappa, \alpha}) \right) \\ &= \frac{1}{2} \sum_{\kappa=1}^2 \sum_{\alpha=1}^N \omega_\alpha \left(\frac{\hat{\omega}_1}{2} \mathbf{U}_h^D(x_{i-\frac{1}{2}}, y_j^{\kappa, \alpha}) + \frac{\hat{\omega}_1}{2} \mathbf{U}_h^D(x_{i+\frac{1}{2}}, y_j^{\kappa, \alpha}) + (1 - \hat{\omega}_1) \mathbb{E}_{1,ij}^\alpha \right), \end{aligned}$$

where $\hat{\omega}_1 = \hat{\omega}_L$ has been used, and

$$\mathbb{E}_{1,ij}^\alpha = \frac{1}{(1-\hat{\omega}_1)} \left(\frac{1}{2} \sum_{\beta=2}^L \hat{\omega}_\beta \mathbf{U}_h^D(\hat{x}_i^{1,\beta}, y_j^{\kappa,\alpha}) + \frac{1}{2} \sum_{\beta=1}^{L-1} \hat{\omega}_\beta \mathbf{U}_h^D(\hat{x}_i^{2,\beta}, y_j^{\kappa,\alpha}) \right) \in G.$$

Similarly, one has

$$\bar{\mathbf{U}}_{ij}^D = \frac{1}{2} \sum_{\kappa=1}^2 \sum_{\alpha=1}^N \omega_\alpha \left(\frac{\hat{\omega}_1}{2} \mathbf{U}_h^D(x_i^{\kappa,\alpha}, y_{j-\frac{1}{2}}) + \frac{\hat{\omega}_1}{2} \mathbf{U}_h^D(x_i^{\kappa,\alpha}, y_{j+\frac{1}{2}}) + (1-\hat{\omega}_1) \mathbb{E}_{2,ij}^\alpha \right),$$

with

$$\mathbb{E}_{2,ij}^\alpha = \frac{1}{(1-\hat{\omega}_1)} \left(\frac{1}{2} \sum_{\beta=2}^L \hat{\omega}_\beta \mathbf{U}_h^D(x_i^{\kappa,\alpha}, \hat{y}_j^{1,\beta}) + \frac{1}{2} \sum_{\beta=1}^{L-1} \hat{\omega}_\beta \mathbf{U}_h^D(x_i^{\kappa,\alpha}, \hat{y}_j^{2,\beta}) \right) \in G.$$

Note that $\mathbf{L}_{h,\mathbf{F}}$ can be reformulated as

$$\mathbf{L}_{h,\mathbf{F}} = \frac{a_x \lambda_x}{\lambda} \left(\bar{\mathbf{U}}_{ij}^D - \frac{\lambda}{(1-\eta)\theta a_x} \delta_{ij}^x(\mathbf{F}_1(\mathbf{U}_h^D)) \right) + \frac{a_y \lambda_y}{\lambda} \left(\bar{\mathbf{U}}_{ij}^D - \frac{\lambda}{(1-\eta)\theta a_y} \delta_{ij}^y(\mathbf{F}_2(\mathbf{U}_h^D)) \right),$$

where $\lambda = a_x \lambda_x + a_y \lambda_y$, $a_x = \tilde{\alpha}_{x,1}^D$, $a_y = \tilde{\alpha}_{y,1}^D$, and

$$\begin{aligned} \bar{\mathbf{U}}_{ij}^D - \frac{\lambda}{(1-\eta)\theta a_x} \delta_{ij}^x(\mathbf{F}_1(\mathbf{U}_h^D)) &= \frac{1}{2} \sum_{\kappa=1}^2 \sum_{\alpha=1}^N \omega_\alpha \left(\frac{\hat{\omega}_1}{2} \mathbb{E}_{1,i-\frac{1}{2},j}^+ + \frac{\hat{\omega}_1}{2} \mathbb{E}_{1,i+\frac{1}{2},j}^- + (1-\hat{\omega}_1) \mathbb{E}_{1,ij}^\alpha \right), \\ \bar{\mathbf{U}}_{ij}^D - \frac{\lambda}{(1-\eta)\theta a_y} \delta_{ij}^y(\mathbf{F}_2(\mathbf{U}_h^D)) &= \frac{1}{2} \sum_{\kappa=1}^2 \sum_{\alpha=1}^N \omega_\alpha \left(\frac{\hat{\omega}_1}{2} \mathbb{E}_{2,i,j-\frac{1}{2}}^+ + \frac{\hat{\omega}_1}{2} \mathbb{E}_{2,i,j+\frac{1}{2}}^- + (1-\hat{\omega}_1) \mathbb{E}_{2,ij}^\alpha \right), \end{aligned}$$

with

$$\begin{aligned} \mathbb{E}_{1,i\mp\frac{1}{2},j}^\pm &= \mathbf{U}_h^D(x_{i\mp\frac{1}{2}}, y_j^{\kappa,\alpha}) \pm \frac{2\lambda}{\hat{\omega}_1(1-\eta)\theta a_x} \mathbf{F}_1(\mathbf{U}_h^D(x_{i\mp\frac{1}{2}}, y_j^{\kappa,\alpha})), \\ \mathbb{E}_{2,i,j\mp\frac{1}{2}}^\pm &= \mathbf{U}_h^D(x_i^{\kappa,\alpha}, y_{j\mp\frac{1}{2}}) \pm \frac{2\lambda}{\hat{\omega}_1(1-\eta)\theta a_y} \mathbf{F}_2(\mathbf{U}_h^D(x_i^{\kappa,\alpha}, y_{j\mp\frac{1}{2}})). \end{aligned}$$

Thanks to Lemma 4.2, we have $\mathbb{E}_{1,i\mp\frac{1}{2},j}^\pm \in G$ and $\mathbb{E}_{2,i,j\mp\frac{1}{2}}^\pm \in G$, as long as

$$\lambda_x \tilde{\alpha}_{x,1}^D + \lambda_y \tilde{\alpha}_{y,1}^D < \frac{(1-\eta)\theta \hat{\omega}_1}{2}. \quad (45)$$

Using the convexity of G , we further obtain $\mathbf{L}_{h,\mathbf{F}} \in G$ under (45). Next, we discuss the term $\mathbf{L}_{h,\mathbf{S}}$. The source term approximations $\langle (S_{2,h}^D, S_{3,h}^D)^\top, 1 \rangle_{ij}$ in the momentum equations are

$$\begin{aligned} \langle (S_{2,h}^D, S_{3,h}^D)^\top, 1 \rangle_{ij} &= \frac{\Delta x \Delta y}{4} \sum_{\kappa,\alpha} \sum_{\tau,\beta} \omega_\alpha \omega_\beta \left(\frac{\rho_h^D(x_i^{\kappa,\alpha}, y_j^{\tau,\beta})}{\rho_h^{s,D}(x_i^{\kappa,\alpha}, y_j^{\tau,\beta})} - \frac{(\overline{\rho_h^D})_{ij}}{(\overline{\rho_h^{s,D}})_{ij}} \right) (\nabla p_h^{s,D})(x_i^{\kappa,\alpha}, y_j^{\tau,\beta}) \\ &\quad + \frac{(\overline{\rho_h^D})_{ij}}{(\overline{\rho_h^{s,D}})_{ij}} \left(\Delta y \delta_{ij}^x(p_h^{s,D}), \Delta x \delta_{ij}^y(p_h^{s,D}) \right)^\top. \end{aligned}$$

Based on

$$\begin{aligned} \int_{I_{ij}} \nabla p_h^{s,D} dx dy &= \frac{\Delta x \Delta y}{4} \sum_{\kappa, \alpha} \sum_{\tau, \beta} \omega_\alpha \omega_\beta \nabla p_h^{s,D}(x_i^{\kappa, \alpha}, y_j^{\tau, \beta}), \\ \int_{\partial I_{ij}} p_h^{s,D} \mathbf{n} ds &= \left(\Delta y \delta_{ij}^x(p_h^{s,D}), \Delta x \delta_{ij}^y(p_h^{s,D}) \right)^\top, \end{aligned}$$

and the identity

$$\int_{\partial I_{ij}} p_h^{s,D} \mathbf{n} ds - \int_{I_{ij}} \nabla p_h^{s,D} dx dy = \left(\llbracket p_h^{s,D} \rrbracket_{ij}^x, \llbracket p_h^{s,D} \rrbracket_{ij}^y \right)^\top,$$

we reformulate $\langle (S_{2,h}^D, S_{3,h}^D)^\top, 1 \rangle_{ij}$ as

$$\begin{aligned} \langle (S_{2,h}^D, S_{3,h}^D)^\top, 1 \rangle_{ij} &= \frac{\Delta x \Delta y}{4} \sum_{\kappa, \alpha} \sum_{\tau, \beta} \omega_\alpha \omega_\beta \frac{\rho_h^D(x_i^{\kappa, \alpha}, y_j^{\tau, \beta})}{\rho_h^{s,D}(x_i^{\kappa, \alpha}, y_j^{\tau, \beta})} (\nabla p_h^{s,D})(x_i^{\kappa, \alpha}, y_j^{\tau, \beta}) \\ &+ \frac{(\overline{\rho_h^D})_{ij}}{(\rho_h^{s,D})_{ij}} \left(\llbracket p_h^{s,D} \rrbracket_{ij}^x, \llbracket p_h^{s,D} \rrbracket_{ij}^y \right)^\top = -\frac{\Delta x \Delta y}{4} \sum_{\kappa, \alpha} \sum_{\tau, \beta} \omega_\alpha \omega_\beta \rho_h^D(x_i^{\kappa, \alpha}, y_j^{\tau, \beta}) \nabla \hat{\phi}_h^D(x_i^{\kappa, \alpha}, y_j^{\tau, \beta}), \end{aligned}$$

where

$$-\nabla \hat{\phi}_h^D(x_i^{\kappa, \alpha}, y_j^{\tau, \beta}) = \frac{\nabla p_h^{s,D}(x_i^{\kappa, \alpha}, y_j^{\tau, \beta})}{\rho_h^{s,D}(x_i^{\kappa, \alpha}, y_j^{\tau, \beta})} + \frac{\left(\llbracket p_h^{s,D} \rrbracket_{ij}^x, \llbracket p_h^{s,D} \rrbracket_{ij}^y \right)^\top}{(\rho_h^{s,D})_{ij} \Delta x \Delta y}.$$

Similarly, we can rewrite $\langle S_{4,h}^D, 1 \rangle_{ij}$ in the energy equation as

$$\langle S_{4,h}^D, 1 \rangle_{ij} = -\frac{\Delta x \Delta y}{4} \sum_{\kappa, \alpha} \sum_{\tau, \beta} \omega_\alpha \omega_\beta \mathbf{m}_h^D(x_i^{\kappa, \alpha}, y_j^{\tau, \beta}) \cdot \nabla \hat{\phi}_h^D(x_i^{\kappa, \alpha}, y_j^{\tau, \beta}).$$

Thus, $\mathbf{L}_{h,S} = \overline{\mathbf{U}}_{ij}^D + \frac{\Delta t}{\eta \theta \Delta x \Delta y} \langle \mathbf{S}_h^D, 1 \rangle_{ij}$ can be reformulated as

$$\mathbf{L}_{h,S} = \sum_{\kappa, \alpha} \sum_{\tau, \beta} \frac{\omega_\alpha \omega_\beta}{4} \left(\mathbf{U}_h^D(x_i^{\kappa, \alpha}, y_j^{\tau, \beta}) + \frac{\Delta t}{\eta \theta} \hat{\mathbf{S}}_h^D(x_i^{\kappa, \alpha}, y_j^{\tau, \beta}) \right),$$

with $\hat{\mathbf{S}}_h^D(x_i^{\kappa, \alpha}, y_j^{\tau, \beta}) := \left(0, -(\rho_h^D \nabla \hat{\phi}_h^D)(x_i^{\kappa, \alpha}, y_j^{\tau, \beta}), -(\mathbf{m}_h^D \cdot \nabla \hat{\phi}_h^D)(x_i^{\kappa, \alpha}, y_j^{\tau, \beta}) \right)^\top$. Thanks to Lemma 4.1, we have $\mathbf{L}_{h,S} \in G$ under the condition

$$\Delta t < \eta \theta \min_{(x,y) \in \mathbb{Q}_{ij}} \left\{ \frac{1}{|\nabla \hat{\phi}_h^D|} \sqrt{\frac{2\rho_h^D}{(\gamma-1)\rho_h^D}} \right\},$$

or equivalently

$$\lambda_x \tilde{\alpha}_{x,2}^D + \lambda_y \tilde{\alpha}_{y,2}^D < \frac{\eta \theta \hat{\omega}_1}{2}.$$

Combining those results, we conclude that if

$$(\lambda_x, \lambda_y) \in \left\{ (\lambda_x, \lambda_y) \in (\mathbb{R}^+)^2 : \lambda_x \tilde{\alpha}_{x,1}^D + \lambda_y \tilde{\alpha}_{y,1}^D < \frac{(1-\eta)\theta \hat{\omega}_1}{2}, \lambda_x \tilde{\alpha}_{x,2}^D + \lambda_y \tilde{\alpha}_{y,2}^D < \frac{\eta \theta \hat{\omega}_1}{2} \right\}, \quad (46)$$

then $\bar{\mathbf{U}}_{ij}^C + \Delta t \mathbf{L}_{ij}^C(\mathbf{U}_h^C, \mathbf{U}_h^D) \in G$. Since the parameters η can be chosen arbitrarily in this proof, we specify

$$\eta = \frac{\lambda_x \tilde{\alpha}_{x,2}^D + \lambda_y \tilde{\alpha}_{y,2}^D}{\lambda_x \tilde{\alpha}_{x,ij}^D + \lambda_y \tilde{\alpha}_{y,ij}^D} = \frac{\lambda_x \tilde{\alpha}_{x,2}^D + \lambda_y \tilde{\alpha}_{y,2}^D}{\lambda_x (\tilde{\alpha}_{x,1}^D + \tilde{\alpha}_{x,2}^D) + \lambda_y (\tilde{\alpha}_{y,1}^D + \tilde{\alpha}_{y,2}^D)},$$

so that the condition (46) becomes

$$\lambda_x (\tilde{\alpha}_{x,1}^D + \tilde{\alpha}_{x,2}^D) + \lambda_y (\tilde{\alpha}_{y,1}^D + \tilde{\alpha}_{y,2}^D) = \lambda_x \tilde{\alpha}_{x,ij}^D + \lambda_y \tilde{\alpha}_{y,ij}^D < \frac{\theta \hat{\omega}_1}{2}.$$

Similar arguments can show that $\bar{\mathbf{U}}_{i+\frac{1}{2},j+\frac{1}{2}}^D + \Delta t \mathbf{L}_{i+\frac{1}{2},j+\frac{1}{2}}^D(\mathbf{U}_h^D, \mathbf{U}_h^C) \in G$. The proof is completed. \blacksquare

Theorem 4.2 provides a sufficient condition for the proposed high-order WB CDG schemes (39) and (40) to be positivity-preserving, when the SSP time discretization is used. The condition (44) can again be enforced by a simple positivity-preserving limiter similar to the one-dimensional case; see Section 4.4. With the positivity-preserving limiter applied at each stage of the SSP Runge-Kutta method, the resulting fully discrete CDG schemes are positivity-preserving.

4.4 Positivity-preserving limiting operators

Introduce the following two sets

$$\bar{\mathbb{G}}_h^{C,k} := \left\{ \mathbf{v} \in [\mathbb{V}_h^{C,k}]^4 : \frac{1}{\Delta x \Delta y} \int_{I_{ij}} \mathbf{v}(x,y) dx dy \in G, \forall i, j \right\},$$

$$\mathbb{G}_h^{C,k} := \left\{ \mathbf{v} \in \bar{\mathbb{G}}_h^{C,k} : \mathbf{v}|_{I_{ij}}(x,y) \in G, \forall (x,y) \in \mathbb{S}_{ij}, \forall i, j \right\}.$$

For any $\mathbf{U}_h^C \in \bar{\mathbb{G}}_h^{C,k}$ with $\mathbf{U}_h^C|_{I_{ij}} := \mathbf{U}_{ij}^C(x,y)$, following [46, 69] we define the positivity-preserving limiting operator $\Pi_h^C : \bar{\mathbb{G}}_h^{C,k} \rightarrow \mathbb{G}_h^{C,k}$ as follows

$$\Pi_h^C \mathbf{U}_h^C|_{I_{ij}} = \theta_{ij}^{(2)} (\hat{\mathbf{U}}_{ij}^C(x,y) - \bar{\mathbf{U}}_{ij}^C) + \bar{\mathbf{U}}_{ij}^C, \quad \theta_{ij}^{(2)} = \min \left\{ 1, \frac{p(\bar{\mathbf{U}}_{ij}^C) - \varepsilon_2}{p(\bar{\mathbf{U}}_{ij}^C) - \min_{(x,y) \in \mathbb{S}_{ij}} p(\hat{\mathbf{U}}_{ij}^C(x,y))} \right\},$$

where $\hat{\mathbf{U}}_{ij}^C(x,y) = (\hat{\rho}_{ij}^C(x,y), \mathbf{m}_{ij}^C(x,y), E_{ij}^C(x,y))^\top$, and $\hat{\rho}_{ij}^C(x,y)$ is a modification of the density $\rho_{ij}^C(x,y)$ given by

$$\hat{\rho}_{ij}^C(x,y) = \theta_{ij}^{(1)} (\rho_{ij}^C(x,y) - \bar{\rho}_{ij}^C) + \bar{\rho}_{ij}^C, \quad \theta_{ij}^{(1)} = \min \left\{ 1, \frac{\bar{\rho}_{ij}^C - \varepsilon_1}{\bar{\rho}_{ij}^C - \min_{(x,y) \in \mathbb{S}_{ij}} \rho_{ij}^C(x,y)} \right\},$$

We take $\varepsilon_1 = \min\{10^{-13}, \bar{\rho}_{ij}^C\}$, $\varepsilon_2 = \min\{10^{-13}, p(\bar{\mathbf{U}}_{ij}^C)\}$. The sets $\bar{\mathbb{G}}_h^{D,k}, \mathbb{G}_h^{D,k}$ and the positivity-preserving limiting operator $\Pi_h^D : \bar{\mathbb{G}}_h^{D,k} \rightarrow \mathbb{G}_h^{D,k}$ defined on the dual mesh $I_{i+\frac{1}{2},j+\frac{1}{2}}$ are very similar, and the details are omitted here.

5 Numerical examples

This section presents several one- and two-dimensional tests to demonstrate the WB and positivity-preserving properties of the proposed CDG methods on uniform Cartesian meshes. The explicit third-order SSP Runge-Kutta method is employed for the time discretization. For comparison, we will also show the numerical results of the standard non-WB CDG schemes with the straightforward source term approximation and the original numerical dissipation term. Unless explained specifically, we use the ideal EOS (2) with $\gamma = 1.4$, the CFL numbers for the third-order and fourth-order CDG methods are taken as 0.25 and 0.15, respectively, and the parameter $\theta = \frac{\Delta t}{\tau_{max}} = 1$. In all the numerical examples, the schemes are implemented by using C/C++ language with double precision.

5.1 One-dimensional tests

5.1.1 Example 1: Accuracy test

We start with a one-dimensional example [41] to demonstrate the accuracy of the proposed WB CDG schemes for the Euler equations under a linear gravitational field $\phi_x = g = 1$. The time-dependent exact solution of this example is given by

$$\begin{aligned}\rho(x,t) &= 1 + 0.2 \sin(\pi(x - u_0 t)), & u(x,t) &= u_0, \\ p(x,t) &= p_0 + u_0 t - x + 0.2 \cos(\pi(x - u_0 t))/\pi,\end{aligned}$$

where the constants $u_0 = 1.0$, $p_0 = 4.5$. The computational domain $\Omega = [0, 2]$ is divided into N uniform cells and the boundary condition is set as the exact solution on $\partial\Omega$. To match the temporal and spatial accuracy, we use $\Delta t = 0.15(\Delta x)^{\frac{4}{3}}/\tilde{\alpha}_x$ for the fourth-order WB CDG scheme. The L^1 errors and corresponding convergence rates at $t = 0.1$ are shown in Tables 1 and 2. We clearly observe that the expected third-order and fourth-order convergence rates are achieved by the WB CDG schemes. This indicates that our novel projection, modification of the dissipation term and WB source term approximation do not destroy the accuracy of our proposed WB CDG schemes.

Table 1: Example 1: L^1 errors at $t = 0.1$ and corresponding convergence rates for the third-order WB CDG scheme at different grid resolutions.

N	ρ		ρu		E	
Mesh	L^1 error	Order	L^1 error	Order	L^1 error	Order
8	1.99e-04	-	2.01e-04	-	1.94e-04	-
16	2.54e-05	2.97	2.54e-05	2.98	2.39e-05	3.02
32	3.16e-06	3.01	3.17e-06	3.00	2.98e-06	3.00
64	3.96e-07	3.00	3.96e-07	3.00	3.72e-07	3.00
128	4.94e-08	3.00	4.95e-08	3.00	4.65e-08	3.00

Table 2: Same as Table 1, except for the fourth-order WB CDG scheme.

N	ρ		ρu		E	
	L^1 error	Order	L^1 error	Order	L^1 error	Order
8	3.12e-06	-	2.93e-06	-	2.70e-06	-
16	1.69e-07	4.21	1.67e-07	4.13	1.61e-07	4.07
32	9.62e-09	4.13	9.68e-09	4.11	9.74e-09	4.05
64	6.67e-10	3.85	6.75e-10	3.84	7.65e-10	3.67
128	4.05e-11	4.04	4.12e-11	4.03	4.79e-11	4.00

5.1.2 Example 2: Isothermal equilibrium test

We consider the isothermal equilibrium problem [6] under a linear gravitational field $\phi_x = g = 1$. The initial data is taken as an isothermal steady state solution

$$\rho(x) = \exp(-x), \quad u(x) = 0, \quad p(x) = \exp(-x). \quad (47)$$

The computational domain is taken as $\Omega = [0, 1]$, and the adiabatic index is $\gamma = 5/3$. We first use this example to verify the WB property of the proposed CDG method. The numerical solution is computed until $t = 2$ by using our third-order WB CDG scheme with respectively 50 and 100 uniform cells. Table 3 lists the L^1 errors between the numerical solution and the projected stationary hydrostatic solution (47). It is clearly observed that all the numerical errors are at the level of rounding error, demonstrating that the proposed CDG method satisfies the WB property.

Table 3: L^1 errors for the isothermal equilibrium test in Example 2.

Mesh	errors in ρ	errors in ρu	errors in E
50	7.71e-15	1.97e-15	4.00e-15
100	1.63e-14	4.50e-15	7.27e-15

Next, in order to check the effectiveness of our WB CDG method in capturing a small perturbation near the isothermal equilibrium solution (47), we modify the initial pressure state as

$$p(x, 0) = \exp(-x) + \eta \exp(-100(x - 0.5)^2),$$

where η is a non-zero perturbation parameter. We simulate two cases: $\eta = 10^{-2}$ and $\eta = 10^{-3}$. Outflow boundary conditions are used at $x = 0$ and $x = 1$. The pressure perturbations at $t = 0.25$ computed by our third-order WB CDG scheme on the mesh of 50 uniform cells, compared with a reference solution with 1000 cells, are displayed in Figure 1. For comparison, we also present the results simulated by the third-order non-WB CDG scheme in the same figure. The initial pressure perturbations are also plotted in the dashed curves. As we can see that the results of the WB CDG scheme agree well with the reference solutions for both cases, while the results obtained by the non-WB CDG scheme fail to capture the small perturbations. This demonstrates that our WB method is more accurate and advantageous in resolving small perturbations near the equilibrium states.

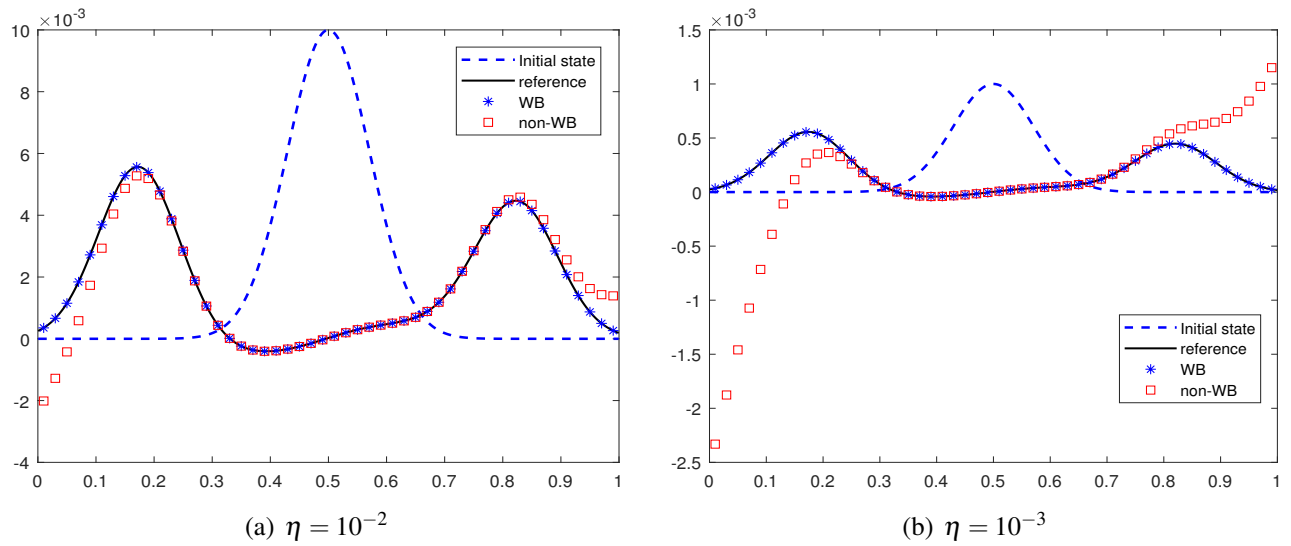


Figure 1: Example 2: Pressure perturbations at $t = 0.25$ obtained by the WB scheme and non-WB scheme with 50 uniform cells. The reference solutions are obtained by the WB scheme using 1000 cells.

5.1.3 Example 3: Rarefaction test with low density and pressure

The purpose of this example is to investigate the positivity-preserving property of our WB CDG method. We consider an extreme rarefaction problem [57] under a quadratic gravitational potential function $\phi(x) = x^2/2$, and the initial data are given by

$$\rho(x,0) = 7, \quad p(x,0) = 0.2, \quad u(x,0) = \begin{cases} -1, & x < 0, \\ 1, & x > 0. \end{cases}$$

The computational domain is set as $\Omega = [-1, 1]$ with outflow boundary conditions at $x = -1$ and $x = 1$. This test involves extremely low density and pressure, so that the positivity-preserving limiting operators are used in our simulation. Figure 2 shows the numerical solutions at $t = 0.6$ computed by our third-order positivity-preserving WB CDG scheme with 400 uniform cells, along with a reference solution with 1000 cells. As we can see that the low density and pressure wave structures are well captured by the proposed method. Our numerical scheme exhibits good robustness, and no negative density or pressure is encountered during the entire simulation.

5.1.4 Example 4: Leblanc shock tube problem under gravitational field

This example considers a Leblanc shock tube problem [57] under a linear gravitational field $\phi(x) = gx$ with $g = 1$. The initial condition is given by

$$(\rho, u, p)(x,0) = \begin{cases} (2, 0, 10^9), & x < 0, \\ (10^{-3}, 0, 1), & x > 0. \end{cases}$$

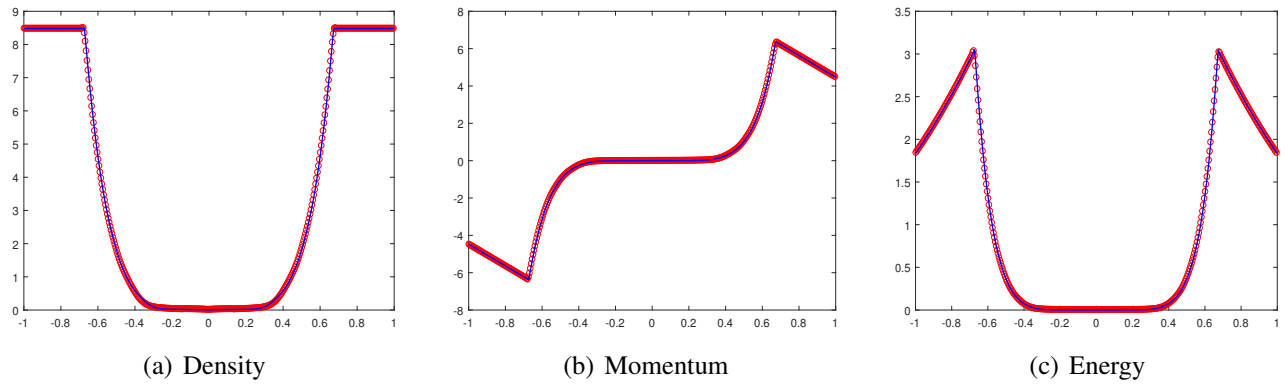


Figure 2: Example 3: Numerical results for the rarefaction test at $t = 0.6$ obtained by the third-order positivity-preserving WB CDG scheme with 400 cells (circles) and 1000 cells (solid lines).

The computational domain is taken as $\Omega = [-10, 10]$ with outflow boundary condition at $x = -10$ and $x = 10$. As the initial data contain a strong discontinuity in the density and the pressure, the WB implementation (see Remark 3.4) of the WENO limiter [37] is applied to the local characteristic fields in some troubled cells, before the positivity-preserving limiting procedure in our simulation. The troubled cells are adaptively identified with parameters $(M_1, M_2, M_3) = (10^{10}, 2 \times 10^6, 5 \times 10^{10})$, where M_i denotes the parameter M in (29) for the i -th component of \mathbf{U} . Figure 3 displays the density, the velocity, and the pressure at $t = 0.0001$ computed by our third-order positivity-preserving WB CDG scheme on a mesh with 800 cells, compared with a reference solution with a refined mesh of 1600 cells. It is seen that our positivity-preserving scheme is highly robust, and the strong discontinuities are captured with high resolution.

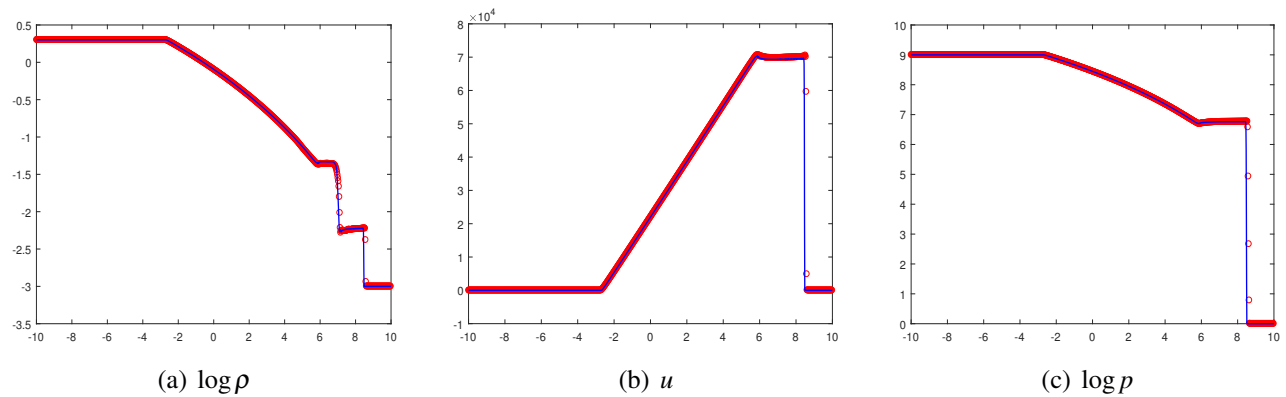


Figure 3: Example 4: Numerical results for the Leblanc shock tube problem at $t = 0.0001$ obtained by the third-order positivity-preserving WB CDG scheme with 800 cells (circles) and 1600 cells (solid lines).

5.2 Two-dimensional tests

5.2.1 Example 5: Accuracy test

This test checks the convergence rates of the WB CDG schemes for the two-dimensional Euler equations under a linear gravitational field $\phi_x = \phi_y = 1$. A time-dependent exact solution [41] takes the form of

$$\begin{aligned}\rho(x, y, t) &= 1 + 0.2 \sin(\pi(x + y - (u_0 + v_0)t)), \\ u_1(x, y, t) &= u_0, \quad u_2(x, y, t) = v_0, \\ p(x, y, t) &= p_0 + (u_0 + v_0)t - x - y + 0.2 \cos(\pi(x + y - (u_0 + v_0)t))/\pi,\end{aligned}$$

where the parameters $u_0 = v_0 = 1$ and $p_0 = 4.5$. The computational domain $\Omega = [0, 2] \times [0, 2]$ is divided into $N \times N$ uniform cells, and the boundary condition is set as the exact solution on $\partial\Omega$. The L^1 errors and corresponding convergence rates at $t = 0.1$ are displayed in Tables 4 and 5. It is seen that the theoretical convergence rates are achieved by our WB CDG schemes, as expected. Our novel projection, modification of the dissipation term, and WB source term approximation do not affect the accuracy of the CDG method.

Table 4: Example 5: L^1 errors at $t = 0.1$ and corresponding convergence rates for the third-order WB CDG scheme at different grid resolutions.

$N \times N$	ρ		ρu_1		ρu_2		E	
	L^1 error	Order	L^1 error	Order	L^1 error	Order	L^1 error	Order
8×8	7.18e-04	-	7.09e-04	-	7.09e-04	-	8.99e-04	-
16×16	8.53e-05	3.07	8.48e-05	3.06	8.48e-05	3.06	1.08e-04	3.06
32×32	1.05e-05	3.02	1.05e-05	3.01	1.05e-05	3.01	1.34e-05	3.01
64×64	1.31e-06	3.00	1.30e-06	3.01	1.30e-06	3.01	1.67e-06	3.00
128×128	1.63e-07	3.01	1.63e-07	3.00	1.63e-07	3.00	2.09e-07	3.00

Table 5: Same as Table 4, except for the fourth-order WB CDG scheme.

$N \times N$	ρ		ρu_1		ρu_2		E	
	L^1 error	Order	L^1 error	Order	L^1 error	Order	L^1 error	Order
8×8	9.65e-05	-	9.35e-05	-	9.35e-05	-	1.16e-04	-
16×16	5.51e-06	4.13	5.43e-06	4.11	5.43e-06	4.11	6.87e-06	4.08
32×32	3.33e-07	4.05	3.30e-07	4.04	3.30e-07	4.04	4.22e-07	4.02
64×64	2.06e-08	4.01	2.05e-08	4.01	2.05e-08	4.01	2.62e-08	4.01
128×128	1.29e-09	4.00	1.29e-09	3.99	1.29e-09	3.99	1.65e-09	3.99

5.2.2 Example 6: Isothermal equilibrium solution

This example considers a two-dimensional isothermal equilibrium problem [41] under the linear gravitational field $\phi_x = \phi_y = g$. The initial condition is specified as

$$\begin{aligned}\rho(x,y) &= \rho_0 \exp\left(-\frac{\rho_0 g}{p_0}(x+y)\right), \\ u_1(x,y) &= u_2(x,y) = 0, \\ p(x,y) &= p_0 \exp\left(-\frac{\rho_0 g}{p_0}(x+y)\right),\end{aligned}\tag{48}$$

where the parameters $\rho_0 = 1.21$, $p_0 = 1$ and $g = 1$. The computational domain is a unit square $\Omega = [0, 1] \times [0, 1]$. We first use this test to demonstrate the WB property of the proposed CDG method. The numerical results at $t = 1$ are obtained by using our third-order WB CDG scheme on two different uniform meshes. Table 6 lists the L^1 errors between the numerical solution and the isothermal equilibrium solution (48). It is clearly observed that all the numerical errors are at the level of machine precision, demonstrating that the proposed CDG method satisfies the WB property in two-dimensional case.

Table 6: L^1 errors for the isothermal equilibrium solution in Example 6.

Mesh	errors in ρ	errors in ρu_1	errors in ρu_2	errors in E
50×50	2.26e-15	8.43e-16	8.44e-16	4.07e-15
80×80	3.96e-15	1.40e-15	1.38e-15	6.49e-15

Next, we investigate the effectiveness of our WB CDG method in capturing the propagation of a small wave perturbation around the isothermal equilibrium solution. Initially, a small Gaussian perturbation is imposed in the pressure state as follows

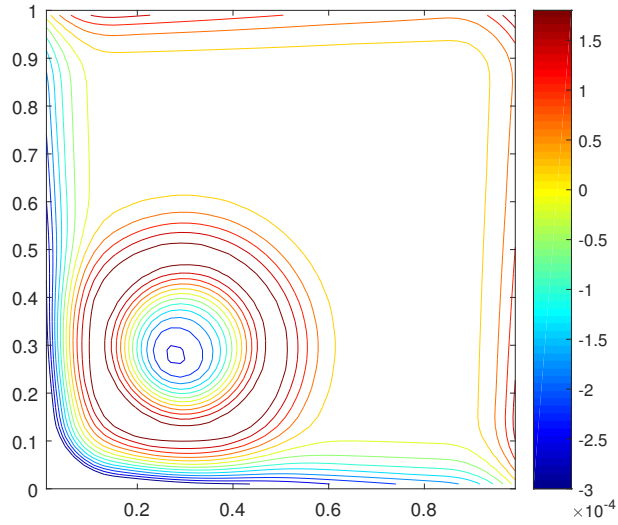
$$p(x,y) = p_0 \exp\left(-\frac{\rho_0 g}{p_0}(x+y)\right) + \eta \exp\left(-100\frac{\rho_0 g}{p_0}\left((x-0.3)^2 + (y-0.3)^2\right)\right),$$

where parameter $\eta = 10^{-3}$, and the density and the velocities are given by the equilibrium state (48). We evolve the numerical solution until $t = 0.15$ on the mesh of 50×50 cells, with the transmissive boundary conditions specified on $\partial\Omega$. The contour plots of the density and pressure perturbations obtained by the third-order WB and non-WB CDG schemes are shown in Figure 4. One can see that the non-WB CDG scheme cannot capture those small perturbations well on the relatively coarse mesh, while the WB method resolves them accurately.

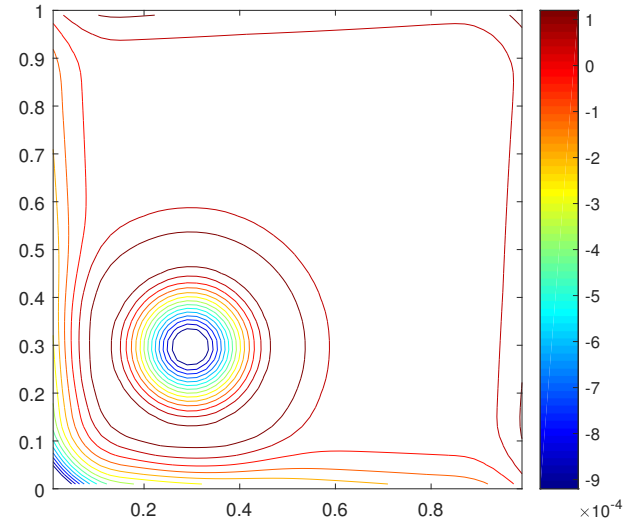
5.2.3 Example 7: Polytopic equilibrium solution

This example considers a two-dimensional polytopic problem arising from astrophysics [17]. This model can be constructed from the hydrostatic equilibrium in spherical symmetry case

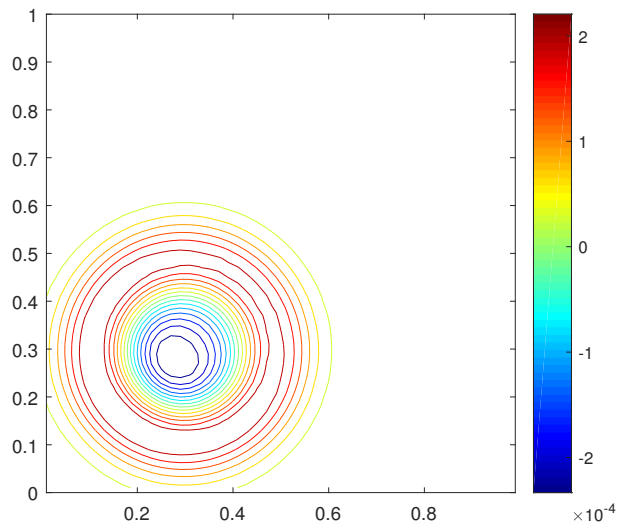
$$\frac{dp}{dr} = -\rho \frac{d\phi}{dr},$$



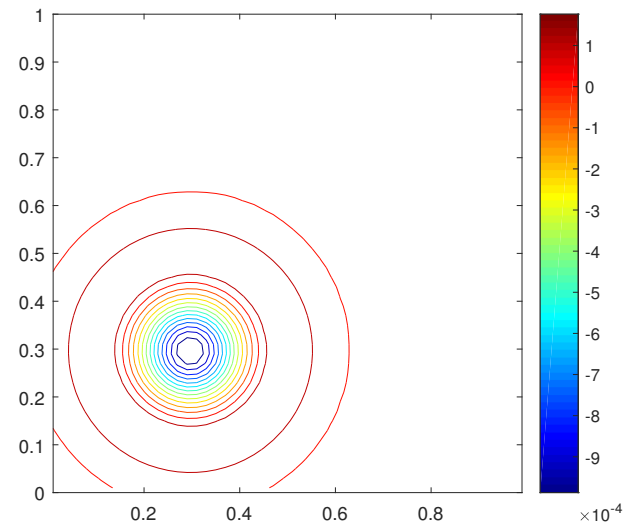
(a) Pressure perturbation of non-WB method



(b) Density perturbation of non-WB method



(c) Pressure perturbation of WB method



(d) Density perturbation of WB method

Figure 4: Example 6: Contour plots of the pressure and density perturbations for the two-dimensional isothermal equilibrium problem at $t = 0.15$ obtained by the WB and non-WB CDG schemes with 50×50 uniform cells.

where $r := \sqrt{x^2 + y^2}$ denotes the radial variable, and the adiabatic index is $\gamma = 2$. One equilibrium solution of this model is given by

$$\rho(r) = \rho_c \frac{\sin(\alpha r)}{\alpha r}, \quad u_1(r) = 0, \quad u_2(r) = 0, \quad p(r) = K\rho(r)^2, \quad (49)$$

coupled with a gravitational potential function

$$\phi(r) = -2K\rho_c \frac{\sin(\alpha r)}{\alpha r}, \quad (50)$$

where $\alpha = \sqrt{\frac{2\pi g}{K}}$ and $K = g = \rho_c = 1$. The computational domain is taken as $\Omega = [-0.5, 0.5] \times [-0.5, 0.5]$.

We first use this example to verify the WB property of the proposed CDG schemes. The initial data are set as the equilibrium solution (49), and we perform the numerical simulations up to $t = 14.8$ on two different uniform meshes. Table 7 lists the L^1 errors between the numerical solution and the projected equilibrium solution (49). It is observed that all the numerical errors are at the level of rounding error, which confirms that the proposed CDG method is WB.

Table 7: L^1 errors for the polytropic equilibrium solution in Example 7.

Mesh	errors in ρ	errors in ρu_1	errors in ρu_2	errors in E
50×50	1.31e-13	1.48e-14	1.55e-14	3.68e-14
80×80	2.25e-13	2.02e-14	2.03e-14	6.39e-14

In order to investigate the capability of our WB CDG method in capturing small perturbations near the polytropic equilibrium solution, we impose a small Gaussian hump perturbation in pressure as follows

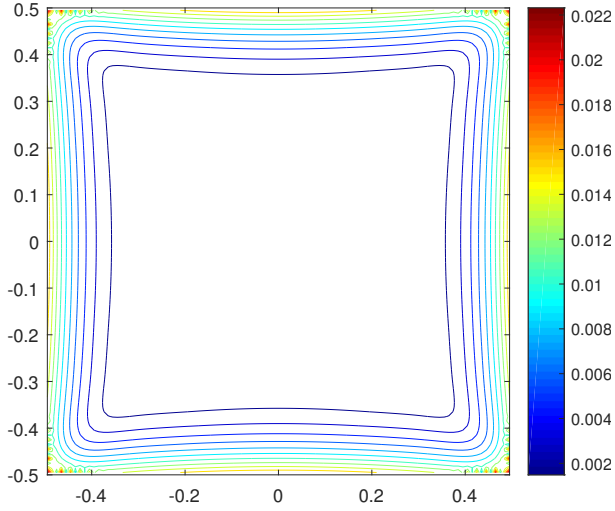
$$p(r) = K\rho(r)^2 + \eta \exp(-100r^2),$$

where the parameter $\eta = 10^{-3}$. We perform the numerical simulation up to $t = 0.2$ on the mesh of 50×50 cells with outflow boundary conditions specified on $\partial\Omega$. The contour plots of the pressure perturbation and the velocity magnitude $\sqrt{u^2 + v^2}$ are displayed in Figure 5. The results show that the non-WB scheme are not capable of capturing the small perturbations on the relatively coarse mesh, while our WB scheme can resolve them accurately. In addition, the WB scheme is able to preserve the axial symmetry, but the non-WB scheme cannot well maintain the symmetry.

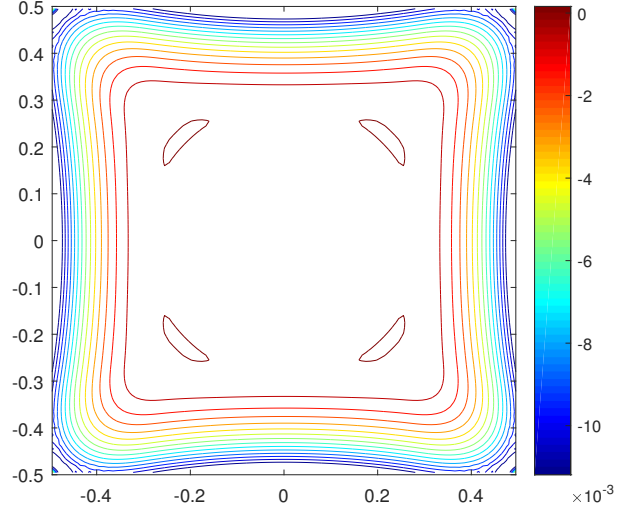
5.2.4 Example 8: Rarefaction test with low density and pressure

This example is used to demonstrate the positivity-preserving property of the proposed CDG schemes. The initial condition is given by

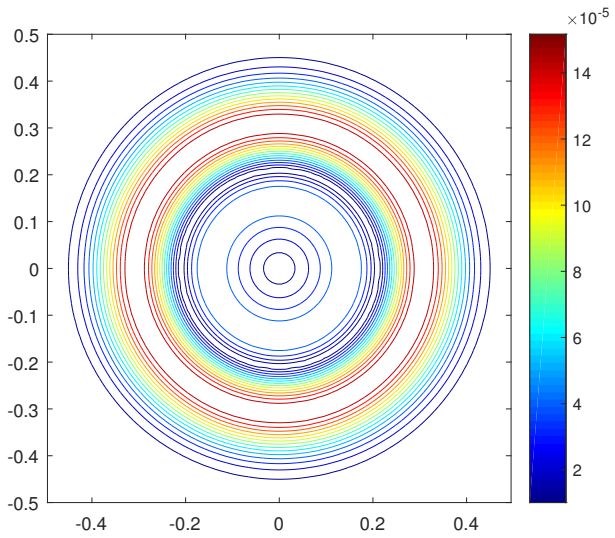
$$\begin{aligned} \rho(x, y, 0) &= \exp(-\phi(x, y)/0.4), & p(x, y, 0) &= 0.4 \exp(-\phi(x, y)/0.4), \\ u_1(x, y, 0) &= \begin{cases} -2, & x < 0.5, \\ 2, & x > 0.5, \end{cases} & u_2(x, y, 0) &= 0, \end{aligned}$$



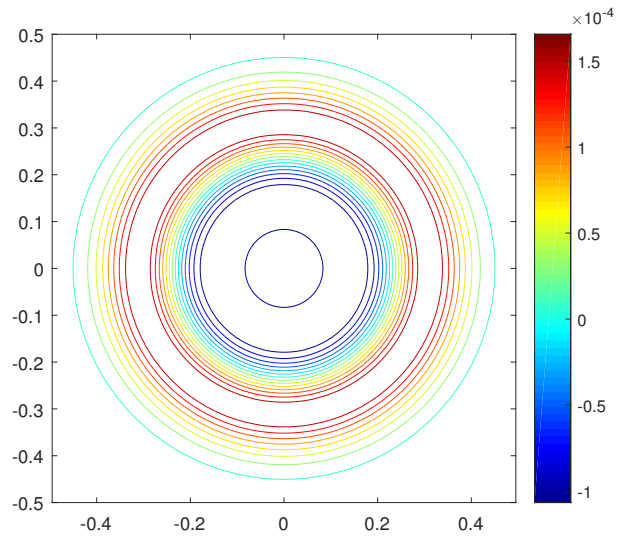
(a) Velocity magnitude of non-WB scheme



(b) Pressure perturbation of non-WB scheme



(c) Velocity magnitude of WB scheme



(d) Pressure perturbation of WB scheme

Figure 5: Example 7: Contour plots of the velocity magnitude $\sqrt{u_1^2 + u_2^2}$ and pressure perturbation for the two-dimensional polytropic equilibrium problem at $t = 0.2$ obtained by the third-order WB and non-WB CDG schemes with 100×100 uniform cells. 10 uniformly spaced contour lines are displayed.

with a quadratic gravitational potential $\phi(x,y) = \frac{1}{2}[(x-0.5)^2 + (y-0.5)^2]$. The computational domain $\Omega = [0, 1] \times [0, 1]$ is divided into 100×100 uniform cells with outflow boundary conditions on $\partial\Omega$. Figure 6 displays the numerical solutions obtained by our third-order positivity-preserving WB CDG method. We observe that the density and the pressure get close to zero but remain positive throughout the simulation. It is noticed that the CDG code would blow-up, if the positivity-preserving limiter is not employed.

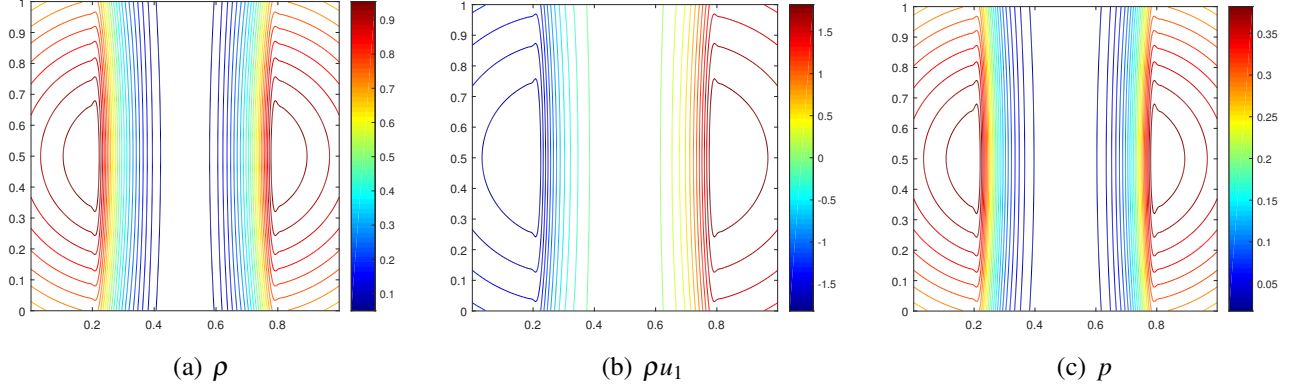


Figure 6: Example 8: Contour plots for the two-dimensional rarefaction test at $t = 0.1$ obtained by the positivity-preserving WB CDG scheme with 100×100 uniform cells.

5.2.5 Example 9: Blast problem

In order to demonstrate the positivity-preserving property and the capability of the proposed WB CDG method in resolving strong discontinuities, we consider a two-dimensional blast problem [57] under the gravitational field (50). The initial condition is obtained by adding a huge jump to the pressure of the polytropic equilibrium solution (49). Specially, the initial pressure is given by

$$p(r) = K\rho(r)^2 + \begin{cases} 100, & r < 0.1, \\ 0, & r \geq 0.1. \end{cases}$$

We set the parameters $K = g = 1$ and $\rho_c = 0.01$, so that the low pressure and the low density appear in the solution and make this test challenging. The computational domain is set as $\Omega = [-0.5, 0.5] \times [-0.5, 0.5]$, and the adiabatic index is $\gamma = 2$.

In this test, both the adaptive WENO limiter [37] (see Remark 3.4 for its WB implementation with the TVB parameter $M = 200$) and the positivity-preserving limiter are implemented. Figure 7 displays the contour plots of the density and the pressure at $t = 0.005$ computed by the third-order positivity-preserving WB CDG method with 200×200 cells. Figure 7 also gives the plots along the line $y = 0$, from which we can clearly observe a strong shock at $|x| \approx 0.4$. It is seen that the discontinuities are captured with high resolution, and the proposed CDG method preserves the positivity of the density and the pressure as well as the axisymmetric structure of the solution.

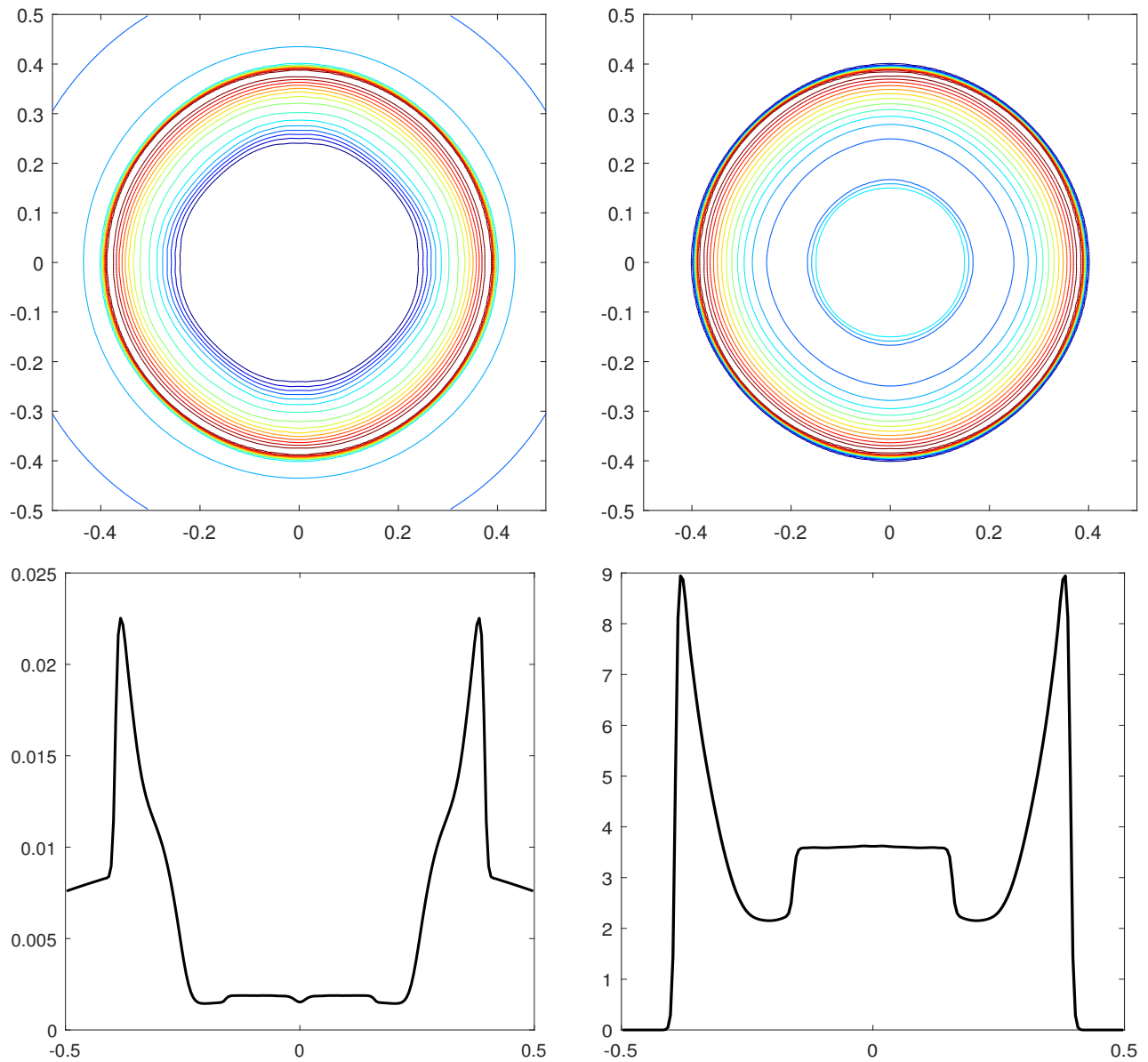


Figure 7: Example 9: Contour plots of the density (top-left) and the pressure (top-right) and corresponding plots (bottom) along the line $y = 0$ for the two-dimensional blast problem at $t = 0.005$, obtained by the positivity-preserving WB CDG scheme on a mesh with 200×200 uniform cells.

5.2.6 Example 10: Rising thermal bubble

This is a benchmark test problem arising from the atmospheric flows [11, 12, 57]. It shows the evolution of a warm bubble in a constant potential temperature environment. Because the bubble is warmer than the ambient air, it rises while deforming as a consequence of the shearing motion caused by the velocity field gradients until it forms a mushroom cloud. The computational domain is set as $\Omega = [0, 1000] \times [0, 1000] \text{ m}^2$. The boundary conditions on all sides are set as the solid walls and the reflective boundary conditions are specified. The initial solution is a stratified atmosphere in hydrostatic balance; see, e.g., the second example in the Appendix of [11]. The constant potential temperature (and thus the reference temperature at $y = 0 \text{ m}$) is 300 K, and the reference pressure is 10^5 N/m^2 . The ambient flow is at rest (i.e. $\mathbf{u} = \mathbf{0} \text{ m/s}$) and experiences a constant gravitational force per unit mass of $g = 9.8 \text{ m/s}^2$, which implies a linear gravitational field with $\phi_x = 0 \text{ m/s}^2$ and $\phi_y = g$. The potential temperature and the Exner pressure of the ambient air are $\Theta = T_0 = 300 \text{ K}$ and $\Pi = 1 - \frac{(\gamma-1)gy}{\gamma RT_0}$, respectively, where $R = 287.058 \text{ J/(kg} \cdot \text{K)}$ is the gas constant for dry air. Initially, the warm bubble is added as a potential temperature perturbation to the hydrostatic balance:

$$\Delta\Theta(x, y, t = 0) = \begin{cases} 0, & r > r_c, \\ \frac{\theta_c}{2}(1 + \cos(\pi r/r_c)), & r \leq r_c, \end{cases} \quad r = \sqrt{(x - x_c)^2 + (y - y_c)^2},$$

where $\theta_c = 0.5 \text{ K}$, $(x_c, y_c) = (500 \text{ m}, 350 \text{ m})$, and $r_c = 250 \text{ m}$. The pressure and density are computed by Θ and Π via the following formulas:

$$p = p_0 \Pi^{\frac{\gamma}{\gamma-1}}, \quad \rho = \frac{p_0}{R\Theta} \Pi^{\frac{1}{\gamma-1}}, \quad (51)$$

with the reference pressure $p_0 = 10^5 \text{ N/m}^2$. Figure 8 shows the evolution of the potential temperature perturbation $\Delta\Theta$ obtained by the proposed fourth-order accurate WB CDG method on the meshes of 100×100 cells (10 m resolution). We observe clearly that the initial circular bubble is deformed to a mushroom-like cloud and the flow structures are well resolved.

5.2.7 Example 11: Rayleigh–Taylor (RT) instability tests

This example simulates three tests, which involve discontinuous stationary hydrostatic solutions.

For the first two tests, we use the same setups as in [6], with the gravitational potential function $\phi(x, y) = y$ and the computational domain $\Omega = [-0.25, 0.25] \times [-1, 1]$. The initial solution is stationary hydrostatic with the pressure and density given by

$$p(x, y, 0) = \begin{cases} p_0 \exp(-y/T_l), & y < 0, \\ p_0 \exp(-y/T_u), & y > 0, \end{cases} \quad \rho(x, y, 0) = \begin{cases} p/T_l, & y < 0, \\ p/T_u, & y > 0, \end{cases} \quad (52)$$

where $p_0 = 1$, $\{T_l, T_u\}$ are two different constant temperatures. Note that the density $\rho(x, y, 0)$ is discontinuous because of the jump in temperature at $y = 0$, while the pressure is continuous at $y = 0$. We consider two configurations [6]:

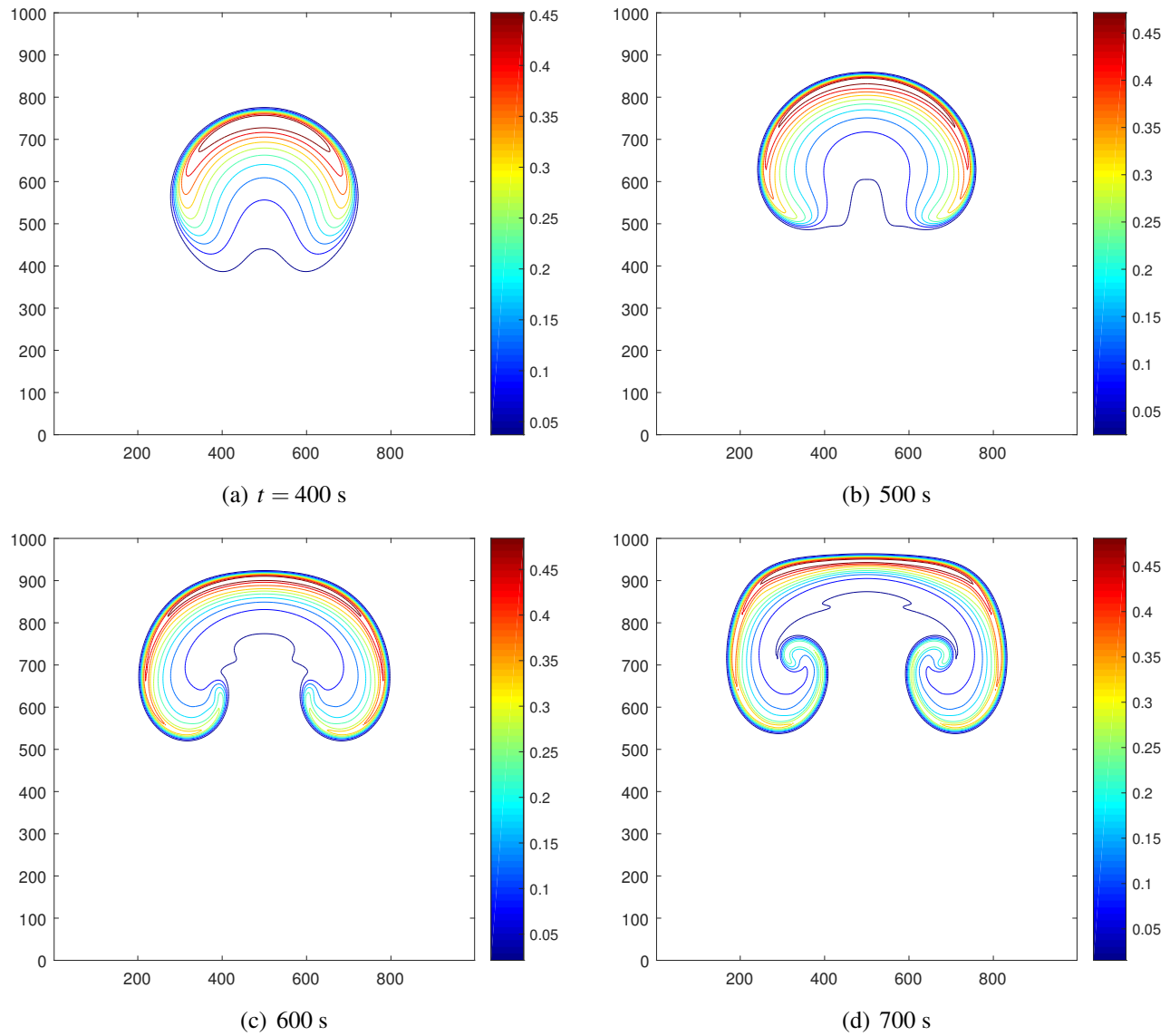


Figure 8: Example 10: Contour plots of the potential temperature perturbation $\Delta\Theta$ at $t = 400$ s, 500 s, 600 s, and 700 s, respectively, obtained by our fourth-order WB CDG method. 10 uniformly spaced contour lines are displayed.

- **RT test 1:** $T_l = 1$ and $T_u = 2$. This is a stable case, because the light fluid is above the heavy fluid.
- **RT test 2:** $T_l = 2$ and $T_u = 1$. This is a physically unstable case, because heavy fluid is above the light fluid.

The numerical solutions for both tests are computed until $t = 0.1$ by using the third-order WB CDG scheme with respectively 25×100 and 50×200 uniform cells. In order to demonstrate our WB implementation of the WENO limiter (see Remark 3.4), we perform the tests with and without the WENO limiter, respectively. Tables 8 and 9 list the L^1 errors between the numerical solutions and the projection of the initial solution (52). We clearly see that all the numerical errors are at the level of rounding error, confirming that the proposed CDG method and our implementation of the WENO limiter exactly preserve the WB property. As the solution remains at the stationary hydrostatic state, we observe that no cell is flagged as “troubled cells” up to $t = 0.1$. Following [6], we also continue the simulation for a very long time. As shown in Figure 9, the steady state solution in the stable case (RT test 1) is still exactly preserved in a long-time simulation until $t = 10$, thanks to the WB property. However, because the configuration of RT test 2 is the physically unstable, in the long-time simulation the small rounding errors will accumulate, as time evolves, and eventually cause the RT instability near the interface $y = 0$ (the WB property is locally preserved away from the interface); see Figure 9.

Table 8: L^1 errors at $t = 0.1$ for RT test 1 in Example 11.

limiter	mesh	errors in ρ	errors in ρu_1	errors in ρu_2	errors in E
No limiter	25×100	$1.43\text{e-}15$	$3.41\text{e-}16$	$5.22\text{e-}16$	$5.54\text{e-}15$
	50×200	$2.93\text{e-}15$	$6.39\text{e-}16$	$9.07\text{e-}16$	$1.17\text{e-}14$
WENO limiter	25×100	$1.43\text{e-}15$	$3.41\text{e-}16$	$5.22\text{e-}16$	$5.54\text{e-}15$
	50×200	$2.93\text{e-}15$	$6.39\text{e-}16$	$9.07\text{e-}16$	$1.17\text{e-}14$

Table 9: L^1 errors $t = 0.1$ for RT test 2 in Example 11.

limiter	mesh	errors in ρ	errors in ρu_1	errors in ρu_2	errors in E
No limiter	25×100	$9.48\text{e-}16$	$2.92\text{e-}16$	$3.20\text{e-}16$	$5.01\text{e-}15$
	50×200	$2.02\text{e-}15$	$5.34\text{e-}16$	$6.05\text{e-}16$	$1.01\text{e-}14$
WENO limiter	25×100	$9.48\text{e-}16$	$2.92\text{e-}16$	$3.20\text{e-}16$	$5.01\text{e-}15$
	50×200	$2.02\text{e-}15$	$5.34\text{e-}16$	$6.05\text{e-}16$	$1.01\text{e-}14$

To check the effectiveness of our WB CDG method in capturing small perturbations near discontinuous equilibrium solutions, we simulate another classical benchmark RT test [39], which is abbreviated as “**RT test 3**” for convenience. This test is usually used to validate the ability of a high-order numerical scheme in capturing complicated small wave structures. For comparison purpose, we

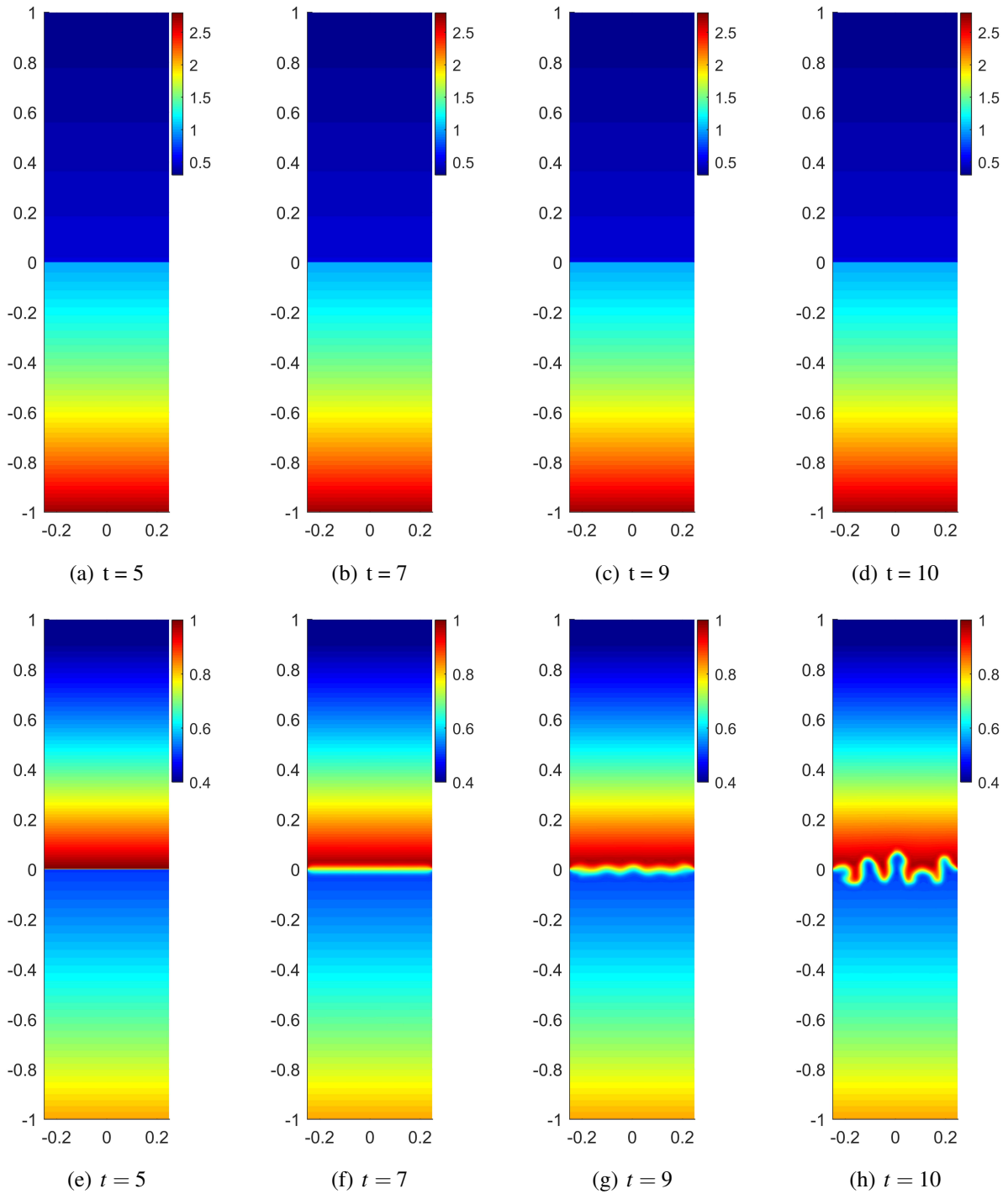


Figure 9: Long-time simulations of RT test 1 (top row; the stable configuration) and RT test 2 (bottom row; the unstable configuration) by using the third-order WB CDG scheme with 50×200 uniform cells. The WB implementation of the WENO limiter is used with the parameter $M = 200$ in the TVB corrected minmod function (29).

use the same setup as in [39]. The gravitational potential function is taken as $\phi(x, y) = -y$, so that the acceleration is in the positive y -direction. The initial condition is a small perturbation to an unstable stationary hydrostatic solution involving a discontinuity in density:

$$(\rho, u_1, u_2, p)(x, y, 0) = \begin{cases} (2, 0, \tilde{u}(x), 2y + 1)^\top, & 0 \leq y < 0.5, \\ (1, 0, \tilde{u}(x), y + 1.5)^\top, & 0.5 \leq y \leq 1, \end{cases}$$

where $\tilde{u}(x) = -0.025\sqrt{\gamma p/\rho} \cos(8\pi x)$. The variables (ρ, u_1, u_2, p) are set as $(1, 0, 0, 2.5)$ on the top boundary and as $(2, 0, 0, 1)$ on the bottom. Reflective boundary conditions are imposed on both the left and right boundaries. The WB implementation of the WENO limiter is used with the parameter $M = 200$ in the TVB corrected minmod function (29). As in [39], the mesh refinement study is carried out here by using three different uniform square meshes: $h = \frac{1}{240}, \frac{1}{480}, \frac{1}{960}$, where h is the spatial step-size in both the x - and y -directions. Figure 10 displays the density contours at time $t = 1.95$. We see that our third-order WB CDG method can clearly resolve the complicated wave structures and that the numerical resolutions are comparable to those computed with WENO9 (a ninth-order WENO scheme) in [39] with the same mesh sizes.

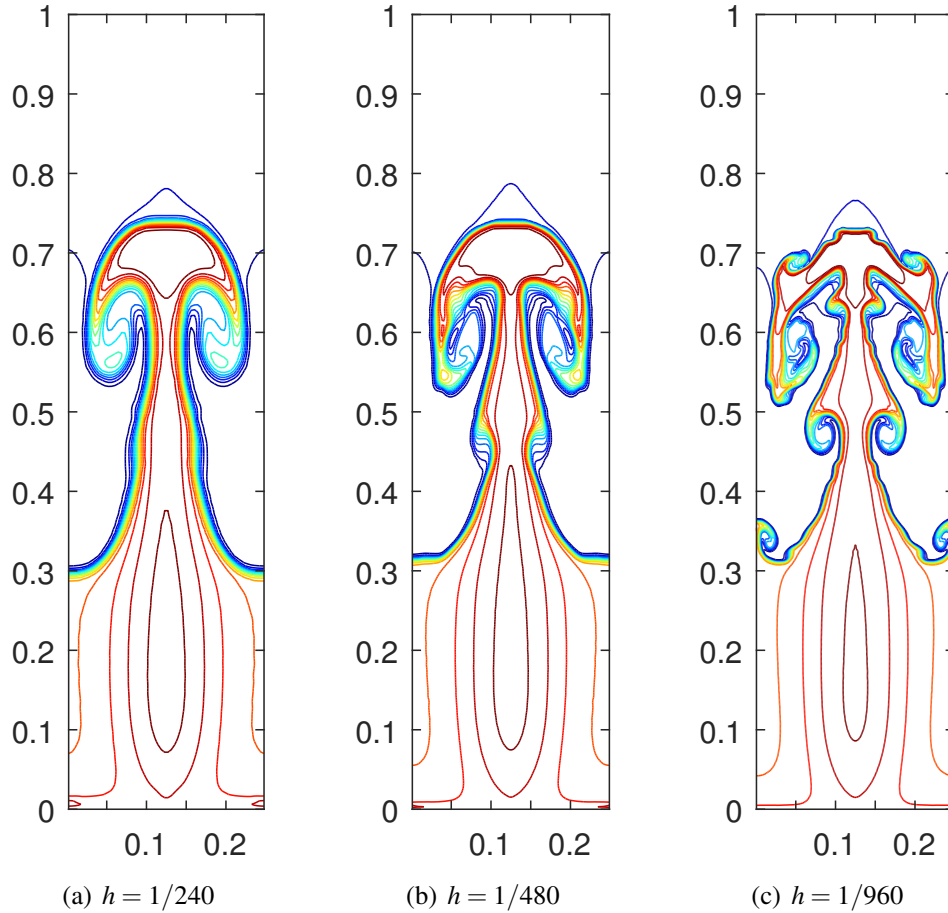


Figure 10: RT test 3 (the perturbation configuration): Contour plots of the density at $t = 1.95$ obtained by the third-order WB CDG scheme with 15 equally spaced contour lines from 0.952269 to 2.14589.

6 Conclusions

This paper designed a high-order positivity-preserving well-balanced (WB) central discontinuous Galerkin (CDG) method for the Euler equations under gravitational fields. A novel WB spatial discretization in the CDG framework was devised with suitable modifications to the numerical dissipation term and the source term approximation, while the desired conservative and positivity-preserving properties were also simultaneously preserved in the discretization. The modifications were based on a novel projection for the stationary hydrostatic solution, which had the same order of accuracy as the standard L^2 -projection, could be explicitly calculated, and was easy to implement without solving any optimization problems. Moreover, the novel projection guaranteed the projected stationary solution having the same cell averages on both the primal and dual meshes. This feature was a key to obtain the desired properties of our schemes. Based on some convex decomposition techniques and several key properties of the admissible states, we rigorously proved that the resulting WB CDG method satisfied a weak positivity-preserving property, which implied that a simple limiter could ensure the positivity-preserving property without losing the high-order accuracy and conservativeness. Extensive one- and two-dimensional numerical examples were provided to demonstrate the robustness, high-order accuracy, WB and positivity-preserving properties of the proposed schemes.

Acknowledgements

H.Z. Tang is partially supported by the National Key R&D Program of China, Project Number 2020YFA0712000, and the National Natural Science Foundation of China (Nos. 12171227 & 12126320). K.L. Wu is partially supported by the National Natural Science Foundation of China, Project Number 12171227. H.L. Jiang wishes to thank Professor Tie Zhou of Peking University very much for his support and the Department of Mathematics of SUSTech for hospitality during the preparation of this paper.

References

- [1] E. AUDUSSE, F. BOUCHUT, M. BRISTEAU, R. KLEIN, AND B. PERTHAME, *A fast and stable well-balanced scheme with hydrostatic reconstruction for shallow water flows*, SIAM Journal on Scientific Computing, 25 (2004), pp. 2050–2065.
- [2] J. P. BERBERICH, R. KÄPPELI, P. CHANDRASHEKAR, AND C. KLINGENBERG, *High order discretely well-balanced methods for arbitrary hydrostatic atmospheres*, Communications in Computational Physics, 30 (2021), pp. 666–708.
- [3] A. BERMUDEZ AND M. E. VAZQUEZ, *Upwind methods for hyperbolic conservation laws with source terms*, Computers & Fluids, 23 (1994), pp. 1049–1071.

- [4] N. BOTTA, R. KLEIN, S. LANGENBERG, AND S. LUTZENKIRCHEN, *Well balanced finite volume methods for nearly hydrostatic flows*, Journal of Computational Physics, 196 (2004), pp. 539–565.
- [5] P. CHANDRASHEKAR AND C. KLINGENBERG, *A second order well-balanced finite volume scheme for Euler equations with gravity*, SIAM Journal on Scientific Computing, 37 (2015), pp. B382–B402.
- [6] P. CHANDRASHEKAR AND M. ZENK, *Well-balanced nodal discontinuous Galerkin method for Euler equations with gravity*, Journal of Scientific Computing, 71 (2017), pp. 1062–1093.
- [7] A. CHERTOCK, S. CUI, A. KURGANOV, Ş. N. ÖZCAN, AND E. TADMOR, *Well-balanced schemes for the Euler equations with gravitation: Conservative formulation using global fluxes*, Journal of Computational Physics, 358 (2018), pp. 36–52.
- [8] B. COCKBURN AND C.-W. SHU, *The Runge–Kutta discontinuous Galerkin method for conservation laws V: multidimensional systems*, Journal of Computational Physics, 141 (1998), pp. 199–224.
- [9] S. DEKEL AND D. LEVIATAN, *The Bramble–Hilbert lemma for convex domains*, SIAM Journal on Mathematical Analysis, 35 (2004), pp. 1203–1212.
- [10] E. FRANCK AND L. S. MENDOZA, *Finite volume scheme with local high order discretization of the hydrostatic equilibrium for the Euler equations with external forces*, Journal of Scientific Computing, 69 (2016), pp. 314–354.
- [11] D. GHOSH AND E. M. CONSTANTINESCU, *Well-balanced, conservative finite difference algorithm for atmospheric flows*, AIAA Journal, 54 (2016), pp. 1370–1385.
- [12] F. X. GIRALDO AND M. RESTELLI, *A study of spectral element and discontinuous Galerkin methods for the Navier–Stokes equations in nonhydrostatic mesoscale atmospheric modeling: Equation sets and test cases*, Journal of Computational Physics, 227 (2008), pp. 3849–3877.
- [13] S. GOTTLIEB, C.-W. SHU, AND E. TADMOR, *Strong stability-preserving high-order time discretization methods*, SIAM Review, 43 (2001), pp. 89–112.
- [14] J. M. GREENBERG AND A.-Y. LEROUX, *A well-balanced scheme for the numerical processing of source terms in hyperbolic equations*, SIAM Journal on Numerical Analysis, 33 (1996), pp. 1–16.
- [15] X. Y. HU, N. A. ADAMS, AND C.-W. SHU, *Positivity-preserving method for high-order conservative schemes solving compressible Euler equations*, Journal of Computational Physics, 242 (2013), pp. 169–180.

- [16] F. KANBAR, R. TOUMA, AND C. KLINGENBERG, *Well-balanced central schemes for the one and two-dimensional Euler systems with gravity*, Applied Numerical Mathematics, 156 (2020), pp. 608–626.
- [17] R. KÄPPELI AND S. MISHRA, *Well-balanced schemes for the Euler equations with gravitation*, Journal of Computational Physics, 259 (2014), pp. 199–219.
- [18] R. KÄPPELI AND S. MISHRA, *A well-balanced finite volume scheme for the Euler equations with gravitation—the exact preservation of hydrostatic equilibrium with arbitrary entropy stratification*, Astronomy & Astrophysics, 587 (2016), p. A94.
- [19] A. KURGANOV AND G. PETROVA, *A second-order well-balanced positivity preserving central-upwind scheme for the Saint–Venant system*, Communications in Mathematical Sciences, 5 (2007), pp. 133–160.
- [20] A. KURGANOV AND E. TADMOR, *New high-resolution central schemes for nonlinear conservation laws and convection–diffusion equations*, Journal of Computational Physics, 160 (2000), pp. 241–282.
- [21] R. J. LEVEQUE, *Balancing source terms and flux gradients in high-resolution Godunov methods*, Journal of Computational Physics, 146 (1998), pp. 346–365.
- [22] F. LI AND L. XU, *Arbitrary order exactly divergence-free central discontinuous Galerkin methods for ideal MHD equations*, Journal of Computational Physics, 231 (2012), pp. 2655–2675.
- [23] F. LI, L. XU, AND S. YAKOVLEV, *Central discontinuous Galerkin methods for ideal MHD equations with the exactly divergence-free magnetic field*, Journal of Computational Physics, 230 (2011), pp. 4828 – 4847.
- [24] F. LI AND S. YAKOVLEV, *A central discontinuous Galerkin method for Hamilton–Jacobi equations*, Journal of Scientific Computing, 45 (2010), pp. 404–428.
- [25] G. LI AND Y. XING, *High order finite volume WENO schemes for the Euler equations under gravitational fields*, Journal of Computational Physics, 316 (2016), pp. 145–163.
- [26] G. LI AND Y. XING, *Well-balanced discontinuous Galerkin methods for the Euler equations under gravitational fields*, Journal of Scientific Computing, 67 (2016), pp. 493–513.
- [27] G. LI AND Y. XING, *Well-balanced discontinuous Galerkin methods with hydrostatic reconstruction for the Euler equations with gravitation*, Journal of Computational Physics, 352 (2018), pp. 445–462.
- [28] G. LI AND Y. XING, *Well-balanced finite difference weighted essentially non-oscillatory schemes for the Euler equations with static gravitational fields*, Computers & Mathematics with Applications, 75 (2018), pp. 2071–2085.

- [29] M. LI, P. GUYENNE, F. LI, AND L. XU, *A positivity-preserving well-balanced central discontinuous Galerkin method for the nonlinear shallow water equations.*, Journal of Scientific Computing, 71 (2017), pp. 994–1034.
- [30] M. LI, F. LI, Z. LI, AND L. XU, *Maximum-principle-satisfying and positivity-preserving high order central discontinuous Galerkin methods for hyperbolic conservation laws*, SIAM Journal on Scientific Computing, 38 (2016), pp. A3720–A3740.
- [31] Y. LIU, *Central schemes on overlapping cells*, Journal of Computational Physics, 209 (2005), pp. 82–104.
- [32] Y. LIU, C.-W. SHU, E. TADMOR, AND M. ZHANG, *Central discontinuous Galerkin methods on overlapping cells with a nonoscillatory hierarchical reconstruction*, SIAM Journal on Numerical Analysis, 45 (2007), pp. 2442–2467.
- [33] Y. LIU, C.-W. SHU, E. TADMOR, AND M. ZHANG, *L^2 stability analysis of the central discontinuous Galerkin method and a comparison between the central and regular discontinuous Galerkin methods*, ESAIM: Mathematical Modelling and Numerical Analysis, 42 (2008), pp. 593–607.
- [34] J. LUO, K. XU, AND N. LIU, *A well-balanced symplecticity-preserving gas-kinetic scheme for hydrodynamic equations under gravitational field*, SIAM Journal on Scientific Computing, 33 (2010), pp. 2356–2381.
- [35] H. NESSYAHU AND E. TADMOR, *Non-oscillatory central differencing for hyperbolic conservation laws*, Journal of Computational Physics, 87 (1990), pp. 408–463.
- [36] T. QIN, C.-W. SHU, AND Y. YANG, *Bound-preserving discontinuous Galerkin methods for relativistic hydrodynamics*, Journal of Computational Physics, 315 (2016), pp. 323–347.
- [37] J. QIU AND C.-W. SHU, *Runge-Kutta discontinuous Galerkin method using WENO limiters*, SIAM Journal on Scientific Computing, 26 (2005), pp. 907–929.
- [38] M. A. REYNA AND F. LI, *Operator bounds and time step conditions for the DG and central DG methods*, Journal of Scientific Computing, 62 (2015), pp. 532–554.
- [39] J. SHI, Y.-T. ZHANG, AND C.-W. SHU, *Resolution of high order WENO schemes for complicated flow structures*, Journal of Computational Physics, 186 (2003), pp. 690–696.
- [40] C.-W. SHU, *Bound-preserving high-order schemes for hyperbolic equations: Survey and recent developments*, in XVI International Conference on Hyperbolic Problems: Theory, Numerics, Applications, Springer, 2016, pp. 591–603.
- [41] C.-W. SHU AND Y. XING, *High order well-balanced WENO scheme for the gas dynamics equations under gravitational fields*, Journal of Scientific Computing, 54 (2013), pp. 645–662.

- [42] A. THOMANN, M. ZENK, AND C. KLINGENBERG, *A second-order positivity-preserving well-balanced finite volume scheme for Euler equations with gravity for arbitrary hydrostatic equilibria*, International Journal for Numerical Methods in Fluids, 89 (2019), pp. 465–482.
- [43] R. TOUMA, U. KOLEY, AND C. KLINGENBERG, *Well-balanced unstaggered central schemes for the Euler equations with gravitation*, SIAM Journal on Scientific Computing, 38 (2016), pp. B773–B807.
- [44] D. VARMA AND P. CHANDRASHEKAR, *A second-order, discretely well-balanced finite volume scheme for Euler equations with gravity*, Computers & Fluids, 181 (2019), pp. 292–313.
- [45] M. H. VEIGA, D. A. VELASCO-ROMERO, R. ABGRALL, AND R. TEYSSIER, *Capturing near-equilibrium solutions: a comparison between high-order discontinuous Galerkin methods and well-balanced schemes*, Communications in Computational Physics, 26 (2019), pp. 1–34.
- [46] C. WANG, X. ZHANG, C.-W. SHU, AND J. NING, *Robust high order discontinuous Galerkin schemes for two-dimensional gaseous detonations*, Journal of Computational Physics, 231 (2012), pp. 653–665.
- [47] K. WU, *Design of provably physical-constraint-preserving methods for general relativistic hydrodynamics*, Physical Review D, 95 (2017), p. 103001.
- [48] K. WU, *Positivity-preserving analysis of numerical schemes for ideal magnetohydrodynamics*, SIAM Journal on Numerical Analysis, 56 (2018), pp. 2124–2147.
- [49] K. WU, *Minimum principle on specific entropy and high-order accurate invariant region preserving numerical methods for relativistic hydrodynamics*, SIAM Journal on Scientific Computing, 43 (2021), pp. B1164–B1197.
- [50] K. WU AND C.-W. SHU, *A provably positive discontinuous Galerkin method for multidimensional ideal magnetohydrodynamics*, SIAM Journal on Scientific Computing, 40 (2018), pp. B1302–B1329.
- [51] K. WU AND C.-W. SHU, *Provably positive high-order schemes for ideal magnetohydrodynamics: analysis on general meshes*, Numerische Mathematik, 142 (2019), pp. 995–1047.
- [52] K. WU AND C.-W. SHU, *Geometric quasilinearization framework for analysis and design of bound-preserving schemes*, arXiv preprint arXiv:2111.04722, (2021).
- [53] K. WU AND C.-W. SHU, *Provably physical-constraint-preserving discontinuous Galerkin methods for multidimensional relativistic MHD equations*, Numerische Mathematik, 148 (2021), pp. 699–741.
- [54] K. WU AND H. TANG, *High-order accurate physical-constraints-preserving finite difference WENO schemes for special relativistic hydrodynamics*, Journal of Computational Physics, 298 (2015), pp. 539–564.

- [55] K. WU AND H. TANG, *Admissible states and physical-constraints-preserving schemes for relativistic magnetohydrodynamic equations*, *Mathematical Models and Methods in Applied Sciences*, 27 (2017), pp. 1871–1928.
- [56] K. WU AND H. TANG, *Physical-constraint-preserving central discontinuous Galerkin methods for special relativistic hydrodynamics with a general equation of state*, *The Astrophysical Journal Supplement Series*, 228 (2017), 3.
- [57] K. WU AND Y. XING, *Uniformly high-order structure-preserving discontinuous Galerkin methods for Euler equations with gravitation: Positivity and well-balancedness*, *SIAM Journal on Scientific Computing*, 43 (2021), pp. A472–A510.
- [58] Y. XING AND C.-W. SHU, *High order finite difference WENO schemes with the exact conservation property for the shallow water equations*, *Journal of Computational Physics*, 208 (2005), pp. 206–227.
- [59] Y. XING AND C.-W. SHU, *High-order finite volume WENO schemes for the shallow water equations with dry states*, *Advances in Water Resources*, 34 (2011), pp. 1026–1038.
- [60] Y. XING AND C.-W. SHU, *A survey of high order schemes for the shallow water equations*, *Journal of Mathematical Study*, 47 (2014), pp. 221–249.
- [61] Y. XING, X. ZHANG, AND C.-W. SHU, *Positivity-preserving high order well-balanced discontinuous Galerkin methods for the shallow water equations*, *Advances in Water Resources*, 33 (2010), pp. 1476 – 1493.
- [62] K. XU, *A well-balanced gas-kinetic scheme for the shallow-water equations with source terms*, *Journal of Computational Physics*, 178 (2002), pp. 533–562.
- [63] K. XU, J. LUO, AND S. CHEN, *A well-balanced kinetic scheme for gas dynamic equations under gravitational field*, *Advances in Applied Mathematics and Mechanics*, 2 (2010), pp. 200–210.
- [64] Z. XU, *Parametrized maximum principle preserving flux limiters for high order schemes solving hyperbolic conservation laws: one-dimensional scalar problem*, *Mathematics of Computation*, 83 (2014), pp. 2213–2238.
- [65] Z. XU AND X. ZHANG, *Bound-preserving high order schemes*, in *Handbook of Numerical Methods for Hyperbolic Problems: Applied and Modern Issues*, edited by R. Abgrall and C.-W. Shu, vol. 18, North-Holland, Amsterdam, 2017, Elsevier.
- [66] W. ZHANG, Y. XIA, AND Y. XU, *Positivity-preserving well-balanced arbitrary Lagrangian–Eulerian discontinuous Galerkin methods for the shallow water equations*, *Journal of Scientific Computing*, 88 (2021), pp. 1–43.

- [67] X. ZHANG, *On positivity-preserving high order discontinuous Galerkin schemes for compressible Navier–Stokes equations*, Journal of Computational Physics, 328 (2017), pp. 301–343.
- [68] X. ZHANG AND C.-W. SHU, *On maximum-principle-satisfying high order schemes for scalar conservation laws*, Journal of Computational Physics, 229 (2010), pp. 3091–3120.
- [69] X. ZHANG AND C.-W. SHU, *On positivity-preserving high order discontinuous Galerkin schemes for compressible Euler equations on rectangular meshes*, Journal of Computational Physics, 229 (2010), pp. 8918–8934.
- [70] X. ZHANG AND C.-W. SHU, *Positivity-preserving high order discontinuous Galerkin schemes for compressible Euler equations with source terms*, Journal of Computational Physics, 230 (2011), pp. 1238–1248.
- [71] X. ZHANG, Y. XIA, AND C.-W. SHU, *Maximum-principle-satisfying and positivity-preserving high order discontinuous Galerkin schemes for conservation laws on triangular meshes*, Journal of Scientific Computing, 50 (2012), pp. 29–62.
- [72] J. ZHAO AND H. Z. TANG, *Runge-kutta central discontinuous Galerkin methods for the special relativistic hydrodynamics*, Communications in Computational Physics, 22 (2017), pp. 643–682.
- [73] J. ZHAO AND H. Z. TANG, *Runge-Kutta discontinuous Galerkin methods for the special relativistic magnetohydrodynamics*, Journal of Computational Physics, 343 (2017), pp. 33–72.